THE REGULATION OF THE EXPRESSION OF HUMAN MAJOR HISTOCOMPATABILITY CLASS I MOLECULES ON CANCER CELLS BY KINASES

A Dissertation

Presented to the Faculty of the Weill Cornell Graduate School

of Medical Sciences

in Partial Fulfillment of the Requirements for the Degree of

Doctor of Philosophy

By

Elliott Joseph Brea

August 2016

THE REGULATION OF THE EXPRESSION OF HUMAN MAJOR HISTOCOMPATABILITY CLASS I MOLECULES ON CANCER CELLS BY KINASES

Elliott Joseph Brea, PhD

Cornell University 2016

The major histocompatability complex (MHC) encodes MHC class I molecules which present antigenic peptides to tumor specific CD8 T cells. Druggable kinases may provide the opportunity to enhance expression of MHC class I molecules on tumor cells. However, the regulation of MHC-I by kinases is largely unstudied, even though many patients with cancer are receiving therapeutic kinase inhibitors. The entire human kinome was screened using a pooled shRNA interference-based approach in a human mesothelioma cell line to uncover kinase regulators of MHC-I. Negative and positive regulators of cell surface HLA levels were discovered. A subset of highly scoring positive and negative kinase hits were subsequently validated by additional RNAi, and pharmacologic inhibitors when available. MAP2K1 (MEK), EGFR, and RET were validated as negative regulators of MHC class I expression in multiple cancer types. We mapped the pathways responsible for increased MHC class I upon kinase inhibition. Interestingly, inhibition of the MAP Kinase pathway broadly influenced expression of other components of the antigen presentation machinery. Moreover, DDR2 and MINK1 were shown

to positively regulate HLA-A*02:01. This had therapeutic relevance, as shown with a therapeutic TCR mimic antibody to a MHC/peptide complex. Druggable kinases may thus serve as immediately applicable targets for modulating immunotherapy for many diseases.

This is the first comprehensive analysis of kinase regulation of the human major histocompatibility complex class I (MHC-class I), a central component of the CD8 T cell-mediated response. Efficient antigen presentation by MHC-I molecules on cancer cells is essential for the success of immunotherapies, including vaccines, checkpoint blockade, adoptive T-cell therapy, and TCR mimic antibodies. We provide a proof of concept of two druggable targets, EGFR and MEK, but expect that these data can broadly influence translational and clinical trial design of targeted therapies combined with immunotherapy.

BIOGRAPHICAL SKETCH

Elliott began his scientific training at the University of Illinois Urbana-Champaign, where he worked in the laboratory of Dr. Chad Rienstra working on protein purification and using Solid State Nuclear Magnetic Resonance for determining protein structures. This experience allowed Elliott to gain basic laboratory skills, and further develop experimental design. After realizing his love and desire in the laboratory, but also his desire to address more clinically relevant topics, he decided to pursue training as a physician-scientist by applying to MD/PhD programs

Elliott matriculated into the Weill Cornell/Rockefeller/Sloan-Kettering Tri-Institutional MD/PhD program. Immediately, he was fascinated by the quality and bredth of research available to him. Elliott enjoyed learning about the pathophysiology of many diseases throughout medical school, with a keen eye on oncology.

After completing his first two years of medical school at Cornell, Elliott transitioned into being a full time graduate school. Elliott joined the laboratory of Dr. David Scheinberg to work on targeting tumor antigens using antibodies, and understand regulation of the Major Histocompatability Complex I, a key molecule in the adaptive immune system recognition of intracellular antigens. The project encompasses basic science techniques in molecular biology and immunology, and also a translational aspect with the goals of developing new therapies for patients with neoplastic diseases. Elliott will return to finish his

clinical portion of medical school, which after graduating plans to continue his clinical training in residency and fellowship with and begin his career as a physician scientist.

ACKNOWLEDGEMENTS

The work presented here was only possible by the rich and collaborative environment that my mentor, Dr. David Scheinberg, has created by choosing the most talented, devoted, and enthusiastic scientists. In addition, working at Sloan-Kettering with the many collaborators has been an incredible privilege, I could not imagine a more ideal environment to train as a physician-scientist in.

The study was supported by US National Institutes of Health grant R01 CA 55349, P01 CA23766, Diversity Research Supplement for the P01CA023766, MARF, P30 CA008748, Memorial Sloan Kettering Cancer Center's (MSKCC's) Experimental Therapeutics Center and the Lymphoma Foundation and Tudor and Glades funds. I would like to thank Patrizia Mondello, Simone Alidori, Claire Oh, Tao Dao, Aaron Chang, Leonid Dubrovsky, Dmitry Pankov, Piro Lito, David Solit, Eric Pamer, Renier Brentjens, Marie Will, Amaia Lujambia, Casey Jarvis and Andrew Scott for their helpful discussions.

Lastly, I would like to thank my mentor, Dr. David Scheinberg, for being a phenomenal mentor to train with during my graduate education. Dr. Scheinberg has always taken his students consideration and career objectives with utmost importance. Without his mentorship, this body of work would not be possible. His clever insight, constant demand for improvement, and joy for research kept the project going during the best and worst of times.

Table of Contents

List of figures

List of tables

List of abbreviations

ADCC	Antibody dependent cellular cytotoxicity
ADCP	Antibody dependent cellular phagocytosis
ALL	Acute lymphoid leukemia
AML	Acute myeloid leukemia
B2M	β_2-microglobulin
BLI	Bioluminescence imaging
BM	Bone marrow
CTL	Cytotoxic T lymphocyte
E:T	Effector to target ratio
EGFR	Epidermal Growth Factor Receptor
EGFRi	EGFR inhibitor
FACS	Fluorescence activated cell sorting
HLA	Human leukocyte antigen
IP	Intra-peritoneal
Luc	Firefly luciferase
mAb	Monoclonal Antibody
MAPK	Mitogen activated protein kinase
MEK	Mitogen-activated protein kinase kinase
MEKi	MEK inhibitor
MHC-I	Major Histocompatability Complex I
MRD	Minimal residual disease
MTD	Maximum tolerated dose
NSCLC	Non small cell lung cancer
NSG	NOD.*Cg-Prkdc*^{scid} *Il2rg*^{tm1Wjl}/SzJ
PBMC	Peripheral blood monocyte
pMHC	Peptide MHC
TAP1	Transporter associated with Antigen Processing 1
TAP2	Transporter associated with Antigen Processing 2
TCR	T cell receptor
TCRm	T cell receptor mimic
TKI	Tyrosine kinase inhibitor
WT1	Wilms Tumor 1

Introduction

Major Histocompatability Complex I

Major histocompatibility class I molecules (MHC-I) are an essential target for effectors of the adaptive immune system response in infectious diseases, cancer, and autoimmunity. The major histocompatibility complex I is present in all vertebrate animals, and is expressed on the surface of all nucleated cells. The molecule, as the name suggests, is a polygenic heterodimer composed of two proteins, HLA and B2M. The first, HLA in humans with homologues found in vertebrates, is highly polymorphic with hundreds of variants. HLA is composed of three domains, the α_1, $\alpha_{2,}$ and α_3 chains. The α_1 and $\alpha_{2,}$ chains bind peptides which are presented to TCR, which specifically binds the peptide in complex with MHC-I(1). The second, B2M, is also required in the complex for stable MHC-I on the cell surface.B2M associates with the α_3 chain and deficiency prevents any MHC-I from being on the surface of cells (2).

MHC-I functions to present peptides from degraded proteins or defective ribosomal translation products(3–5). These peptides can be either foreign proteins, which are bacterial or viral in origin, or native proteins(6, 7). Proteins are degraded by the proteasome into smaller peptide fragments. These can then enter into the endoplasmic reticulum via two transporters, TAP1 or TAP2. Once in the endoplasmic reticulum, more processing occurs to generate 9-10 amino acid peptides that can bind to MHC-I(8, 9). The binding

between MHC-I, specifically the HLA portion, is highly sequence dependent, and also depends on the allele.

The peptides in complex with MHC-I are shuttled to the cell surface, where a cognate TCR present on a CD8+ T-cell can bind. This binding between the TCR and peptide/MHC complex acts as signal 1 for the T-cell to elicit killing. Many secondary signals exist to either amplify or repress the T-cell signaling which will ultimately lead to the CD8+ T-cell killing the target cell presenting peptide/MHC-I.

Immunotherapy targeting antigens presented on MHC-I

While MHC-I has long been known to play a major role in infectious disease due to the role it plays in presentation of viral and bacterial antigens, it has been more recently appreciated for the role it plays in cancer. Native proteins, when degraded, are presented on MHC-I. While most of these antigens are tolerized against centrally by the thymus, and therefore are unlikely to have a pre-existing active CD8+ T-cell against the peptide/MHC-I, some antigens have not been encountered and tolerized against and can thus serve as tumor antigens(10, 11). These have been shown to be bonafide antigens that can elicit a CD8+ mediated T-cell response, not unlike the one seen when a foreign antigen is presented on MHC-I(12). It has been appreciated that tumors, through dysregulated pathways or neo-antigens derived from non-synonymous mutations, can have high levels of these tumor antigens available for MHC-I binding(13–16).

An early recognized human tumor antigen, MAGE, was recognized to be expressed in a variety of melanomas with limited expression in normal tissue, with the exception of the testes(17). More importantly, anti-MAGE CD8+ T-cells were shown to be specific and could elicit cytolytic killing of the tumor cells expressing both MAGE and the HLA-A1 allele. This demonstrated that tumor antigens, encoded in the human genome, could serve as targets of T-cells and allow tumor-specific killing. The requirementsfor T-cell tumor killing were a sufficiently immunogenic tumor antigen, and expression of MHC-I(18). Further research demonstrated that certain parts of the MAGE protein were immunogenic, and the specific peptide could be identified and tested for CTL recognition.

MAGE was not unique, and many other tumor associated antigens encoded in the germline were recognized over the subsequent years(19).Many strategies were subsequently developed aimed at targeting tumor antigens. Vaccine therapy is one approach, utilizing the knowledge of specific peptides which are presented on the MHC-I derived from tumor associated antigens(20). Patients have been safely vaccinated for many years against TAA, but little clinical efficacy has been observed. Little correlation between T-cell response and clinical benefit has been seen(21). Many theories exist why these vaccines have failed, possible due to immunosuppressive environment in the tumor, T-cell anergy, or a limited number of antigen specific T-cells that expand after vaccine administration(22, 23).

Another strategy to overcome the limited clinical effect is administration of adoptive T-cell therapy. This strategy employs identification of a tumor antigen and in vitro expansion of T-cells specific for the tumor antigen, and then reinfusion back into the patient(24). These tumor infiltrating lymphocytes have demonstrated clinical efficacy in melanoma and other cancers. A much higher percent of tumor specific TIL was observed than what was seen with vaccine therapy(25).

Other strategies utilizing TCR based therapy include using retrovirally encoded TCR, which can be cloned from tumor antigen reactive T-cells. This allows peripheral blood lymphocytes to be specifically trained to kill tumor specific antigens. T-cells can be harvested from patients, retrovirally transduced with tumor antigen specific TCR encoded retrovirus, expanded, and reinfused back into patients. The advantage of this approach is that it does not require the patient to have a pre-existing tumor reactive T-cell population. This approach has been used for multiple tumor antigens, including MART-1, WT1, GP100 tumor antigen, and others(26–28). A similar strategy using soluble TCR, fused to a anti CD3 specific scFv allows for bulk nonspecific T-cells to be redirected toward specific tumor antigen expressing cells (29).

Finally, another immunotherapy strategy that depends on tumor antigen presentation is T-cell checkpoint blockade. In normal conditions, co-stimulatory and inhibitory signals are expressed on cells presented antigens to T-cells. Expression of both co-stimulatory and immune checkpoint blockade is

necessary to prevent autoimmunity and protect tissue from non-specific killing during infection.

One of the first described immune checkpoint receptors was CTLA4. Expression of CTLA4 on the T-cell can lead to decreased T-cell activation through inhibitory signaling and outcompeting activating CD28(30, 31). Loss of CTLA4 using knockout mouse models showed lethal autoimmunity(32). Despite the lethal autoimmunity, it was demonstrated that therapeutic blockade could be safely administered and showed anti-tumor activity(33). This paved the way for clinical trials on CTLA4 blocking antibodies ipilibumab and tremelimumab in melanoma. Ipilibumab fared better in trials, demonstrating survival benefit in metastatic melanoma, which was long term beyond two years (18%). Interestingly enough, doses of ipilibumab were given over a short course of 3 months, yet a long term benefit was observed. This led to FDA approval of ipilibumab(34).

Another major checkpoint blockade therapy utilizes the PD1/PD-L1 axis. PD-1 limits the activity of T-cells during inflammation to decrease autoimmunity associated with chronic T-cell activation(35). More recently, this has been observed as a major mechanism of immune escape by tumors co-opting this pathway as well(36). PD1 engages with the ligands PD-L1 and PD-L2, which are upregulated on tumor cells, to trigger inhibition of kinases necessary for T-cell activation(37). Mouse models demonstrated anti-tumor activity upon blockade of PD1 and/or PD-L1/L2(38). Interestingly, the knockout mouse models of PD-1 or PD-L1/L2 showed milder phenotypes than what was

observed when the gene encoding CTLA4 was knocked out, indicating a potentially better therapeutic window. Clinical trials were subsequently performed using human mAbs blocking PD-1 and PD-L1 in various cancers such as melanoma, NSCLC, and others with high response rates greater than 20% of patients observed for melanoma and NSCLC(39).

One advantage of targeting tumor antigens on MHC-I is that it opens an entirely new potential to target undruggable targets, such as transcription factors, or other proteins which may be difficult to inhibit with small molecule inhibitors. Work in our group demonstrated druggability of the oncogene WT1, a transcription factor essential for many leukemias and some solid tumors (40, 41). Previous work from our lab and others identifying WT1, a tumor antigen with limited expression in normal tissue and overexpression in broad types of cancers, as an excellent target undruggable by small molecule inhibitors. It was ranked as the number one target by an independent panel at the NIH (42).

WT1 was shown to be immunogenic by using peptide epitopes derived from the protein sequence that bound to HLA-A*02. In particular, one 9mer peptide, RMFPNAPYL, was identified to bind well and elicit CTL responses in vitro (43). In vivo tumor immunity in mice was observed with the WT1 peptide vaccine against WT1+ tumors, with minimal toxicity to normal tissue(44). This paved the way for human vaccination studies to be performed with WT1+ tumors. While immune responses were observed in patients with leukemia, mesothelioma, and NSCLC, little long term benefit was seen(45, 46).

While TCR-based therapies in their various forms provide tumor specificity, there are limitations to their uses due to feasibility or lack of predictable pharmacokinetic properties. In contrast, mAb therapies are readily applicable as therapeutic agents. Recently work targeting tumor antigens has utilized development of TCR mimic antibodies as a strategy to target tumor antigens presented on MHC-I (47). These TCRm antibodies target a specific tumor antigen in the context of HLA, similar to how a TCR on a CD8+ T-cell would target an antigen. The advantage of TCRm is the scalability, predictable pharmacokinetics, and ability to increase potency by use of BiTE or CAR-T cell based methods. TCRm have shown both in vitro and in vivo activity against human tumors expressing a variety of antigens, including WT1 (48–50). The activity is highly dependent on the level of antigen presentation and expression of MHC-I, given that it interacts with this complex of peptide/MHC-I. Work in this thesis will show the feasibility of using the TCRm ESKM as a mAb therapy for various cancers, and work into its development as a potent and specific mAb. In particular, we demonstrate the potential to combine ESKM with other therapies, such as TKIs in ALL or with MEKi and EGFRi in mesothelioma.

Downregulation of MHC-I as a mechanism of immune escape

In order to subvert the immune system, downregulation of MHC-I is often observed in broad tumor types. Given that antigens in complex with

MHC-I serve as the activation signal to T-cells, there exists a strong selective pressure by tumor cells to avoid the immune system by downregulation of these stimulatory signals, while upregulating inhibitory signals for T-cells(51–53). In some cancers, such as Hodgkin's lymphoma, a high rate of loss of MHC-I through alterations of B2M(54). Mutations have also been observed in the HLA-A, B, and C genes in pan-cancer analyses that may lead to ineffective CD8+ T cell engagement or proper antigen binding (55). Some data has shown that decreased MHC-I is associated with increased NK cell killing, but this is usually not sufficient to lead to tumor elimination (56, 57).

While specific immunotherapies for cancer directed to MHC-I presentation of neoantigens, (such as checkpoint inhibition, vaccines, adoptive TCR cells and TCR mimic antibodies) continue to expand as effective therapeutic strategies, there is limited understanding of readily druggable pathways underlying the control of presentation of tumor antigens and MHC molecules. The most well understood and used pharmacologic agent for increasing MHC-I expression is the cytokine IFN-gamma. IFN is a type II interferon that is secreted by lymphocytes. IFN-gamma binds to the IFN-gamma receptor, whereby it triggers downstream signaling via the JAK-STAT pathway. Many different pathways are affected by IFN-gamma, in particular the HLA locus, TAP1, TAP2, and B2M are induced by IFN-gamma(58–60). JAK phosphorylates STAT1 at Y701 and S727, which are important for transcriptional activation of target genes by STAT1(61). Once in the active form, STAT1 translocates to the nucleus whereby it can act on target genes.

IFN-γ induces expression of MHC-I components by targeting the conserved enhancer A, IFN stimulated response element, and SXY sites(62). Binding sites for transcription factors NF-κB and IRF are located in the enhancer A and ISRE sites(63, 64).In addition, components of the immunoproteasome are also induced by IFN-gamma, an inducible proteasome with a different preference of substrates based on amino acid sequence(65). All of these in concert lead to a drastic upregulation of MHC-I on the surface of cells.

One would simply suggest that IFN-gamma is an ideal candidate for immunotherapy, and should be useful alone to increase tumor antigen presentation on MHC-I. Despite this, it has proven to be ineffective as a therapeutic agent in multiple cancer types(66). One possibility is that IFN-γ is a known upregulation of PD-L1 and PD-L2 on cells, and may limit T-cell activity(67). In addition, systemic high doses of IFN-γ required for anti-tumor efficacy are associated with severe toxicity(68).

Rationale for current work

With the plethora of targeted therapies and immunomodulating therapies present, it would be ideal to predict and study which rational combinations will work best. Targeting tumor antigens with immunotherapies is difficult because of rare cell surface presentation of individual tumor antigens. Hence, the regulation of this process pharmacologically might have important applications.

Kinases are involved in most aspects of cellular functions. We hypothesized that gene products involved in surface MHC-I expression could be identified by screening a custom library of shRNAs targeting the human kinome and using binding of specific antibodies to MHC-I as a readout. We surmised that by picking kinase therapies that could target oncogenic pathways, in addition to increasing antigen presentation in combination with an immunotherapy dependent on antigen presentation we could yield beneficial combination therapy strategies which would be difficult to discover or time consuming by testing in vivo combinations or clinical trials.A genome wide RNAi screen was performed on MHC-II surface expression by another group and successfully discovered novel regulators(69). Multiple kinases altering HLA-A expression in a human mesothelioma cell line were identified. Preliminary hits have been validated with other genetic means and pharmacologically. Several have been confirmed in other cancer cell lines. Previously described and novel gene products were discovered. One of the validated kinases was MAP2K1, also known as MEK. This kinase acts as a negative regulator of surface HLA-A and thus, inhibition led to increased surface expression of HLA-A. We were able to phenocopy the effect of the RNAi against MEK using a specific MEK inhibitor. The addition of a MEK inhibitor increased the cytotoxic efficacy of a monoclonal antibody against the MHC on the human mesothelioma cell line in vitro. Utilizing loss and gain of function screens, the discovery of regulators of MHC-I may have broad implications for pharmacologic intervention in multiple diseases in which

pathophysiology or therapy is dependent on MHC and antigen presentation. This includes TCR mimic antibody therapies, infectious diseases, vaccine therapy, TCR engineered T cell therapy, bone marrow transplantation, donor leukocyte infusions, and autoimmune disease.

CHAPTER I: UTILIZING POOLED shRNA SCREENS TO DISCOVER NOVEL REGULATORS OF SURFACE MHC-I EXPRESSION

INTRODUCTION

The use of RNA interference (RNAi) for loss of function experiments is powerful and reliable technique to demonstrate the involvement of a gene in a pathway. In particular, use of shRNA has allowed for sustained knockdown and observation of phenotype. RNAi works by targeting the mRNA of a gene by using complementary RNA to yield a hybrid double stranded RNA molecule. The target gene mRNA is destroyed by the host cell RNA induced silencing complex (RISC)(70). This technique has been validated as a rapid and effective way of performing loss of function screens(71).

The advantage of using shRNA for silencing genes is that a shRNA hairpin can be designed to knock down a given gene and then can be stably incorporated into the genome using either retroviral or lentiviral methods. This allows for cells to be transduced with a given shRNA construct and selected for cells that have stable knock down of a given gene for evaluation of phenotypic differences. We employed the use of a pooled shRNA screen, whereby a population of cells is transduced with a library of shRNA targeting hundreds of genes. Gene products causing an increase or decrease in surface HLA-A can then be selected using fluorescence activated cell sorting for cells with high or low surface HLA-A using an HLA-A specific, fluorophore tagged mAb. Once the cells are isolated, gDNA can be extracted from cells and then

a PCR can be performed for the shRNA barcode present in the cells. The PCR product is then subjected to massively paralleled sequencing, where the abundance and identity of each shRNA for a given population is determined.

We decided to target the human kinome, which represents a set of genes involved in many different regulation pathways, has many tools to evaluate the state of a given pathway using western blot techniques, and is readily druggable with many small molecule inhibitors available for use(72, 73). The mir30 based shRNA platform was utilized for creation of a kinome library. The mir30 based shRNA has been utilized before for pooled shRNA screens to yield druggable targets of leukemia (74). We utilized the TRMPV shRNA construct, which allows for tetracycline inducible knockdown, coupled with the dsRed fluorophore to track shRNA expression(75). The construct also includes the Venus fluorophore and NeoR cassette for selection of cells which were successfully transduced (Figure 1.1). We applied this system to screen for regulators of surface HLA-A in the JMN human mesothelioma cell line, stably expressing the rt-TA3 gene.

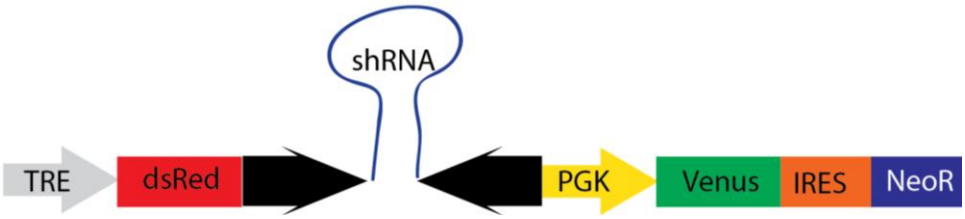

Figure1.1. A TRMPV inducible shRNA retroviral vector was used for transducing JMN (HLA-A*02:01 positive human mesothelioma line). TRE is the Tet responsive element, which drives expression of the fluorophore dsRed and the shRNA hairpin. The constitutive PGK promoter drives the Venus fluorophore along with Neomycin resistance cassette.

MATERIALS AND METHODS

Cell lines and culture conditions: After informed consent on Memorial Sloan-Kettering Cancer Center (MSK) Institutional Review Board–approved protocols, PBMCs from HLA-typed healthy donors and patients were obtained by Ficoll density centrifugation. The sources for obtaining human mesothelioma cell lines are described previously(50). Cell lines were maintained in RPMI supplemented with 10% FBS and 2 mM L-glutamine unless otherwise mentioned. HEK293T were grown in Dulbecco's modified media with 10% FBS and 2 mM L-glutamine. Cells were checked regularly for mycoplasma.

ADCC: The HLA-A*02:01 positive mesothelioma cell line JMN transduced with either a control shRenilla (shRen) construct or shHLA-A constructwere used in the ADCC assay as the targets. Cells were stably selected using 1 mg ml^{-1} neomycin for 7 days. Once selected, the shRNA were induced with 2 ug/ml doxycycline for 96 h. ADCC was then performed. Antibodies ESKMor its isotype control hIgG1 at 3 ug/ml were incubated with target cells and fresh healthy donor PBMCs at different effector/target ratios for 6 hours, RPMI supplemented with 10% FBS. The supernatant was harvested, and the cytotoxicity was measured by a ^{51}Cr release assay (Perkin Elmer).

Retroviral transduction of vectors: JMN mesothelioma cell line was initially transduced with a vector containing the mouse ecotropic receptor, along with rt-TA3 and PuroR gene. Cells were selected with 5 ug/ml puromycin for 5

days. Retrovirus was generated from ecoptropic HEK293T (ATCC Manasses, VA USA) packaging cells by transfecting the cells with TRMPV vectors. Viral supernatant was then used to transduce JMN, and cells were selected for 7-10 d with 1 mg/ml G418 (Life Technologies)

Flow cytometry studies: Cells were induced with 2 ug/ml doxycycle for knockdown of target gene for 96 h. Cells were then analyzed by western blot of flow cytometry for HLA-A expression. BB7.2 was used for flow cytometry studies for surface HLA-A02 (Abcam). Western blot for HLA-A was performed with HLA-A specific goat polyclonal sc-23446 (Santa Cruz Biotechnology).

Pooled RNAi screening

A custom shRNA library targeting the full complement of 526 human kinases was designed using miR30-adapted DSIR predictions refined with “sensor” rules (six shRNAs per gene) and constructed by PCR-cloning a pool of oligonucleotides synthesized on 12k customized arrays (Agilent Technologies and CustomArray) as previously described (Supplementary Table 1)(75). The list of genes was obtained from KinBase Database (http://kinase.com/human/kinome/) and was manually curated. After sequence verification, 3156 shRNAs (5-6 per gene) were combined with positive control HLA-A - and negative-control Renilla targeting shRNAs at equal concentrations in one pool. JMN mesothelioma cells stably expressing the Tet-On rt-TA3 gene were used. This pool was subcloned into the TRMPV-Neo vector and transduced in triplicates into Tet-on JMN mesothelioma cancer cells using conditions that predominantly lead to a single retroviral integration

and represent each shRNA in a calculated number of at least 1,000 cells. (Figure 1.1) Transduced cells were selected for 6 days using 1 mg ml^{-1} G418 (Invitrogen); at each passage more than 30 million cells were maintained to preserve library representation throughout the experiment. After induction, T0 samples were obtained (~30 million cells per replicate (n = 3)) and cells were subsequently cultured in the presence of 2 µg ml^{-1} doxycycline to induce shRNA expression. After four days (Tf), about three million shRNA-expressing ($dsRed^{+}$/$Venus^{+}$) cells were sorted for each replicate using a FACSAriaII (BD Biosciences). DAPI negative, dsRed+/Venus+ cells were sorted by FACS into three populations of BB7 low, BB7 middle, and BB7 high binding (Figure 1). Genomic DNA from Tf samples was isolated by two rounds of phenol extraction using PhaseLock tubes (5prime) followed by isopropanol precipitation. Deep-sequencing template libraries were generated by PCR amplification of shRNA guide strands as previously described(75). Libraries were analyzed on an Illumina Genome Analyzer at a final concentration of 8 pM; 50 nucleotides of the guide strand were sequenced using a custom primer (miR30*Eco*RISeq, TAGCCCCTTGAATTCCGAGGCAGTAGGCA). Hits with lower than 100 reads from the Illumina HiSeq were eliminated because they were not above background levels.

Relative representations of each individual shRNA were determined and compared in each given sorted population. We separated hits phenotypically into negative regulators (the population one standard deviation below the

mean fluorescence intensity) or positive regulators (the population one standard deviation above the mean fluorescence intensity) of HLA-A*02:01. The ratio of the shRNA ranking between the high and low population was compared, with a high ratio indicating a putative negative regulator of surface HLA-A*02:01. The scoring criteria for a gene being a *negative* regulator of HLA-A*02:01 was based on having 2 or more shRNA constructs score in the top 5% for fold difference in relative representation between BB7 high population and BB7 low population, with other constructs scoring within 1 SD of the mean fold change. The gene products with at least two shRNA sequences in the top 5% ratio were selected for further validation by other methods. The same discovery pipeline was used for identifying *positive* regulators of HLA-A*02:01.

For validation, the LT3GEPIR shRNA vector was used(76). Cells were transduced and selected with puromycin, then induced with 2 ug/ml doxycycline for 96 h before evaluating levels of either BB7, W6/32 or ESK, by flow cytometry.

RESULTS

The human mesothelioma cell line was profiled using the IMPACT platform for any mutations or copy number changes in known oncogenes and tumor suppressors, in addition to components of MHC-I. No mutation or loss/gain of copy number was observed in HLA-A or B2M (Table 1.1 and 1.2)

Table 1.1. MSK Memorial Hospital IMPACT genomic sequencing data for the JMN human mesothelioma cell line. Non-synonymous mutations in JMN using the IMPACT-410 platform.

Gene	Protein	Type	Allele freq	Copy #
TP53	***G245S***	**Missense**	1	Diploid
BRCA2	***E2258K***	**Missense**	0.65	Diploid
NF2	***D511Afs*2***	**Frameshift**	1	Diploid
ZFHX3	***R3381_Q3387del***	**Deletion**	0.12	Diploid
ARID1B	***P450dup***	**Insertion**	0.58	Diploid
ARID2	***Y92Vfs*19***	**Frameshift**	0.93	Diploid
ATM	***C117Y***	**Missense**	0.21	Diploid
EGFR	***K728N***	**Missense**	0.16	Diploid
EPHA7	***R529****	**Nonsense**	0.28	Diploid
ERBB3	***H1085L***	**Missense**	0.61	Diploid
ERCC3	***E48D***	**Missense**	1	Diploid
FANCA	***H1417D***	**Missense**	0.63	Diploid
FLT3	***L689****	**Frameshift**	0.53	Diploid
GRIN2A	***V967L***	**Missense**	1	Diploid
KDM5C	***K363N***	**Missense**	0.32	Diploid
NSD1	***V1394I***	**Missense**	0.24	Diploid
PALB2	***P864S***	**Missense**	1	Diploid
PBRM1	***R365C***	**Missense**	1	Diploid
POLD1	***Q411H***	**Missense**	0.25	Diploid
SPEN	***S263F***	**Missense**	0.23	Diploid
TERT	***Promoter***	**5'Flank**	0.99	Diploid
AR	***G473dup***	**Insertion**	0.11	Diploid

Table 1.2. Copy number alterations using the IMPACT-410 platform in JMN.

Gene	CNA	Cytoband
CDKN2B	**DeepDel**	9p21
CDKN2AP16INK4A	**DeepDel**	9p21
CDKN2AP14ARF	**DeepDel**	9p21

Knockdown of HLA-A*02:01 by use of an shRNA to this gene product in the TRMPV vector was tested as a positive control and caused strong knockdown by both western blot analysis and flow cytometry (Figure 1.2AB). This was also confirmed to decrease killing of ESKM in an in vitro ADCC assay (Figure 1.2C).

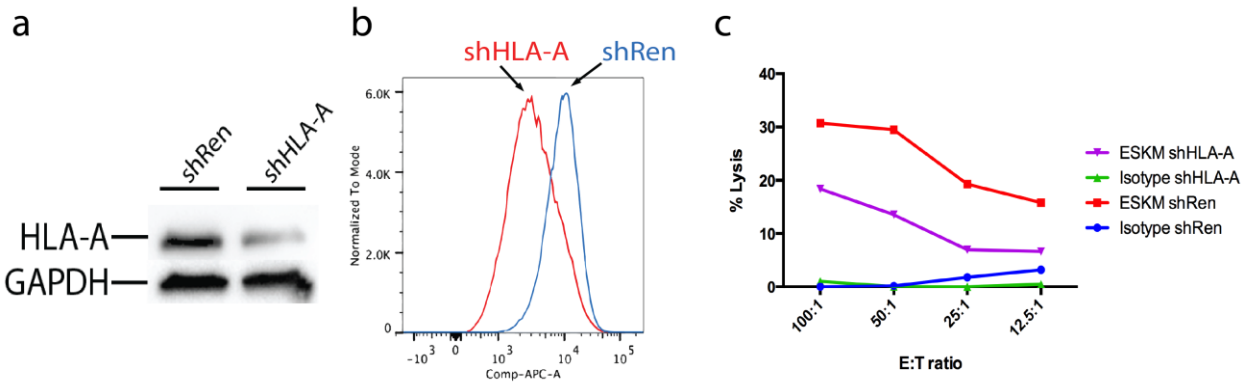

Figure 1.2. Knockdown of HLA-A with TRMPV shRNA construct. **(A)** Western blot showing knockdown of HLA-A using TRMPV retroviral system with a positive control shRNA to HLA-A02. The shRen is a negative control shRNA designed against the Renilla gene **(B)** Flow cytometry data showing knockdown of HLA-A using TRMPV retroviral system using a HLA-A specifc mAb **(C)** Knockdown of HLA-A causes resistance to antibody dependent cellular cytotoxicity by the ESK-M mAb. JMN transduced with either control shRen or shHLA-A and induced for 96 h was used for in vitro ADCC assay. Isotype or ESK-M was used as described in material and methods.

These data validated that if a phenotypic difference upon knockdown of HLA-A could be observed by flow cytometry based methods, that other gene products could be discovered in a similar manner to regulate surface HLA-A.

The JMN cell line was screened as described in the methods for shRNA against genes acting as negative or positive regulators of surface HLA-A. Cell surface HLA-A was detected by flow cytometry with the HLA-A*02:01 specific antibody BB7.2 and fluorescence activated cell sorting was used to sort populations based on HLA expression (illustrated as in Figure 1.3A). Compared to control shRen dsRed+ cells, the positive control shHLA-A showed an enrichment in the HLA-A low population of >8 fold. This similar strategy was applied to shRNA kinome transduced cells, which were sorted by HLA-A expression using FACS, and then gDNA was isolated from the HLA-A low and HLA-A high populations. The gDNA was sequenced using next generation Illumina Hiseq for the shRNA barcode, which gave the identity and relative abundance of the shRNA in each population. The top 5 hits for negative and positive regulation of HLA-A are shown(Table 1.3).

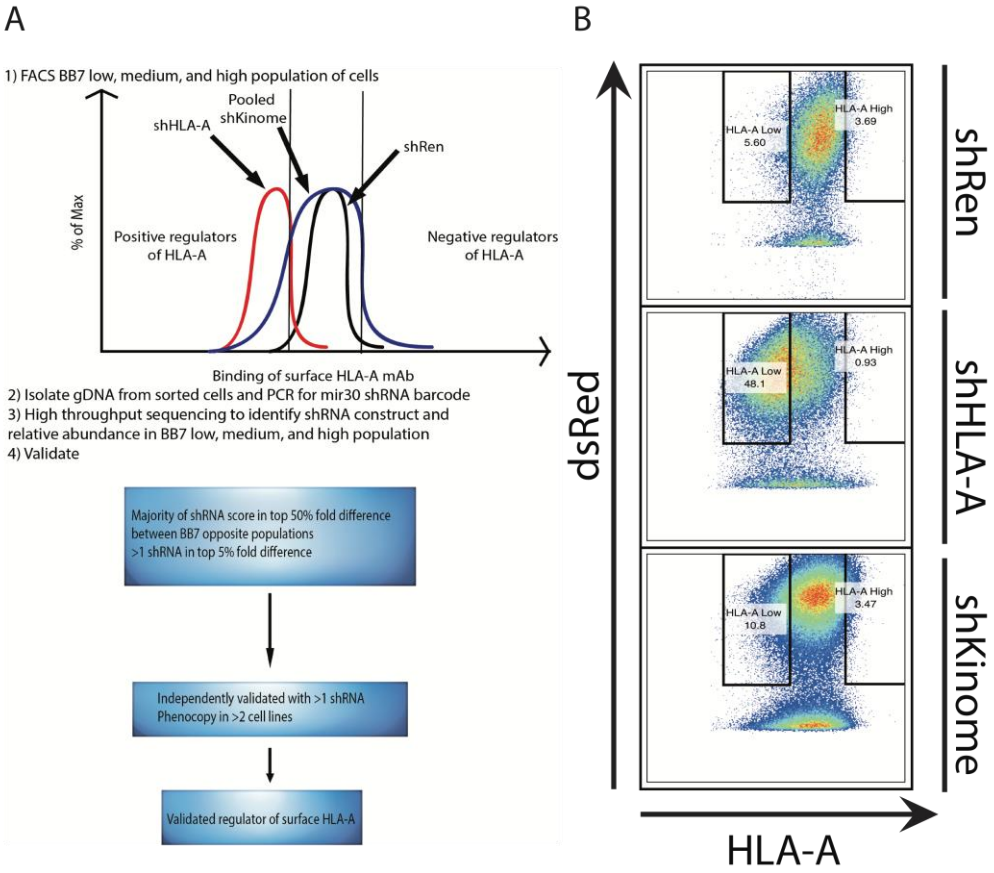

Figure 1.3. Screen for regulators of surface HLA-A. **A**. Schematic depicting outline for screen. **B.** Flow cytometry data for JMN cells transduced with various TRMPV vectors and induced for 96 h with doxycycline. Flow cytometry was performed for dsRed+ (TRMPV expressing) and HLA-A expression.

Table 1.3. Top 5 negative regulatory and top 5 positive regulatory kinase genes that were hits from the screen for regulating surface HLA-A expression. Bold genes have been validated. The percentile ranking of the top 5% of shRNA constructs for each gene listed is shown out of 3168 constructs tested.

Genes	GeneID	Percentile Rank of top shRNA	Validated
GRK7	131890	99.8%, 98.7%	Yes
MAP2K1	5604	99.7%, 98.1%, 95.1%	Yes
EGFR	1956	99.5%, 95.3%	Yes
RET	5979	99.3%, 95.8%	Yes
BRSK1	84446	99.3%, 97.3%	Yes
DAPK3	1613	0.22%, 1.1%	No
DDR2	4921	0.28%, 2.8%	Yes
CDK7	1022	0.41%, 3.3%	Yes
MINK1	50488	0.47%, 2.1%	Yes
MAPK3	5595	0.51%, 4.9%	No

The relative representation of the MAP2K1 and EGFR shRNA constructs that were present in the shRNA library showed an enrichment in the population of sorted cells with high levels of HLA-A02 (Figure 1.4).

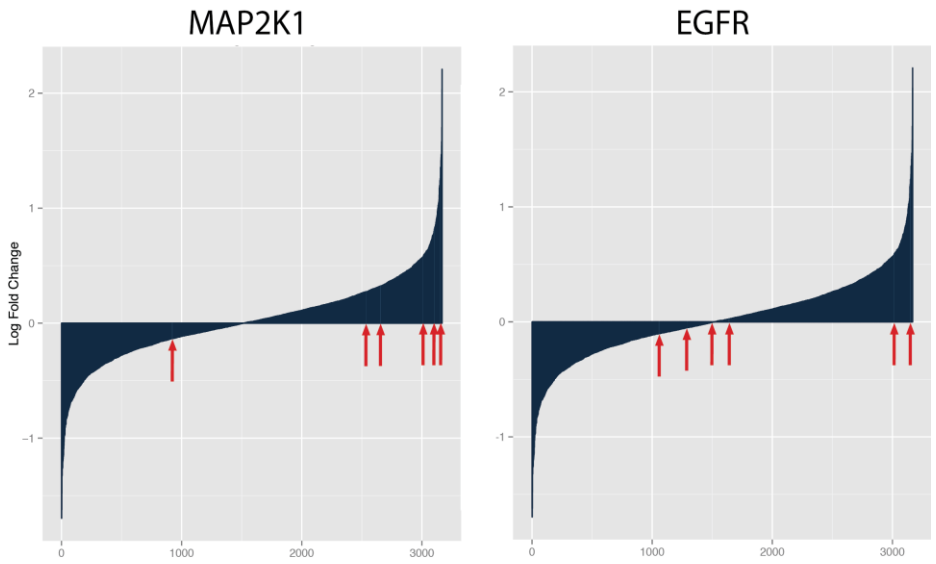

Figure 1.4. Waterfall plot showing distribution of shRNA constructs against MAP2K1 and EGFR as log fold difference between BB7 high sorted population and BB7 low sorted population.

Validation was performed for the hits using the LT3GEPIR shRNA construct, which allows for an all in one inducible shRNA knockdown of the target gene. Data are shown for the validation of MAP2K1 and EGFR in the JMN human mesothelioma cell line. Validation was performed on an additional mesothelioma cell line, Meso34, and other mesothelioma cell lines which are HLA-A02 as well. The validation data confirmed that MAP2K1, also known as MEK, negatively regulates HLA-A, and inhibition leads to increased surface HLA-A and also HLA-ABC.

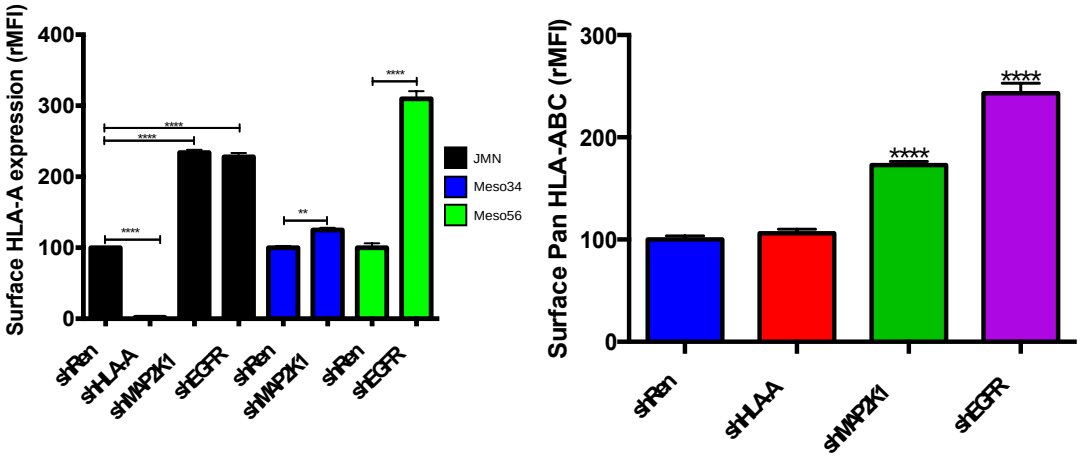

Figure 1.5. A. shRNA knockdown of MAP2K1 and EGFR in JMN cells validates them as a negative regulator of surface HLA-A. BB7.2 is a mAb specific for HLA-A02. shRNA against Renilla was used as a negative control, while an shRNA against HLA-A was used as a positive control. Validation was also shown for the Meso34 and Meso56 cell line. Student's t-test was done to compare each shRNA gene knockdown MFI to the shRen control. (*≤0.05, **≤0.01, ***≤0.001, ****≤0.0001) B. shRNA knockdown of MAP2K1 and EGFR in JMN cells shows increased pan surface MHC-I (HLA-A, HLA-B, HLA-C).

As a proof of concept, two positive regulators of surface HLA-A in JMN were chosen, DDR2 and MINK1, to demonstrate the ability of the screen to also detect positive regulators. Knockdown of DDR2 and MINK1 led to decreased surface HLA-A in JMN, and was validated in other cell lines as well.

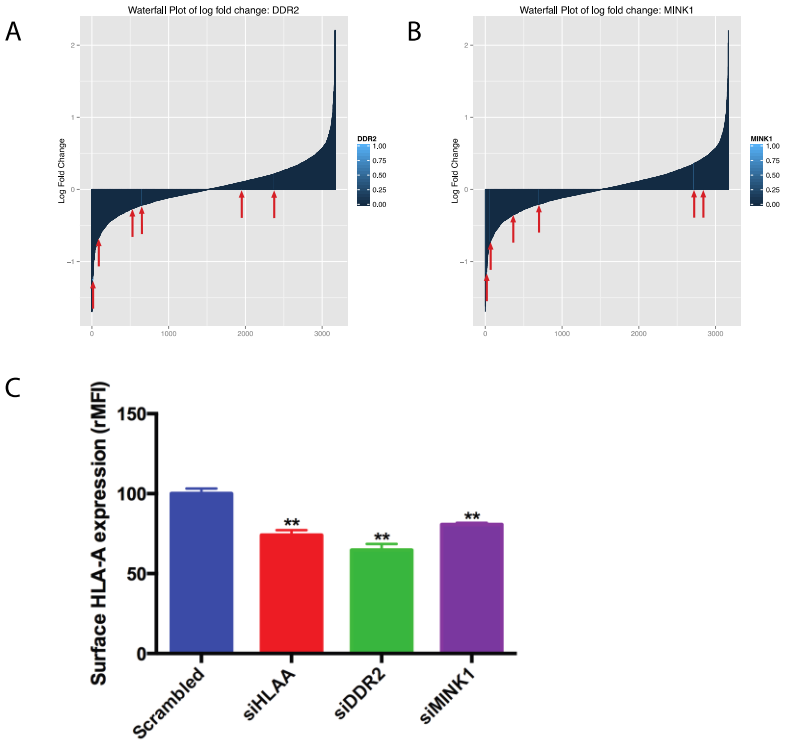

Figure 1.6.DDR2 and MINK1 acts as positive regulators of surface HLA-A. A. Waterfall plot showing fold difference between BB7 high and low sorted population and distribution of shRNA constructs against DDR2. B. Waterfall plot showing fold difference between BB7 high and low sorted population and distribution of shRNA constructs against MINK1. C. DDR2 and MINK1 knockdown decreases surface HLA-A expression in JMN. Cells were transfected with siRNA against either a scrambled siRNA, an siRNA against HLA-A, or an siRNA against DDR2 or MINK1. After 96 hours, flow cytometry was performed as previously described. Statistical significance was compared to scrambled siRNA using unpaired student T-test on triplicate samples.

DISCUSSION

The validation of MAP2K1 and EGFR as regulators of surface HLA-A and also MHC-I using shRNA mediated knockdown of both genes allowed for further investigation into the pathways governing surface MHC-I regulation and whether they could be manipulated by specific inhibitors. Activation of kinase signaling is a common occurrence in cancers, and many mutations present in cancer activate kinase signaling (77, 78). The validated targets which regulate MHC-I in mesothelioma, and also validated in other cell lines provide an interesting opportunity to target a pathway not only essential for proliferation of tumor cells, but also to increase immunogenicity of tumor cells as well, providing fertile ground for combination drug strategies.

Two of the identified regulators of MHC-I, EGFR and MAP2K1 or MEK1, both signal in the mitogen activated kinase pathway (79)(MAPK). The MAPK pathway is involved in cellular proliferation, differentiation, and transformation, and is highly conserved throughout eukaryotes. The MAPK pathway consists of extracellular growth factor regulated kinases (ERK), or stress regulated kinases. ERK1/2 is generally regulated by receptor tyrosine kinase stimulation, whereas the ERK5, c-Jun kinase JNK, and p38 kinases are regulated by stress response and growth factor stimulation (78).

The ERK1/2 MAPK pathway is involved in signaling when upstream cell surface receptor tyrosine kinases, such as EGFR, bind their respective growth factor, such as EGF. This causes the receptor to signal downstream to

cytoplasmic Ras, a guanine nucleotide binding protein(80). Ras then signals downstream to Raf, a serine/threonine kinase in the MAPK signaling cascade. Raf then signals to MEK, another serine/threonine kinase (81). MEK will then signal downstream to ERK1/2, which has numerous substrates such as transcription factors, and other kinases.

EGFR and MEK both signal to the MAPK pathway whereby active signaling through the MAPK pathway leads to down regulation of MHC-I. Knockdown of kinases in the MAPK pathway at the level of EGFR or MEK. Given that both EGFR and MEK have specific small molecule inhibitors which can be used to inhibit their kinase activity, we decided to investigate pharmacologic inhibition as a means of up regulation MHC-I.

Chapter 2: The MAPK pathway regulates MHC-I and antigen presentation in cancer cells

INTRODUCTION

Targeted therapy for treatment of cancer has expanded largely since it was first demonstrated to be effective for treatment of acute promyelocytic leukemia(82). Targeted therapy is based on looking for aberrant pathways activated in tumor cells which are absent or minimally present in normal tissue. Characterization of the molecular pathways cancer is dependent on has led to numerous FDA approved therapies that can now be utilized for targeting specific pathways activated in cancer.

After discovering the pathways underlying neoplasia and oncogenesis, kinases were shown to play crucial roles in sustained signaling necessary for transformation. Examples of kinase pathways contributing to oncogenesis include the MAPK pathway, which integrates growth signaling necessary for sustained proliferation and avoidance of apoptosis, or the PI3K pathway which is necessary for protein synthesis, metabolism, survival, and transcription of genes. Experiments showed that cancer cells were addicted to signaling through these pathways, which led to the development of small molecule inhibitors of kinases within oncogenic pathways.

One of the most successful early examples of this was the use of imatinib, a kinase inhibitor of Abl in BCR-Abl translocated chronic myelogenous leukemia. Since the translocation is only present in transformed leukemia cells, and the leukemia is dependent on signaling through BCR-Abl

for growth and proliferation, this was an attractive and specific therapeutic target(83). After discovering a potent and specific BCR-Abl inhibitor which demonstrated in vitro efficacy against CML, clinical trials in humans showed similar promising data, with most patients having complete responses to imatinib as a single agent(84).

These data provided the ground work for targeting kinases with aberrant signaling derived from mutations, translocations, fusion proteins, or amplifications of the kinase gene. Sequencing of large cohorts of patient derived tumors validated that many mutations are present in kinases, such as melanoma where up to 70% have BRAF mutations, or pancreatic adenocarcinoma where 95% have KRAS mutations(85, 86). Many of these pathways were necessary for oncogenic transformation and maintenance of the tumor growth, proliferation, metastasis, angiogenesis, and many other hallmarks of cancer.

The MAPK pathway had been shown to be essential in tumor growth and proliferation in many solid tumors. As such, inhibiting kinases that feed into the MAPK pathway has been demonstrated to be a viable strategy for targeted therapy in cancer. One example is in melanoma, where mutations in the kinase BRAF V600E, present in up to 40% of melanomas, have been targeted using a BRAF V600E specific inhibitor vemurafinib or dabrafenib(87, 88). This has been demonstrated in vitro, and in vivo. These tumors are highly dependent on signaling downstream of BRAF to MEK, and ERK for sustained growth and proliferation. More recently, work has shown that BRAF mutant

melanomas are exquisitely sensitive to MEK inhibition. Despite MEK being a common component in other tissues requires MAPK pathway signaling, BRAF mutant melanomas are much more sensitive to MEKi given their dependence on MAPK (89).

This work has validated that MAPK inhibition is useful in cancer therapy for targeting growth and proliferation. One understudied consequence of MAPK inhibition has been the immunologic effect of kinase inhibition. More specifically, our unbiased search led us to discover two key components of the MAPK pathway, EGFR and MEK, to regulate surface levels of MHC-I and antigen presentation. We decided to use specific small molecule inhibitors to further investigate the pathway of MAPK inhibition of surface MHC-I and how this regulation could be manipulated. Inhibition of MAPK signaling may serve as a useful therapeutic strategy not only for slowing tumor growth but also increasing immunogenicity of tumors.

MATERIALS AND METHODS

Cell lines and culture conditions: After informed consent on Memorial Sloan-Kettering Cancer Center (MSK) Institutional Review Board–approved protocols, PBMCs from HLA-typed healthy donors and patients were obtained by Ficoll density centrifugation. The sources for obtaining human mesothelioma cell lines are described previously (50). SKMEL5, PC9, and UACC257 were obtained from ATCC (Manasses, VA USA). The NSCLC cell lines were obtained from the Scott Lowe laboratory. TPC1 cell line was a kind gift from the James Fagin lab. Cell lines were maintained in RPMI supplemented with 10% FBS and 2 mM L-glutamine unless otherwise mentioned. HEK293T were grown in Dulbecco's modified media with 10% FBS and 2 mM L-glutamine. Cells were checked regularly for mycoplasma.

Small molecule inhibitor studies: Compounds were obtained from SelleckChem (Houston, TX USA). Drugs were used at sub-cytostatic doses by titration using the Cell Titer Glo assay (Promega). All drugs were used in vitro at indicated doses in 1% DMSO. Experiments were performed at least twice with similar results, and data shown are representative.

Flow cytometric studies: Cell lines were seeded in triplicate in a 6-well tissue culture plate at a density of 1E5 cells/well, and allowed to adhere overnight. The next day, cells were treated with either vehicle control (0.1% DMSO) or inhibitor at indicated concentrations. Cells were then isolated at 72 hours after inhibitor treatment, and washed with PBS. Cells were subsequently stained

with BB7.2 (HLA-A02 specific mAb) or W6/32 (HLA-ABC specific mAb). Cells were stained with propidium iodide for viability. Cells were analyzed on BD Accuri C6 flow cytometer.

Western blot analysis: Protein lysate was isolated from cultured cells using RIPA buffer with protease inhibitor (50mM Tris pH 8, 150 mM NaCl, 0.5% sodium deoxycholate, 1% NP-40). Protein quantification was performed using DC Lowry assay. Antibodies for pERK(#4370), ERK1/2 (#9102), pEGFR, EGFR (#4267), GAPDH, and B2M were obtained from Cell Signaling Technologies. Antibodies for HLA-A were obtained from Santa Cruz Technology.

Treatment with EGF ligand: Recombinant EGF was obtained from Life Technologies and cells were treated with 100 ng/ml EGF for 72 h before flow cytometric analysis of surface HLA-A (BB7.2) and surface HLA-ABC (W6/32) was performed.

Overexpression of mutant EGFR and NRAS: The pBABE retroviral vector encoding either EGFR harboring the L858R mutation was used to stably transduce H1299 cell line using HEK293T/Amphoteric cells and were selected in 2.5 ug/ml puromycin for 5 days. EGFR L858R was a gift from Matthew Meyerson (Addgene plasmid # 11012).

For overexpression of NRAS the pBABE NRAS Q61K plasmid was used to transduce H827 cells similar to described above, and selected in 2 ug/ml puromycin. pBabe N-Ras 61K was a gift from Channing Der (Addgene plasmid # 12543).

Transgenic EGFR L858R mouse model: FVB CC10-rtTA/EGFR-L858R mice were obtained as a kind gift from the Harold Varmus lab. Mice were bred in accordance with MSKCC institutional review board under protocol 96-11-044. Mice used for the experiment were heterozygous for CC10-rtTA and EGFR-L858R as detected by quantitative PCR genotyping. At 4-6 weeks of age, mice were put on doxycycline via food pellets (625 mg/kg) (Harlan-Teklad) for >6 weeks. Mice were imaged by anesthetizing under 2% isoflurane and lung field images were acquired on Bruker 4.7T Biospec scanner (Bruker Biospin Inc.) MRI in the Small animal imaging core at MSKCC. Images were analyzed with Osirix Imaging Software (Geneva, Switzerland). Once confirmed to have reticulonodular appearances and consolidations by axial and coronal MR images, consistent with previous data published on the transgenic mice (90).

Mice were sacrificed once confirmed to have lung tumors (non induced control mice were also used, which genotypically were identical but did not receive dox diet). The lungs were isolated and treated with Collagenase IV in HBSS with Ca^{2+} and Mg^{2+} for 1 h 37ºC. Cells were then collected, blocked with mouse FcR block (Miltenyi), counted, and stained with mouse CD45 (30-F11 Biolegend), human EGFR(AY13 clone Biolegend), and mouse H2-kq (KH114 clone Abcam) antibodies. Flow cytometry analysis was performed on Fortessa (BD Biosciences).

RESULTS

MAPK pathway regulation of MHC-I

EGFR an MEK both have numerous specific small molecule inhibitors, with some being FDA approved for use in various cancers(91, 92). We phenocopied the inhibition of shRNA mediated knockdown of EGFR and MEK with the small molecule inhibitors trametinib and erlotinib in a panel of mesothelioma, NSCLC, melanoma, colorectal, pancreatic, and thyroid cell lines. Interestingly, the JMN mesothelioma and PC9 NSCLC showed up regulation of surface HLA-A when treated with the EGFR inhibitor afatanib, while all had some degree of sensitivity to the MEKi trametinib (Figure 2.1A). Of note, many cell lines had known driver mutations of the MAPK pathway, such as SKMEL5 and UACC257 melanoma lines, which have BRAF V600E mutations, or SW480 colorectal carcinoma and CFPAC pancreatic adenocarcinoma cell lines which had KRAS G12V mutations. The TPC papillary thyroid cancer had the RET/PTC1 rearrangement. We further showed that this effect was valid not only for surface HLA-A, but more broadly on pan MHC-I using W6/32, a mAb specific for HLA-ABC in a selected number of cell lines (Figure 2.1B)

Not only did we demonstrate that EGFRi and MEKi leads to increased surface HLA-A, but we also used TCR mimic antibodies which bind to 9-10 amino acid epitopes derived from intracellular proteins that are presented on HLA-A02. We chose two TCR mimics established in the lab, ESKM and PRAME, which bind to peptides derived from the oncoproteins WT1 and

PRAME respectively. Using these TCRm antibodies, we demonstrated increased presentation of WT1 and PRAME derived peptide on JMN, Meso34, TPC1, and SKMEL5 (Figure 2.1C). Strong concordance was observed with the up regulation of HLA-A and the up regulation of TCRm binding.

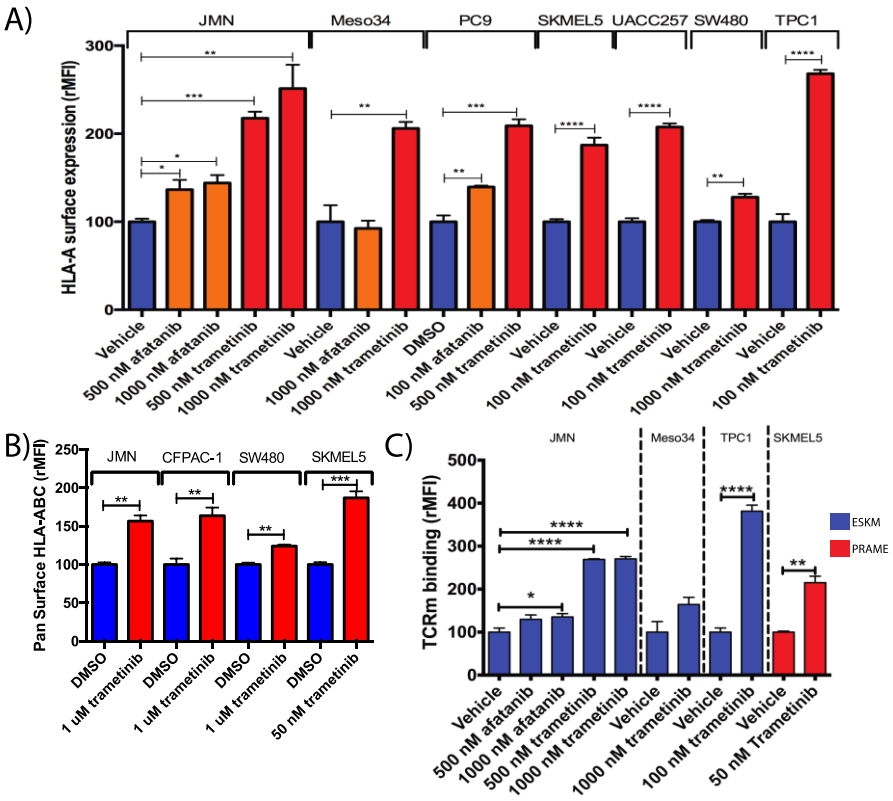

Figure 2.1. Use of selective EGFRi and MEKi, increases cell surface HLA-A expression and tumor antigen presentation **A**. MEK inhibition and EGFR inhibition for 72 h with indicated inhibitors increases HLA-A (BB7 binding) by flow cytometry in JMN, Meso34, PC-9, UACC257, SK-MEL-5, SW480, and TPC1 cell lines. 1% DMSO was used as a vehicle control.**B.** MEKi with trametinib shows increased pan surface HLA-ABC using W6/32 by flow cytometry. Experimental setup similar to 2.1A**C**. Binding of TCRm antibodies to peptide /MHC epitopes. In blue use of ESK antibody to a peptide derived from the oncoprotein WT1 that is presented on HLA-A0201. Binding increases after inhibition of EGFR and MEK for 72 h in JMN, Meso34, and TPC1. In red PRAME is a TCRm antibody against an epitope of PRAME tumor antigen presented on HLA-A0201 on SKMEL5. Experimental setup was similar to A.

We next wanted to explore how the MAPK pathway controlled surface HLA-A and MHC-I expression. While inhibition on the MAPK pathway either at the level of EGFR or MEK lead to increased surface HLA-A and MHC-I, we wanted to see if stimulating the pathway would lead to decreased HLA-A and MHC-I. We exposed JMN to EGF, in order to further stimulate the EGFR. A decrease on surface HLA-A and MHC-I was observed, consistent with higher MAPK activity leading to lower MHC-I (Figure 2.2).

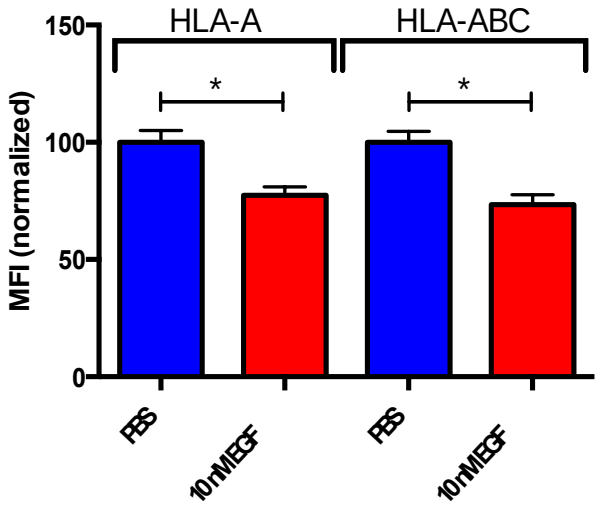

Figure 2.2 Treatment of JMN with 10 nM EGF for 72 h, causing activation of the downstream MAPK pathway, leads to decreased surface HLA-A and total HLA-ABC.

In order to further evaluate the effects of EGFRi and MEKi on surface MHC-I, we turned to a panel of well genotypically and phenotypically defined NSCLC cell lines. H827 contains the activating EGFR ELREA746 deletion, H1975 contains a combined EGFR L858R and gatekeeper T790M mutation, rendering it resistance to first generation TKI such as erlotinib and gefitinib. H1299 contains an activating NRAS Q61K mutation, and is insensitive to EGFRi. A549 contains an activating KRAS G12S mutation, also rendering it insensitive to EGFRi. The up regulation of MHC-I was dependent on the response downstream of EGFR for the two sensitive cell lines, as measured by pEGFR and pERK, in H827 and H1975. H1975 was resistant to the effects of erlotinib, a first generation TKI which resistance has been demonstrated before due to the gatekeeper T790M mutation(93), but sensitive to newer second and third generation TKI(94). H1299 and A549 were resistant to EGFRi mediated up regulation of MHC-I, and did not show a decrease in pERK on treatment with erlotinib or afatanib but did respond to MEKi with trametinib (Figure 2.3). These results show that genotype of the tumors can predict response to MHC-I up regulation based on MAPK inhibition.

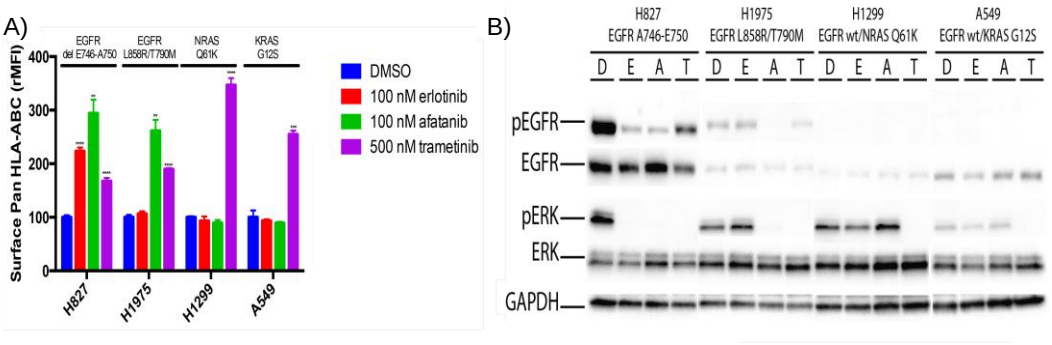

Figure 2.3A. UseofEGFRierlotinibandafatanib, alongwithMEKitrametinibonH827 (EGFRE746del-A750 mutation), H1975 (L858R/T790M), H1299 (EGFRwt, NRASQ61K), andA549 (EGFRwt/KRASG12S) toaltersurfaceHLA-ABClevels. Student'st-testwasdonetocompareeachtreatmenttovehiclecontrol. *Pvaluesannotatedasinfigure 2.1. **B.** WesternblotanalysisshowinglevelofinhibitionoftheMAPkinasepathwayonpanelofNSCLCcelllinesusing 1% DMSO (D), 100 nMerlotinib (E), 100 nMafatanib (A), or 500 nMtrametinib (T).

One interesting result was that while MEKi and EGFRi both led to a similar level of suppression of pERK activity, EGFRi had a statistically significant higher up regulation of MHC-I than MEKi in EGFR mutant cell lines. This led us to determine whether EGFR was capable of suppressing MHC-I in the presence of an already active MAPK pathway due to a downstream mutation. H1299 has an NRAS Q61K mutation, causes signaling downstream to RAF, MEK, and ERK. We ectopically expressed the constitutively active EGFR L858R mutation in H1299, leading to a phenotypically EGFR mutant/NRAS mutant cell line. When comparing the cell line to the vector alone, EGFR L858R coexpression led to further suppression of MHC-I, despite similar levels of pERK in both lines (Figure 2.4). It is possible that there are

non MAPK functions of EGFR signaling responsible for the suppression of surface MHC-I.

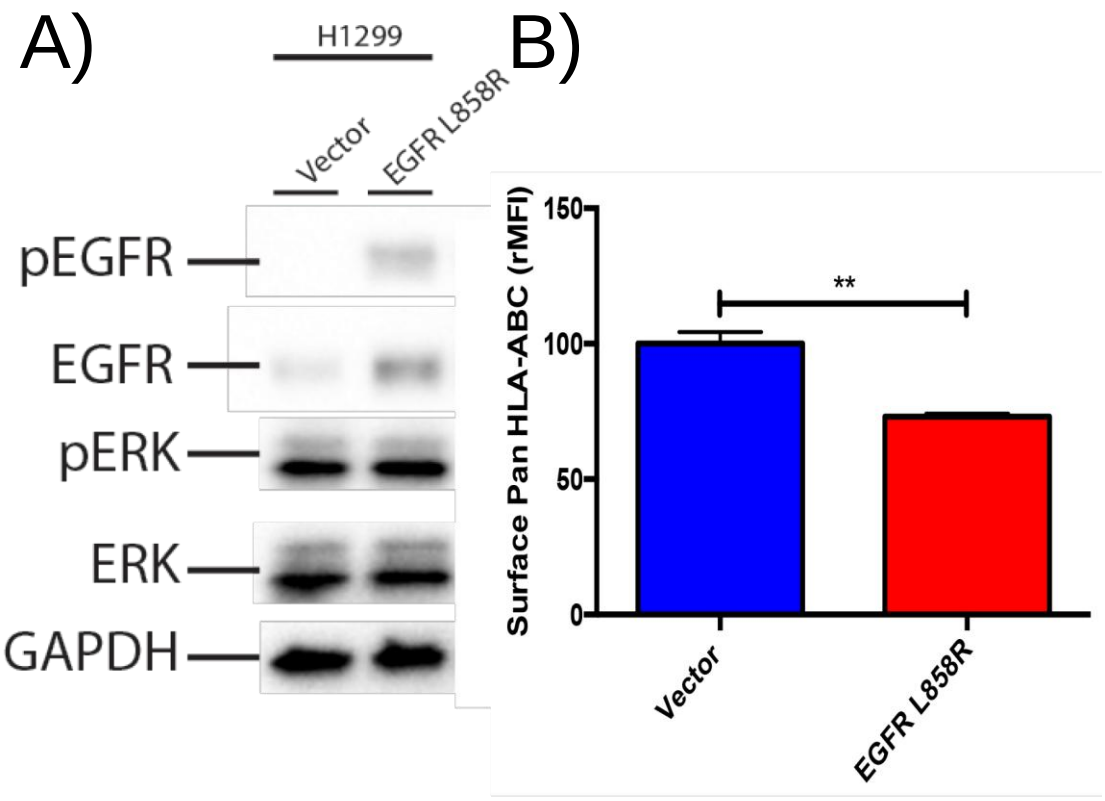

Figure 2.4. Surface MHC-I can be down regulated by constitutively active EGFR in the context downstream RAS mutations. **A.** H1299 cells were transduced with retroviral vectors expressing EGFR L858R. Western blot analysis of vector transduced versus EGFR L858R transduced cell lysate shows activated pEGFR signaling. **B.** H1299 with either vector alone or EGFR L858R expressing were analyzed for surface pan HLA-ABC using W6/32.

We further demonstrated in the H827 EGFRm cell line that EGFRi alone was able to increase MHC-I as much as when combined with MEKi, whereas the single agent MEKi alone did not cause as large of an increase (Figure 2.4A). Both MEKi, EGFRi, and the combination caused similar levels of inhibition of pERK. The H827 cell line was transduced with either vector alone or NRAS

Q61K, which has been demonstrated to be a mechanism of resistance of EGFRi (95). Despite resistance to MAPK suppression in NRAS Q61K expressing cells with EGFRi, as seen by pERK output, a change was observed in surface MHC-I expression, though lower than with MEKi (Figure2.5B).

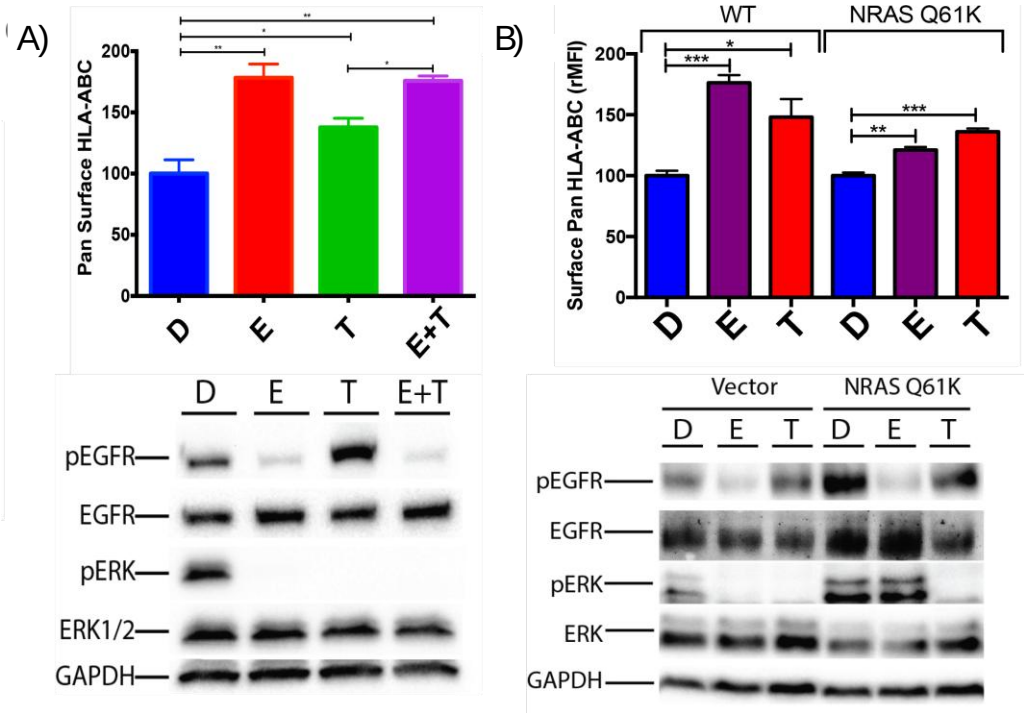

Figure 2.5.A. EGFR inhibition upregulates surface HLA-ABC greater than MEKi despite equivalent levels of inhibition of pERK output. **B.** EGFRi up-regulates MHC-I despite downstream mutations causing constitutive MAPK activation. The NRAS Q61K mutation was introduced into H827 and cells were treated with EGFRi or MEKi as done in 2.4A

We next explored mechanistically how surface MHC-I is regulated upon inhibition of the MAPK pathway. Treatment with EGFRi and MEKi in a panel of cell lines lead to increased transcript levels of the mRNA for HLA-A, along with B2M. We also assessed increase in components of the antigen presentation machinery, such as TAP1 and TAP2. We also observed increases in transcripts for these genes as well (Figure 2.6).

Figure 2.6. MEK and EGFR inhibition for 48 h leads to increased levels of HLA-A, along with TAP1, TAP2, and B2M in JMN, Meso34, SK-MEL-5 and UACC257, H827, and PC9 cell lines

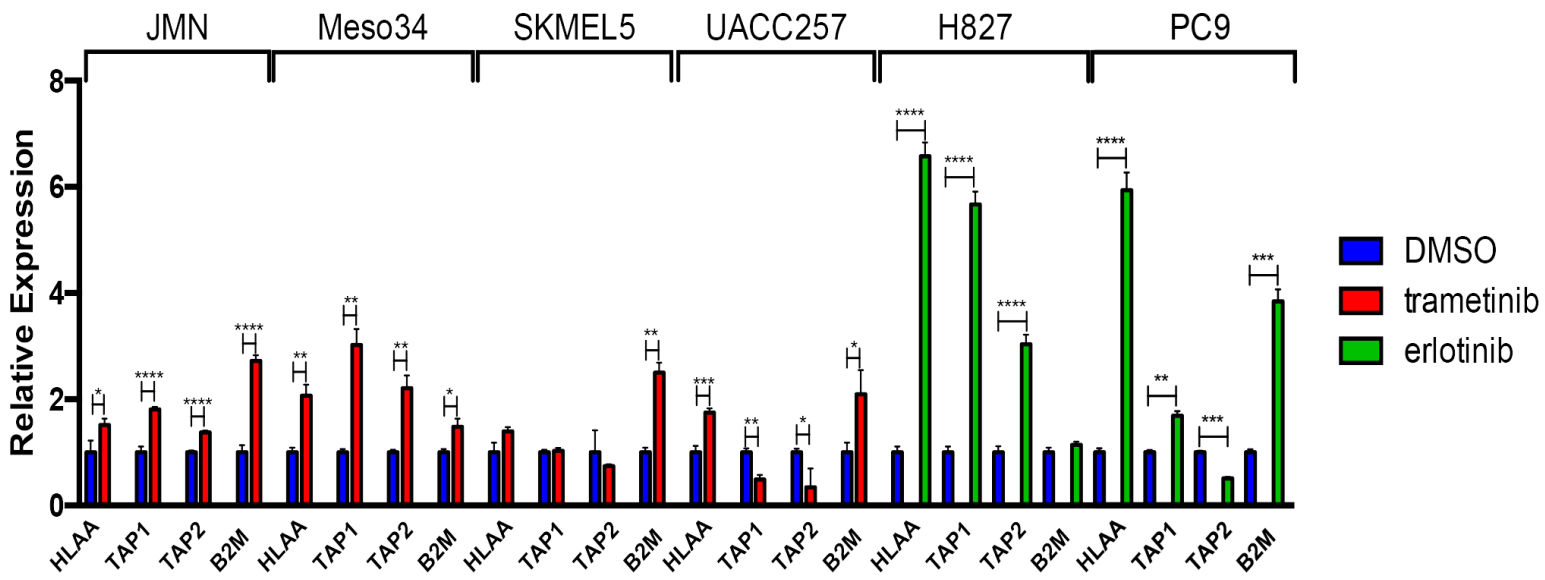
JMN
Meso34
SKMEL5
UACC257
H827
PC9
Relative Expression
0
2
4
6
8
HLAA
TAP1
TAP2
B2M
DMSO
trametinib
erlotinib

In order to demonstrate that the effect of up regulation of MHC-I was a dose dependent process, we treated JMN and SKMEL5 cell lines with increasing amounts of MEKi trametinib, and assessed pERK levels by western blot and surface HLA-A by flow cytometry. Interestingly, SKMEL5 was sensitive to the effects of trametinib at lower doses than JMN (Figure 2.7).

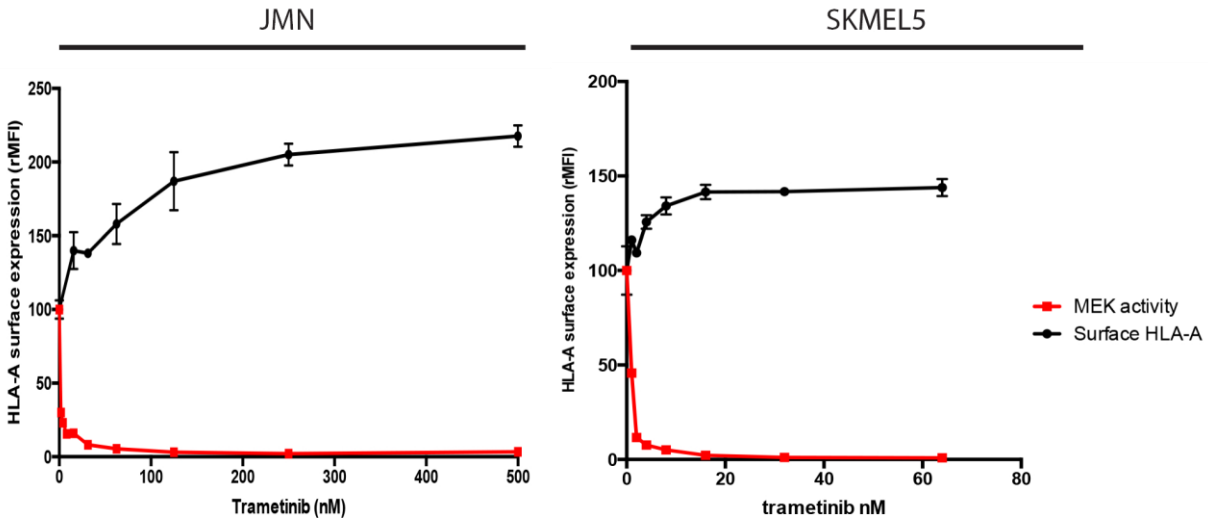

Figure 2.7. Dose dependent increase in surface HLA-A with increasing MEKi in JMN and SKMEL5. Cells were analyzed by flow cytometry at 72 h

Sensitivity to MEKi based on genotype has been previously reported that melanomas with BRAF V600E mutations are much more sensitive to MEKi than wild type BRAF cell lines, which is the case for JMN and Meso34 (89). This was likely due to feedback inhibition, as the JMN and Meso34 cell lines pERK levels were sensitive at an earlier timepoint of 1 h treatment with trametinib (Figure 2.8A), whereas later timepoints at 72 h showed rebounding of pERK (Figure 2.8B). In comparison, the melanoma BRAF V600E mutant

cell lines remained sensitive at t=72 h to MEKi with trametinib at low levels (Figure 2.7C).

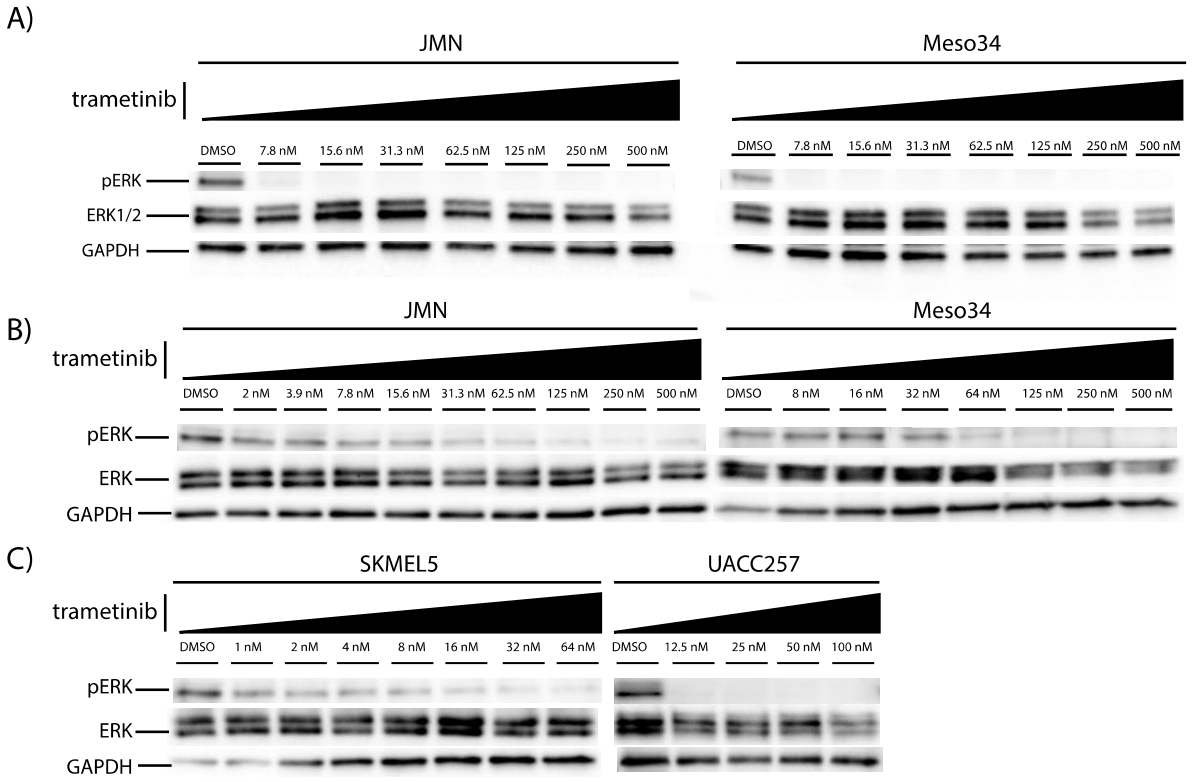

Figure 2.8. Titration of trametinib to determine optimal inhibition of MEK using pERK as a marker of inhibition. A. JMN and Meso34 were incubated with increasing doses of trametinib for 1 h and analyzed by western blot for pERK and ERK. B. Cells were incubated with trametinib for 72 h. C. SKMEL5 and UACC257 were analyzed by western blot at 72 h for pERK and ERK.

We further demonstrated that not only did transcript levels of HLA-A and B2M increase, but also protein levels in mesothelioma cell lines upon MEKi. We also confirmed a similar dose dependent pattern with EGFRi (Figure 2.9).

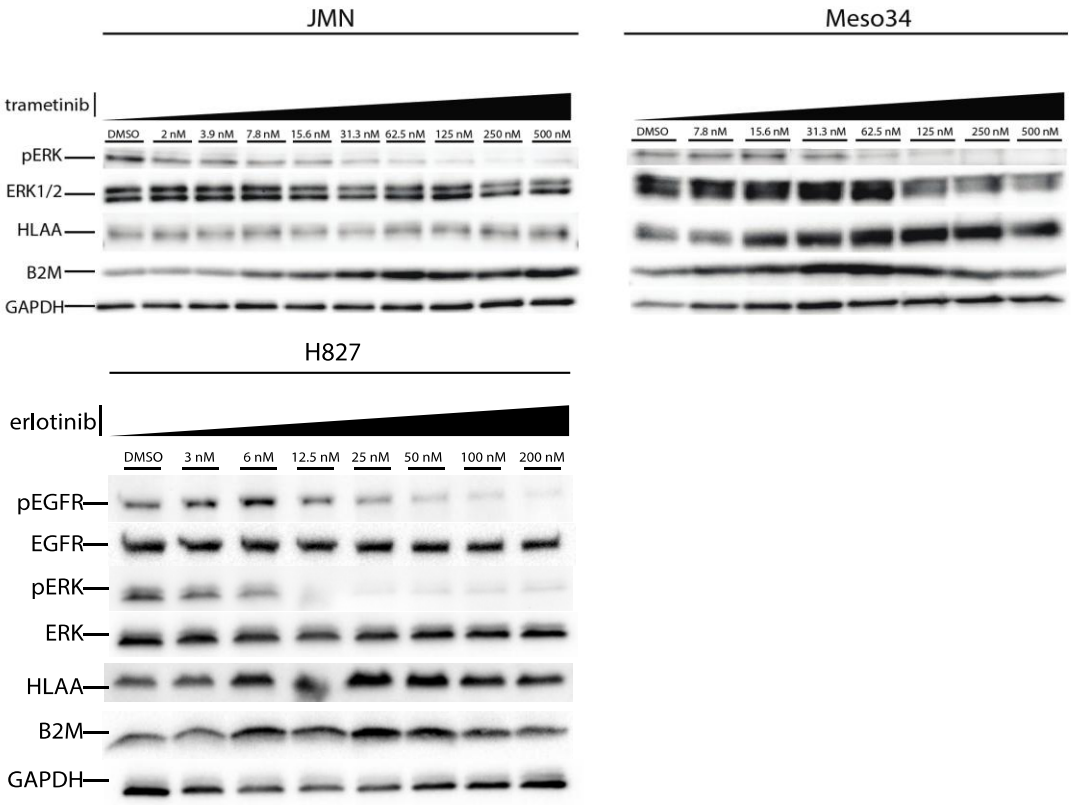

Figure 2.9. MEK inhibition or EGFR inhibition leads to increasing levels of HLA-A and B2M protein. Cells were treated with indicating amounts of trametinib (MEKi) or erlotinib (EGFRi) for 72 hours and specific antibodies against indicated proteins were blotted

One striking finding was how in some cases, transcript levels and protein levels of B2M increased drastically, while levels of HLA-A did not increase by as much or at all. We hypothesized that increased B2M may be sufficient to drive increased surface MHC-I, as it is a necessary protein that heterodimerizes with HLA to remain as a stable complex on the surface of cells. We overexpressed B2M and showed that this was sufficient to drive increased surface HLA-A and pan HLA-ABC (Figure 2.10).

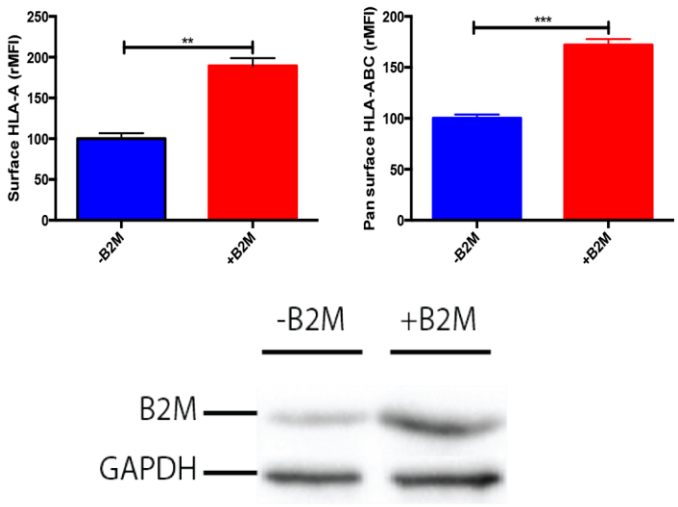

Figure 2.10. Overexpression of B2M leads to increased surface HLA-A and HLA-ABC. Western blot showing increased protein levels of B2M

We next demonstrated that upon MEKi, activity on the promoters of HLA-A and B2M increases using a luciferase promoter assay, which the HLA-A and B2M promoters were cloned upstream of the gaussian luciferase gene. IFN-gamma is a known positive regulator of HLA-A and B2M, acting via the JAK-STAT pathway, and lead to an increase in activity on both the HLA-A and B2M promoters as well (Figure 2.11)(96–99).

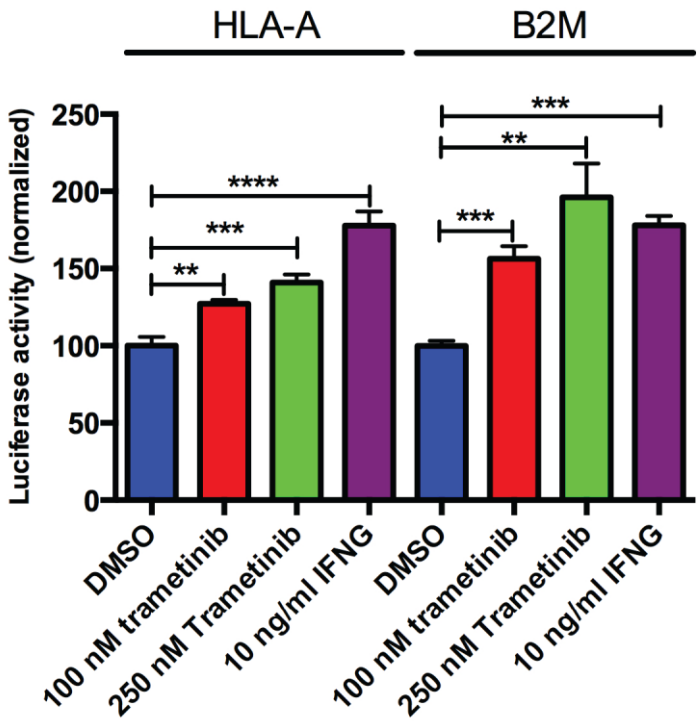

Figure 2.11. Treatment of JMN with MEKi trametinib for 72 h leads to increased activity on the HLA-A and B2M promoter. The HLA-A and B2M promoter was cloned upstream of the Gaussian Luciferase gene. SEAP under the CMV promoter was used as a normalization factor**.**

The HLA-A and B2M gene expression is regulated by multiple regulatory domains in the promoter region, including the ISRE site, E box, and NF-κB sites. Knockdown of the STAT1, STAT3, and RelA (component of NF-κB complex) were performed on JMN cells, along with treatment with MEKi. STAT1 knockdown had the largest effect in blunting up-regulation of surface HLA-A after MEKi, suggesting a role for STAT1 in response to MEKi (Figure 2.12).

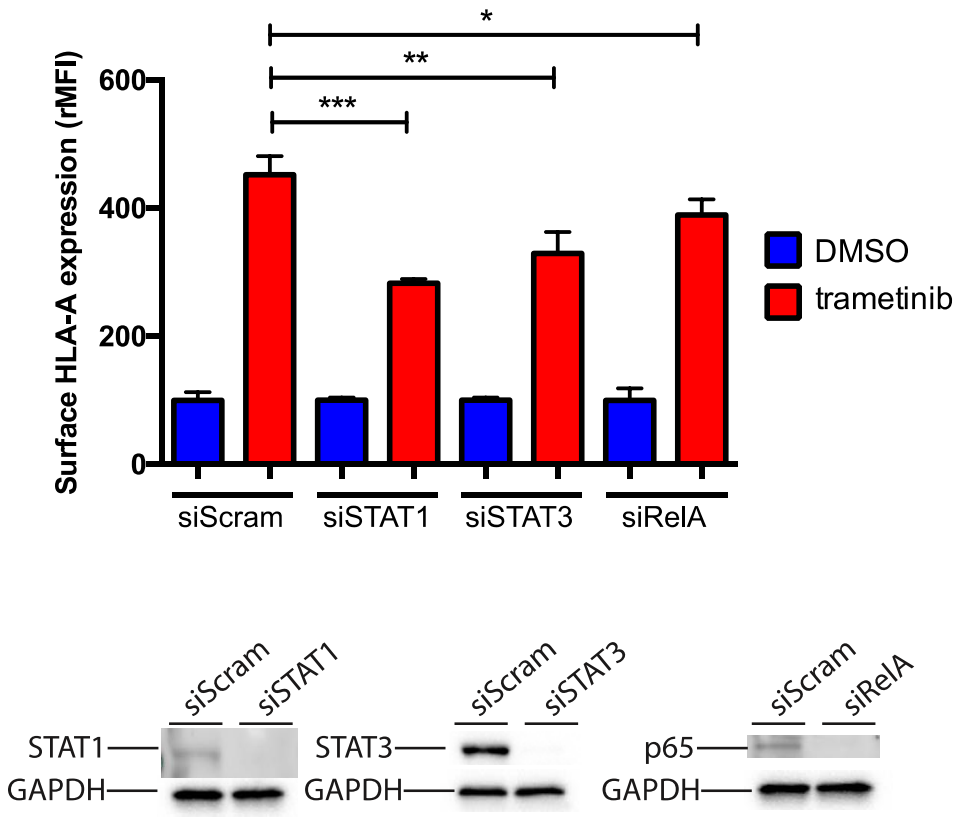

Figure 2.12. Knockdown of STAT1, on JMN cells treated with MEKi demonstrates role in mediating surface HLA-A up-regulation. JMN cells were transfected with siRNA against genes shown and treated with either DMSO or 1 uM trametinib 24 h after siRNA transfection, then assayed by flow cytometry for surface HLA-A expression 72 h after treatment.

We next wanted to see whether activation of the MAPK pathway would lead to decreased levels of MHC-I and antigen presentation components in vivo. Microarray profiling of the lung bearing tumors from transgenic EGFR L858R, which activates the MAPK pathway, compared to normal lungs, demonstrated suppression of mouse MHC-I and antigen presentation components H2-KD, and B2M, thereby confirming the effects of this pathway in vivo (100)(Figure 2.12).

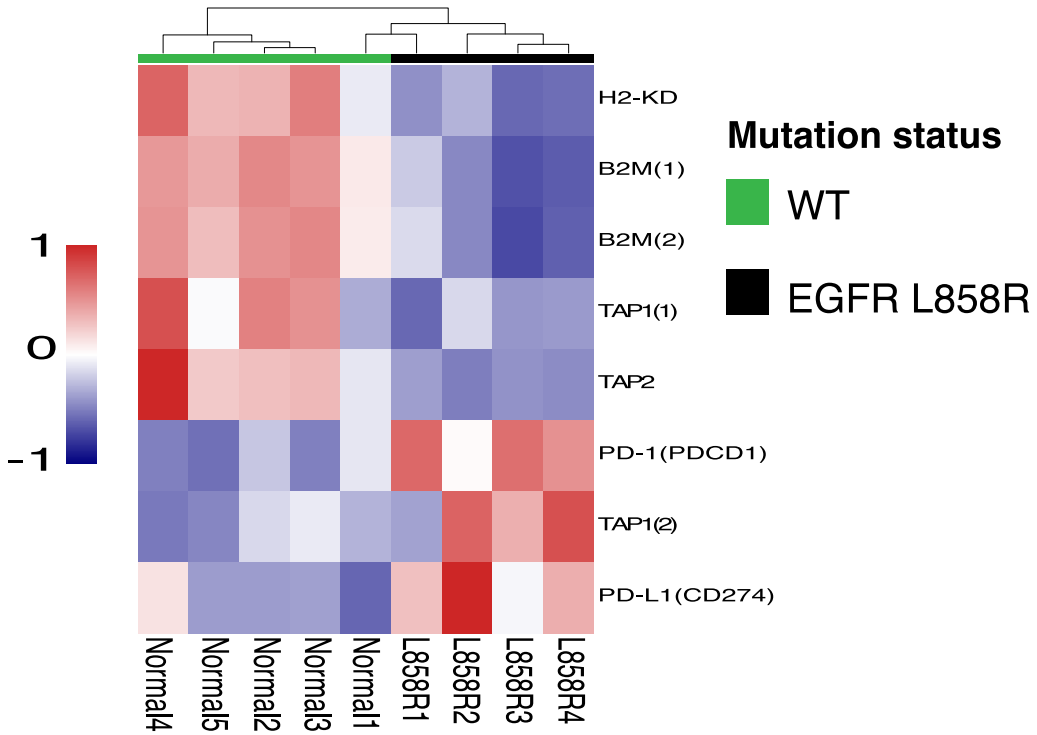

Figure 2.13. Unsupervised hierarchical clustering microarray expression profiling analysis of lung tumors from CC10/L858R mice with EGFR L858R tumor bearing lungs (right side, black) or normal lungs (left side, green) focusing on H2-KD, B2M, TAP1, TAP2, PD-L1(PDCD1), and PD1 (CD274) gene expression.

Up-regulation of PD-1 and PD-L1 markers in the tumors was also observed as previously published (101). Expression of EGFR L858R in the transgenic mice with treatment on doxycycline for >6 weeks was demonstrated by increased binding of a human EGFR specific fluorescently labeled mAb (Figure 2.13A). Mice were confirmed to have development of lung adenocarcinoma by MR, with development of a reticulonodular infiltrate in the lung consist with previous publications(90). The CD45-/hEGFR+ population in the lung in the EGFR L858R expressing mice demonstrated decreased binding of a MHC-I specific mAb by flow cytometry, when compared to a wild type mouse which did not express the EGFR L858R mutation. (Figure 2.14B).

Figure 2.14.A. FlowcytometrydataofFVBCC10-rtTA/TetOEGFRL858Rexpressingmice. Micewereinducedwithdoxycyclinefor>6 weeksbeforesacrificed (mice E-G). Control mice were kept on normal diet, but genotypically identical (A-D). LungswereisolatedandstainedwithmarkersforCD45 (panleukocyte), hEGFR, andH2-kq (MHC-I). **B**. TheCD45- lungpopulationwasstainedwithmouseH2-kqspecificmAb. CD45-/hEGR- populationshowshigherMHC-IexpressionthanCD45-/hEGFR+ population. Representative MRI images of mouse lungs are shown for two samples.

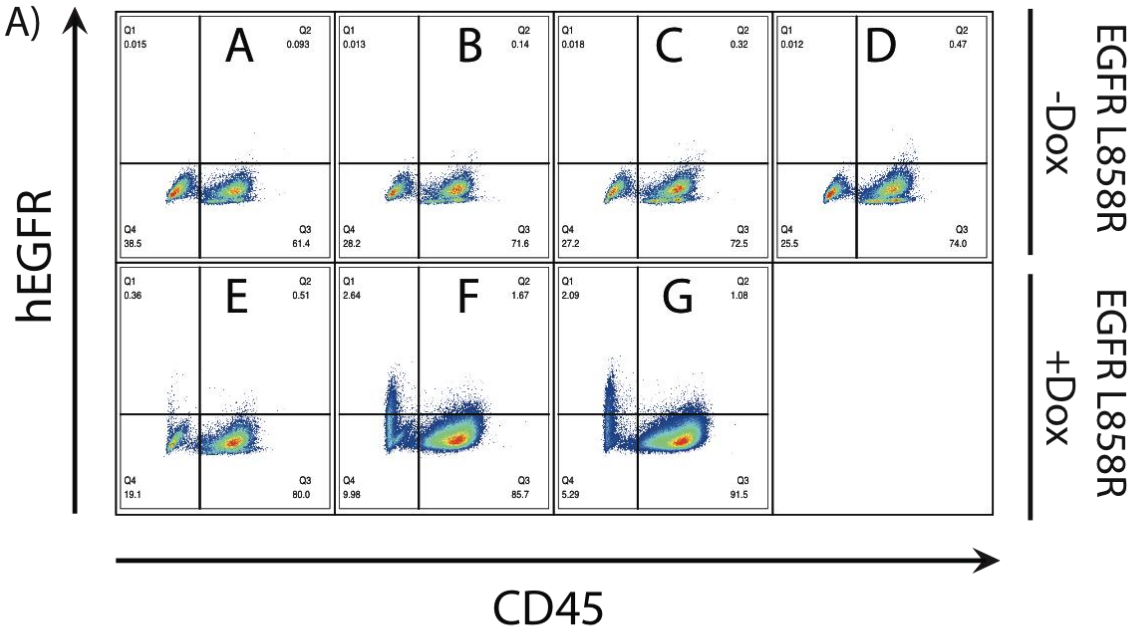
A)
hEGFR
CD45
A
B
C
D
E
F
G
EGFR L858R -Dox
EGFR L858R +Dox

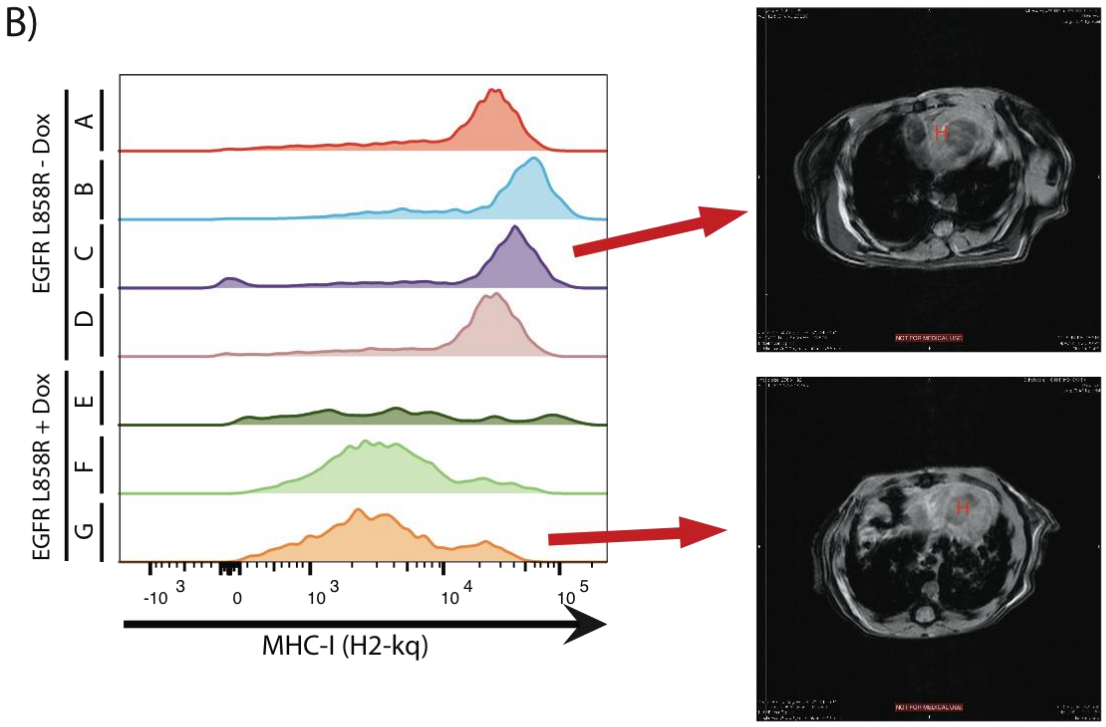
B)
EGFR L858R - Dox
EGFR L858R + Dox
A
B
C
D
E
F
G
-10 3
0
10 3
10 4
10 5
MHC-I (H2-kq)

Improving immunotherapy by increasing MHC-I expression and antigen presentation using MEKi

We finally wanted to demonstrate that regulation MHC-I and antigen presentation with kinase inhibitors had a beneficial effect to immunotherapy for cancer. We utilized two TCR mimic mAbs, ESKM and PR-20. ESKM is a TCRm directed towards an epitope from WT1, an oncoprotein present in numerous hematopoietic and solid tumors (21, 50, 102, 103). PR-20 is a TCRm targeted an epitope derived from the PRAME oncoprotein also present in various hematopoietic and solid tumors (104, 105). We demonstrated that in two HLA-A02+/WT1+ cell lines, combination therapy with the MEKi trametinib along with ESKM resulted in superior killing in an ADCC assay, when compared to vehicle or single agent alone (Figure 2.15AB). This also worked for the PR-20 antibody against an HLA-A02+/PRAME+ melanoma cell line (Figure 2.15C).

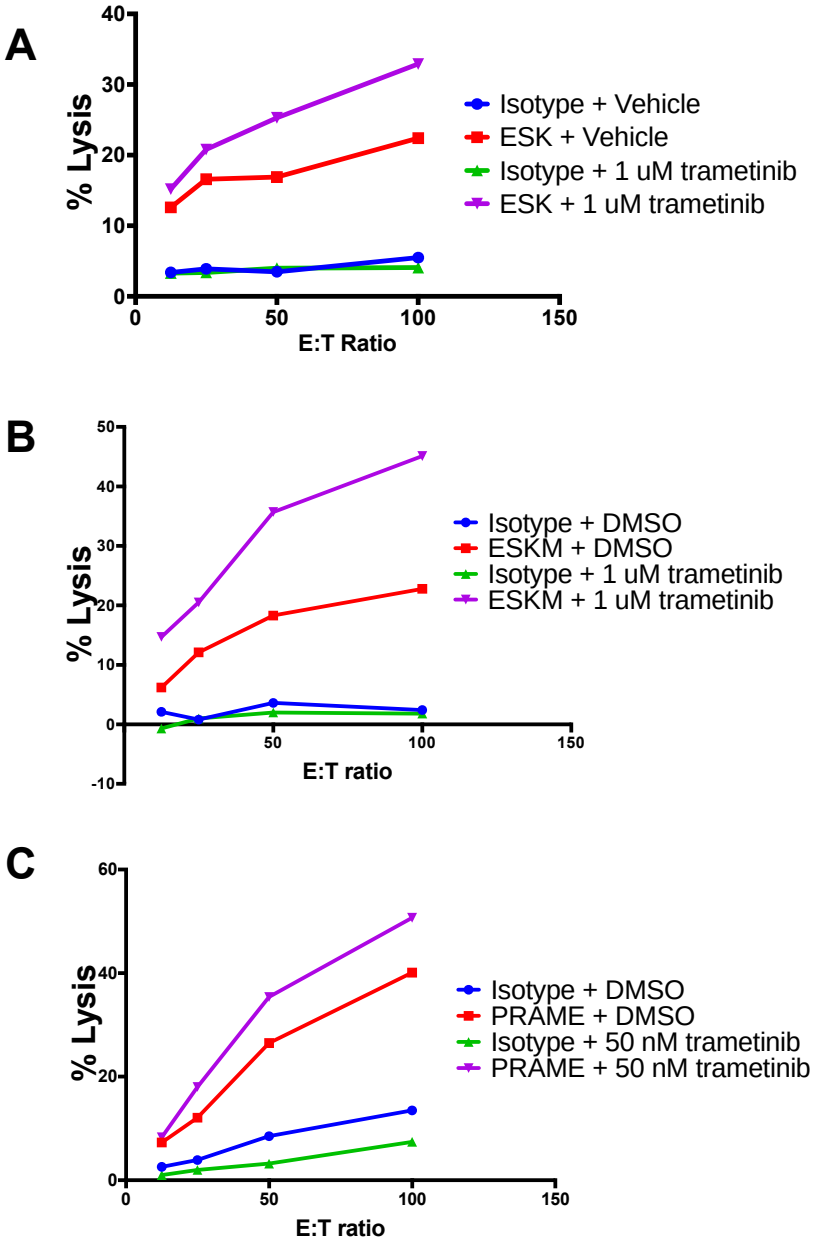

Figure 2.15. Improving immunotherapy efficacy by up-regulating cell surface MHC-I**A**. Antibody dependent cellular cytotoxicity assay was performed on JMN human mesothelioma cell line. Cells were incubated for 72 h with either vehicle control or trametinib and subsequently exposed to either isotype antibody or ESKM in ADCC assay **B**. ADCC assay on Meso34 (human mesothelioma). Experimental setup was similar to 2.14A. **C**. ADCC assay on SKMEL5 (human melanoma) using TCRm mAb PRAME against the PRAME epitope, experimental setup similar to 2.14A.

Another model that we investigated was using T-cell based killing in combination with MEKi. The B6.Cg-Thy1a/Cy Tg(TcraTcrb)8Rest/J mice express TCR specific for the gp100 pmel tumor antigen(20). We harvested T-cells from the spleen of a pmel transgenic mouse and used these cells as effectors. After treating the pmel+ B16F10 murine melanoma with either vehicle or 1 uM trametinib, we exposed them to pmel specific T-cells in an overnight killing assay, then performed a clonogenic assay to assess killing(106). Finally, we also demonstrated increased killing by specific T cells following use of MEKi to up-regulate MHC-I. The pmel-1 gp100 specific mouse T cells were more effective at killing of the gp100 positive target B16F10 melanoma cells following trametinib treatment, which correlated with pERK inhibition and MHC-I up-regulation (Figure 2.16ABC)

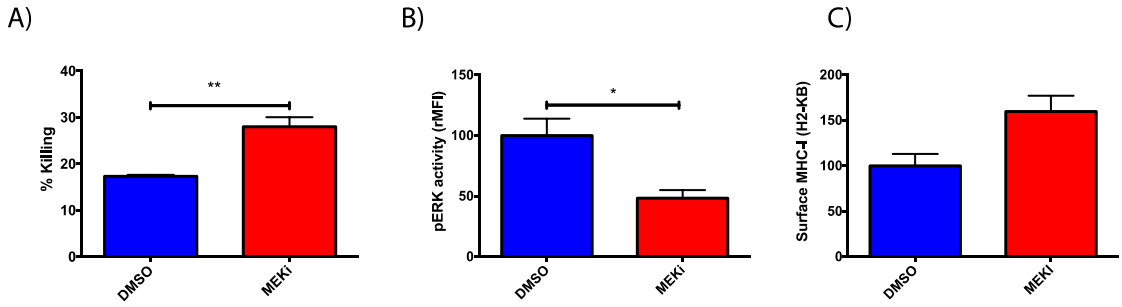

Figure 2.16. B16F10 cells were exposed to pmel-1 (gp100) specific TCR T-cells for 24 h, then killing was assessed using a clonogenic assay described previously.**A.** B16F10 cells were exposed to pmel-1 (gp100) specific TCR T-cells for 24 h, then killing was assessed using a clonogenic assay described previously (50). **B.** B16F10 pERK levels, as measured by pERK intracellular staining, in cells treated with vehicle or 1 uM trametinib. **C.** B16F10 MHC-I expression assessed by flow cytometry after treatment with 1 uM trametinib for 72 h.

DISCUSSION

Immunotherapy of cancer is emerging as a successful and important component of treatment. MHC molecules presenting antigens are the target of multiple therapeutic strategies that involve vaccines, T cells or TCR's, TCR mimic antibodies, or T cell checkpoint blockade. The latter, a highly effective recent example in cancer therapy, appears to require presentation of neoantigens on MHC-I on the surface of cancer cells (107–109). Many immunotherapies have focused on intrinsic effector cell mechanisms, such as the T-cells, for modulating the immune response, but not the target of the immune attack. The ability to regulate such responses by affecting target cells could have an important impact on both disease and therapy. We propose that kinases are a readily druggable pathway that might be used in conjunction with immunotherapy to enhance efficacy. The beneficial effect of the combination of immunotherapy with kinase inhibition was shown in mouse models of combined PD-1/PD-L1 blockade with MEKi (110). A second model of adoptive T-cell therapy in combination with MEKi in BRAF mutant murine melanoma has demonstrated superiority to single agent alone (111). Our work has provided a mechanistic understanding of these combination therapies leading to up-regulated MHC-I and antigen presentation, essential for the adaptive immune response. Indeed, many of the patients treated currently with immunotherapies also receive kinase inhibitor therapies as distinct treatments.

The loss and gain of function screen described here allowed unbiased interrogation of the currently annotated human kinases for their regulation of cell surface MHC-I. We then explored mechanistically how such kinase regulators could be inhibited for altering surface expression of MHC-I, as a way of validating the screen, understanding the process, and also for extending the findings to functional modulation of a model immunotherapy proof of concept that directly depends on MHC-I presentation. In this case, we were able to specifically isolate the MHC as the sole target of the therapy by use of therapeutic TCR mimic antibodies directed to antigens presented by MHC.

This study also provides a proof of concept for use of a flow cytometry based loss of function pooled shRNA screen in an application to the study of regulation of other cell surface molecules, and potentially intracellular antigens as well. This technique will allow many laboratories without robotics and high throughput flow cytometry equipment to investigate pathways that can be easily perturbed with loss of function RNAi screens or other techniques such as CRISPR loss of function.

While we demonstrate the effect of the MAPK pathway on MHC-I in vivo, the study of certain kinases, such as MEK, to increase MHC-I surface expression and antigen presentation is complex because T-cells and NK cells also rely on similar kinase signaling pathways for activation. More work needs to be done

to determine optimal pathways or schedules or doses to target MHC in tumor cells specifically, while sparing signaling pathways of the effector cells (112). Some work has suggested conflicting effects of MEKi on T-cell effector function, and may be dependent on the tumor model evaluated (113, 114). Optimal dosing schedules will be needed in models in vivo and in humans to show that use of kinase inhibition to regulate immunotherapy has therapeutic benefits while sparing immune effector cells of the detrimental effects. These investigations will be complicated by the effects of some of the drugs on the T cell effectors themselves.

The data provide a mechanistic explanation of how MHC-I is regulated by the MAPK pathway. MHC-I mRNA expression is regulated through upstream enhancer elements, with involvement of the NF-κB transcription factor (96, 115). MHC-I is also induced by TNF, IL-1, interferon beta, and interferon gamma, which up-regulates HLA-A via the JAK/STAT pathway (99, 116). The CIITA transcription factor can also act on MHC-I gene expression (97). Interferon gamma has been shown to increase MHC-I and antigen presentation, but thus far has had limited applications for this use (117). MEK has been proposed by others to be a regulator of MHC-I expression. EGFR inhibition can augment MHC-I and MHC-II expression in keratinocytes (118). MEK is a negative regulator of HLA-A*02:01 in esophageal and gastric cancer (119). We validated these targets in the screen as an important negative regulator of MHC-I and discovered a mechanistic role of the MAP kinase

pathway in regulating surface levels of MHC-I. Interestingly, activating EGFR mutations may contribute to immune escape due to PD-L1 expression. Down-regulation of MHC-I, which was observed from our study, may also contribute to this finding (101). Our data also suggest that using combination therapy of MAP kinase inhibition can be powerful not only as a direct cancer therapy to prevent growth, but also indirectly to promote immunotherapy.

For autoimmune disease, the HLA genes have been shown to be a risk factor for diseases such as ankolysing spondylitis, multiple sclerosis, and other diseases (120–122). In addition to up-regulation by certain kinases, we were also able to show down-regulation of MHC-I through new kinase targets. These targets are not currently addressed by immunosuppressive therapies, which inhibit the effector arm of the immune response with concomitant toxicity. These new targets warrant further development of specific inhibitors and mouse models to elucidate the utility of using kinases to alter autoimmune disease, also beyond the scope of this report.

A requirement of many immunotherapies therapies is the availability of recognizable antigens that are presented on MHC-I. Tumors can down regulate MHC-I to avoid immune system detection of the rare neo-antigens created in tumors by mutations, in addition to up-regulation of inhibitory receptors. By modulating the levels of these limited antigens, improved clinical efficacy could be seen with certain immunotherapies in conjunction with

current FDA approved small molecules targeting EGFR and MEK. We also discovered that the inhibition of the kinase pathways caused a more general up-regulation of the antigen presentation machinery, including Tap (responsible for transporting peptides) and B2M (responsible for stabilizing MHC). Many of the recently approved immunotherapies, such as CTLA-4 blockade and PD-1 blockade, release the T-cell inhibition promoted by target tumor cells. These immunotherapies provide a promising approach to addressing multiple malignancies, and by rationally combining with targeted small molecule inhibitors, this approach may allow for novel synergistic treatment strategies to be developed.

CHAPTER 3: STRUCTURE OF A THERAPEUTIC TCR MIMIC ANTIBODY WITH TARGET PREDICTS PHARMACOGENETICS [1,2]

INTRODUCTION

Antibodies are ideal drugs for cancer therapy, given their ability to specifically target antigens, predictable pharmacokinetics, high affinity binding, track record of success in the clinic, and ease of production. Antibody targeted therapies have been highly successful in selectively killing cancer cells by various mechanisms with reduced adverse effects. More than a dozen cancer therapeutic antibodies are used clinically (123). Antibody therapies target extracellular proteins, and a major unmet challenge has been targeting *intracellular* cancer specific proteins, which are more common and often more specific to the cancer. Also, many intracellular targets are considered undruggable, including many transcription factors which are known to be involved in oncogenesis (124). One strategy to target intracellular antigens is to direct antibodies to peptides derived from oncoproteins that are displayed on the cell surface by major histocompatibility complex (MHC) class I receptors, which may have limited expression in normal tissue (48, 125).

The Wilms Tumor 1 protein (WT1) is overexpressed in most hematological and solid tumor cancers (40, 126), and peptides derived from WT1 are displayed by HLA receptors as 9-10 amino acid T-cell epitopes for presentation to the TCR (43, 127). We used ESK1 as a model TCRm, which

[1]Modified from Ataie N, Xiang J, Cheng N, Brea EJ*et al.*J Mol Bio. 2014
[2]Some experiments were designed and conducted by or in collaboration with Niloufar Ataie and J. Xiang as noted in the text.

we have demonstrated has in vitro and in vivo activity in solid and hematopoetic tumors. ESK1 binds the WT1 derived peptide epitope RMFPNAPYL (RMF)/HLA-A*02:01 complex with 0.2 nM affinity and triggers WT1-specific cancer cell death (128–130).

X-ray crystal structures of TCR and TCRm have been used in the past to yield novel insight into binding orientations and allow for comparison with each other. TCR in complex with peptide/MHC-I have very little variability in binding orientation, with most binding in similar locations (131, 132). TCR mimics have demonstrated diverse binding orientations (133, 134).

Insight into binding will also allow for prediction of off-targets of ESK1. Given the ability for potent antibody therapy, TCR based therapy, CAR-T cell and bispecific enganging antibodies to destroy targets, a thorough examination of off targets is also necessary. Cases of off target reactions have been seen with TCR therapy against MAGE antigen, which cross reacted with an epitope from titin and caused cardiovascular toxicity in a patient(135).

In collaboration with N. Ataie, J. Xiang, H. Ng, and C. Lui, we solved the crystal structure of the RMF/HLA-A*02:01/ESK1 (Fab) complex to 3.05 Å. The ESK1 variable domains bind the HLA and peptide in a different mode than TCRs. ESK1 CDR loops contact regions of HLA that TCRs typically do not reach. Our structure and binding studies also show that RMF acts as an electrostatic key in mediating ESK1 specificity and activity with Arg1 playing a central role. RMF Pro4 also contributes to ESK1 binding.

The rest of the binding interface is limited to interactions between ESK1 and a region on the HLA receptor that is conserved between subtypes, suggesting that binding is compatible with other common HLA-A*02 subtypes, which we experimentally confirmed. While HLA-A*02:01 is the most common HLA-A*02 subtype in the United States and Europe, other subtypes bearing different peptide and TCR binding specificities are found across different ethnic groups worldwide (136, 137). Unlike TCR, which are restricted to subtype and would cause allograft reactions, this unique ability of ESK1 potentially broadens the target patient populations for this drug beyond the HLA-A*02:01 subtype found predominantly in Caucasians to multiple other ethnic groups. The crystal structure allowed additional predictions of possible cross-reactive human self-peptides, which were confirmed in vitro. In this way, we use structural data as a tool for pre-clinical antibody pharmacogenetics and toxicology.

MATERIALS AND METHODS

ESK1 design, construction, purification

The antibody ESK1 was prepared as described previously (128). Briefly, ESK1 was derived from the top clone selected from the Eureka Therapeutics human single-chain variable fragment (scFv) phage library with specific binding for the RMF/HLA-A*02:01 complex. The full-length human IgG1 form of ESK1 antibody was produced in the Chinese Hamster Ovary (CHO) cell line. ESK1 antibody was affinity purified by Protein A chromatograph with an AKTA FPLC system.

ESK1 flow cytometry binding assay to RMF peptides

T2 cells, a TAP1/2 deficient HLA-A*02 expressing cell line that does not present endogenous peptides, were used for pulsing peptides. T2 cells were purchased from ATCC and cultured in RPMI with 10% FBS. Peptides were purchased from Genemed Synthesis (San Antonio, TX USA) with >90% purity. Peptides were resuspended to 20 mg/ml in DMSO and diluted to working stocks in PBS. T2 cells, at $1x10^6$ cells/ml, were pulsed with peptides at various concentrations overnight in RPMI with 10% dialyzed FBS and 10 ug/ml β_2-microglobulin. T2 cells were incubated with peptide overnight at 37ºC with 5% CO_2. Cells were then spun down, washed with PBS, and blocked in human FcR block for 15 minutes on ice. T2 cells were then stained with ESK1 labeled

with APC at 3 ug/ml final antibody for 45 minutes on ice. Cells were then spun down and resuspended in FACS buffer and run on FACS Calibur.

Off target binding of ESK1

Protein BLAST from NCBI, along with analysis using NetMHC 3.0(138) for peptides with a binding of <500 nM to HLA*A0201 was used to determine novel off targets of ESK1. The search criteria used for the protein BLAST were: RMFPXXXXL, RMFPXXXXV, RMFPXXXXI, RLFPXXXXL, RLPFXXXXV, RLFPXXXXI. Peptides were pulsed on T2 cells, as previously described, at various concentrations, and binding of ESK1 was measured by flow cytometry.

HLA subtype binding assays

Binding affinity was determined by measuring surface plasmon resonance on a Biacore X100. In brief, 50 µg/mL of modified streptavidin was immobilized onto a Sensor Chip CAP by flowing the Biotin CAPture Reagent through the flow cells at 2 µL/min for 5 minutes. 10 ug/mL biotinylated MHC complex carrying the RMFPNAPYL peptide was loaded onto the flow cell at a rate of 30 µL/min for 3 minutes. Following the standard protocol for single-cycle kinetics, a series of injection of ESK1 were performed at 0.313, 0.625, 1.25, 2.5, and 5 µg/mL, with each step consisting of a 3 minute injection at 30 µL/min and 3 minute disassociation. Afterwards, the surface was regenerated for 2 minutes

with a solution consisting of 75% v/v 8M guanidine-HCl and 25% v/v 1M NaOH. Kinetic constants were derived by global fitting to a 1:1 Langmuir binding model using the BIAcore X100 Evaluation Software (Version 2.0.1).

HLA subtype construction, purification, and analysis

HLA-A*02:01, 02:02, 02:03, 02:05, 02:06, 02:07, 02:11 sequences were obtained from *The HLA Factsbook*(139). HLA subtype MHC complexes were generated using a modified protocol(140). In brief, each HLA-A*02 subunit as well as the □2-microglubulin (B2M) subunit were overexpressed in E. coli in inclusion bodies and then solubilized in 8M urea. The RMF peptide, HLA-A*02 solution, and B2M urea solutions were mixed together in the refolding buffer at 4 degree for 2 days. The refolding solution was further concentrated and buffer exchanged into PBS. The desired MHC complex was purified by size exclusion chromatography (SEC) using an AKTA FPLC system.

Crystallization

ESK1 Fab fragments were produced from intact IgG ESK1 and purified with the Pierce Fab Purification kit. Fab fragments were concentrated to 100 uM, mixed with equimolar HLA-A*0201 receptor/□-microglobulin/RMF complex, and equilibrated on ice for one hour. The sample was concentrated to 12.5 mg/ml using a 10 kDa cutoff Amicon concentrator and exchanged into 50mM Tris (hydroxymethyl) aminomethane, 25 mM NaCl, pH 7.5, and 0.5 mg/ml

RMF peptide. Crystals grew within 1 – 3 weeks when the protein solution was mixed 3:1 with Microlytic MCSG-1 H9 solution (0.1 M Bis-Tris HCl pH 5.5, 25% (w/v) PEG 3350) at 18° C in sitting drops. Crystals were whisked through Paratone-N for 10-20 seconds and cryocooled in liquid nitrogen prior to data collection.

Data collection and refinement

Diffraction data to 3.05 Å were collected remotely at Beamline 12-2 at the Stanford Synchrotron Radiation Laboratory (141) under a nitrogen cryostream on a Pilatus detector. Data were processed with HKL3000 (142) and XDS (143). The structure was solved by molecular replacement using the structures of HLA-A2 (PDB 3HPJ) and the Fab fragment from antibody HC84-1 (PDB 4JZN) using MOLREP (144) and Phaser (145). The structure was refined with REFMAC (146) with manual rebuilding with Coot (147). Processing and refinement statistics are provided in Table S1. The crystal structure coordinates and diffraction reflections are deposited in the PDB (4WUU).

Structure analysis and modeling

Modeling was performed with PyMol and Coot. Interaction surface properties were calculated with Pisa (148).

RESULTS

OverallStructure

The ESK1 Fab fragment binds primarily the first five residues, RMFPN of the peptide-MHC (pMHC). The ESK1 Fab variable domain contacts 160 $Å^2$ (Figure 3.1A). RMF peptide interacts with 873 $Å^2$ of the HLA receptor with a similar structure to the HLA-A02 without peptide (149). ESK1 antibody-HLA contacts 890 $Å^2$ and the total ESK1-pMHC surface is 1050 $Å^2$ (Figure 3.1BC). The variable domains of ESK1 bind to both the peptide RMF and HLA-A02 molecule (Figure 3.1D). The binding region of the ESK1 Fab is predominantly contacting the first five amino acid residues of RMF with the interactions of the CDR loop with the pMHC. Four tyrosines on the heavy CDRs stabilize the interface. (Figure 3.1E).

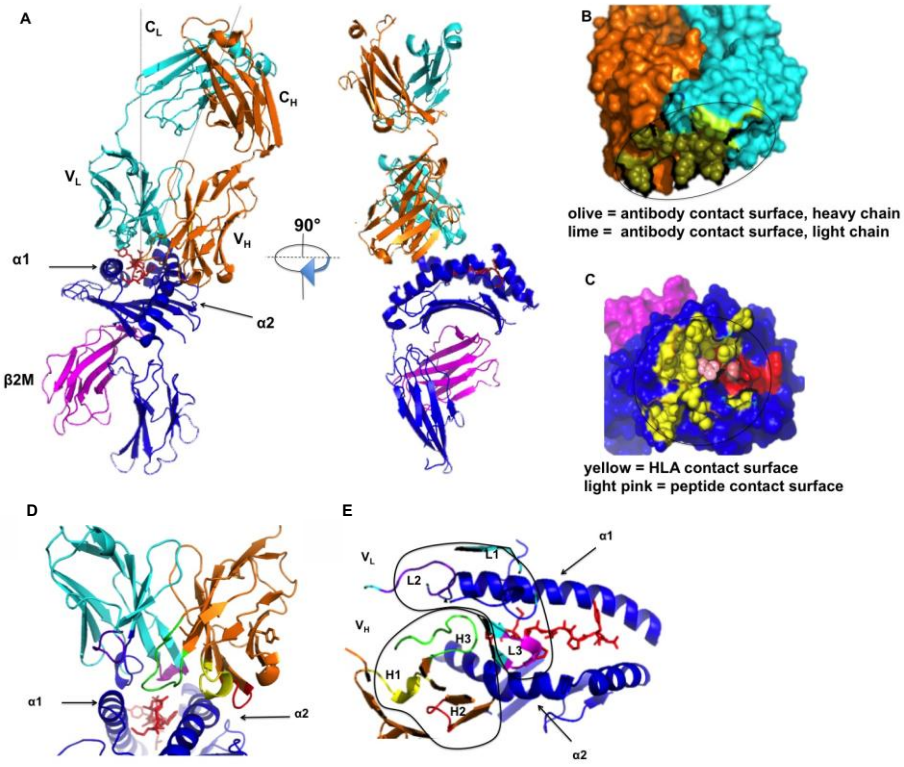

Figure 3.1 Overall structure of ESK1 Fab. **A**.The cartoon backbone rendering of the ESK1/pMHC complex is shown. HLA-A*02:01and β2-microglobulin are colored blue and magenta respectively. HLA helices α1 and α2 in the RMF binding site are red. The light and heavy antibody Fab fragments are cyan and orange respectively and are labeled by their variable (V_L, V_H,) or constant (C_L, C_H) domains. **B**. The surface of the variable domains of the antibody is shown where the heavy chain contact surface is colored olive and the light chain contact surface is lime. **C**. The top down view of the HLA surface is shown with the HLA contact surface colored yellow and the RMF contact surface colored pink. **D**.The variable loop regions of the light and heavy chains are shown at the antigen binding site. V_L loops L1, L2, and L3 are colored blue, purple, and magenta, respectively. V_H loops H1, H2, and H3 are colored yellow, red, and green respectively. **E**. The top-down view shows the RMF binding site with the variable loops circled. (Conducted by N. Ataie).

Comparison to other TCRS and TCR-like antibodies

We compared the structure of ESK1 + HLA-A*02 to HLA-A*02 with twenty other TCRs and TCR mimic antibodies (134, 150–156) to determine the mechanism for the 1000-fold higher affinity for ESK1 compared to these other ligands (**Figure 3.2**). The four TCR mimic antibodies compared differ widely in binding orientations. None of the other three antibodies binds to the same arginine cluster as ESK1. ESK1 CDR loops reach HLA-A*02 regions untouched by TCRs that interact with the HLA arginine cluster. Compared to the sub-nanomolar affinity of ESK1, TCRs typically bind with a maximum of 1 μM binding affinity (157). While ESK does not have the largest contact surface compared to the other pMHCs, it has the highest affinity (Table 3.1)(158, 159).

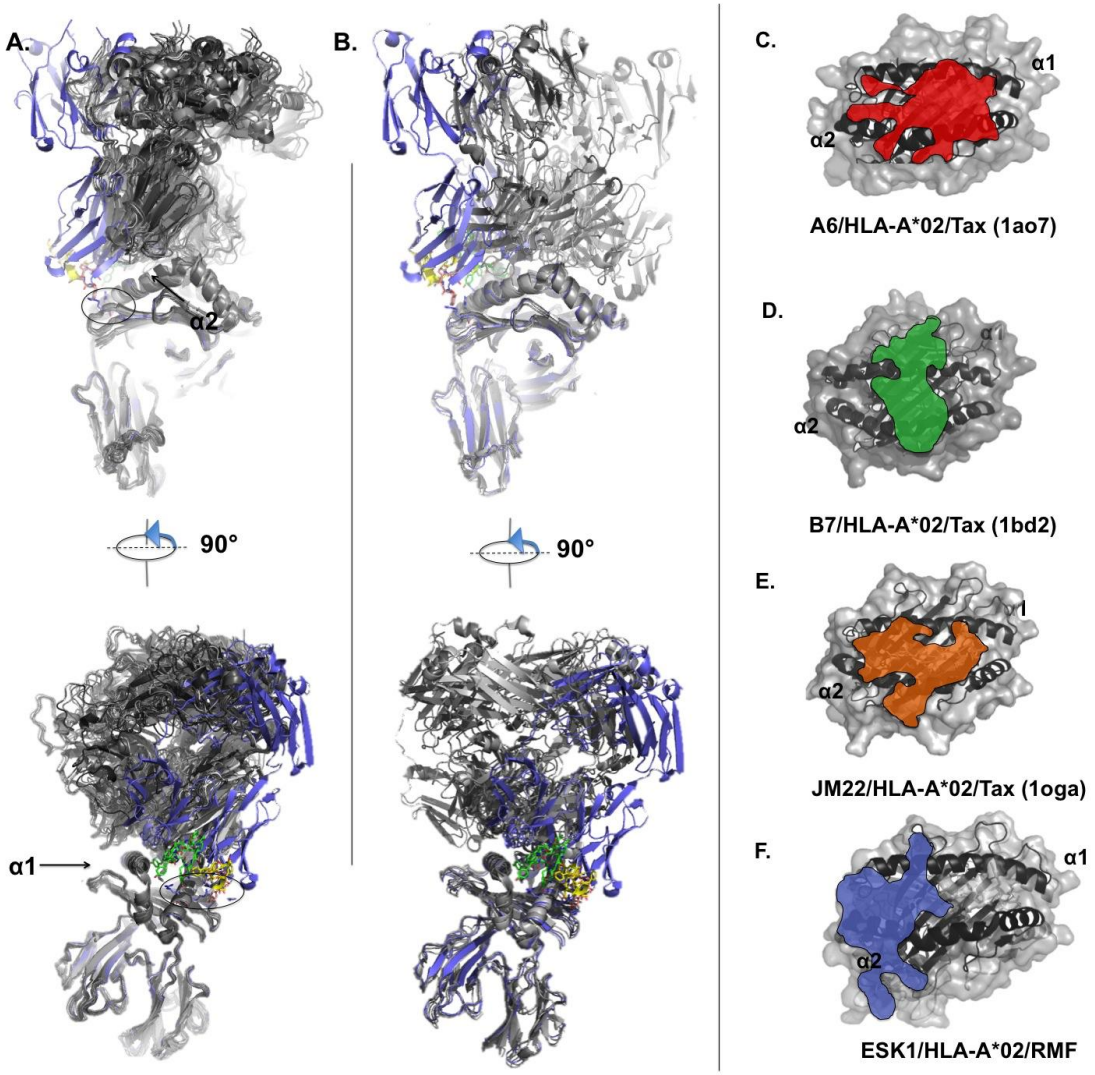

Figure 3.2. Structural comparison between ESK1 and other TCRs and TCR-like antibodies. **A.** Structural alignment between ESK1 and 20 TCR/HLA-A*02:01/peptide structures shows that ESK1 CDR loops reach regions of HLA α2 that TCR loops do not. This includes the circled arginine-rich region: Arg108, Arg169, and Arg170. The blue ESK1/pHLA structure has V_H domains H1, H2, and H3, colored yellow, red, and green, respectively. **B.** Structural alignment of TCRm antibody/HLA-A*02 structures shows that antibodies are more diverse in binding position and angle than TCRs, though none binds to HLA via the arginine-rich ESK1 binding site. **C-F**. The footprints of three TCRs and ESK1 show that TCRs bind to the mid-helical region, in contact with the peptide, whereas ESK1 reaches beyond the canonical TCR binding site. (Conducted by N. Ataie).

Table 3.1. A comparison of interface interactions between ESK1/pHLA-A*02:01 and three TCR/HLA-A*02:01 structures showing the contact surface area and binding free energy calculated from experimental dissociation constants. ESK1 has the strongest binding free energy despite having a total contact surface area comparable to TCRs. Surface areas were calculated with PISA (Conducted by J. Xiang).

TCR/HLA-A*02/peptide	MHC/TCR contact surface Å² (PISA)	Peptide/TCR contact surface Å² (PISA)	Total TCR contact surface Å² (PISA)	ΔG (kcal/mol)
A6/HLA-A*02/Tax (1ao7)	555 (α) + 198 (β) = 753	182 (α) + 214 (β) = 396	1149	-7.7
B7/HLA-A*02/Tax (1bd2)	548 (α) + 171 (β) = 719	164 (α) + 173 (β) = 337	1056	-8.0
JM22/HLA-A*02/MP58 (1oga)	206 (α) + 435 (β) = 641	80 (α) + 199 (β) = 279	920	-7.1
ESK1(antibody)/HLA-A*02/RMF	585 (h) + 305 (l) = 890	70 (h) + 90 (l) = 160	1050	-14

Peptide Binding Specificity

ESK1 binds the HLA receptor where RMF Arg1 is buried (**Figure3.3A**)**.** ESK1 primarily interacts with RMF Arg1 and Pro4. RMF Met2, Phe3, Ala6, Phe7, and Leu9 side chains contact the bottom of the HLA peptide binding region (**Figure3.3B**). Asn5 and Tyr8 face the solvent and do not contact ESK1.

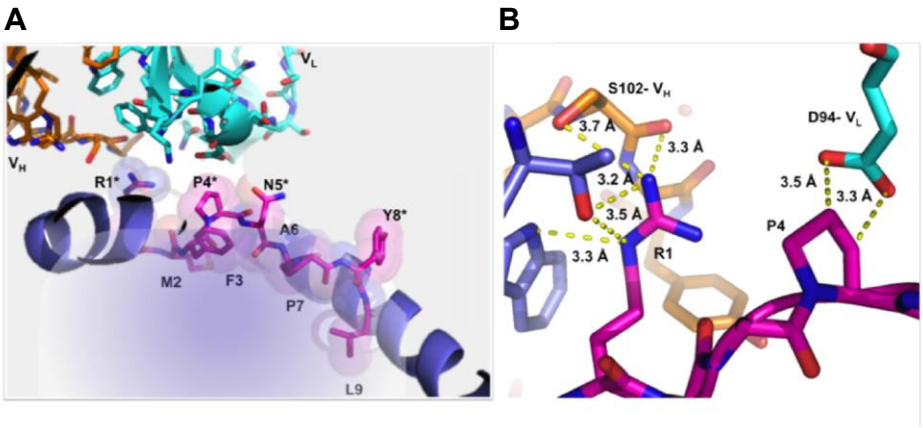

Figure 3.3. Peptide interactions. **A**. RMF binds HLA with Met2, Phe3, Pro7, and Leu9 facing the HLA receptor and Arg1, Pro4, Asn5, and Tyr8 facing solvent and/or antibody. The heavy and light chains are in orange and cyan. Arg1, Pro4, and Asn5 are within van der Waals distance to ESK1. **B.** RMF Arg1 is located near hydrogen bond distance of Ser102. Arg1 also forms potential hydrogen bonds to HLA Thr163 and Trp167 and is within van der Waals distance to ESK1 Tyr104. Also shown is the proximity of RMF Pro4 to ESK1 light chain Asp94 (Conducted by N. Ataie)

In order to probe the structural requirements of the ESK1 antibody to the HLA-A02/RMF complex, we made substitutions along the length of the RMF peptide. Substitutions were made throughout RMF and ESK1 binding to the peptide/MHC complex was measured in the TAP1/2 deficient T2 lymphoblastoid cell line by pulsing various peptides onto HLA-A02.

Substitution at position 1with citrulline, sterically similar to arginine, but uncharged, eliminated binding. Lysine substitution at position 1 decreased binding 40-fold. Substitution at position 1 with ornithine, similar to lysine, but shorter by a carbon atom, or with histidine, eliminated ESK1 binding (Figure 3.4). Overall, the binding data support a highly specific fit of the ESK1 electrostatic lock for arginine. Arg1 is near several charged residues in a

buried hydrophobic pocket capped by a highly negatively charged loop from the ESK1 heavy chain.

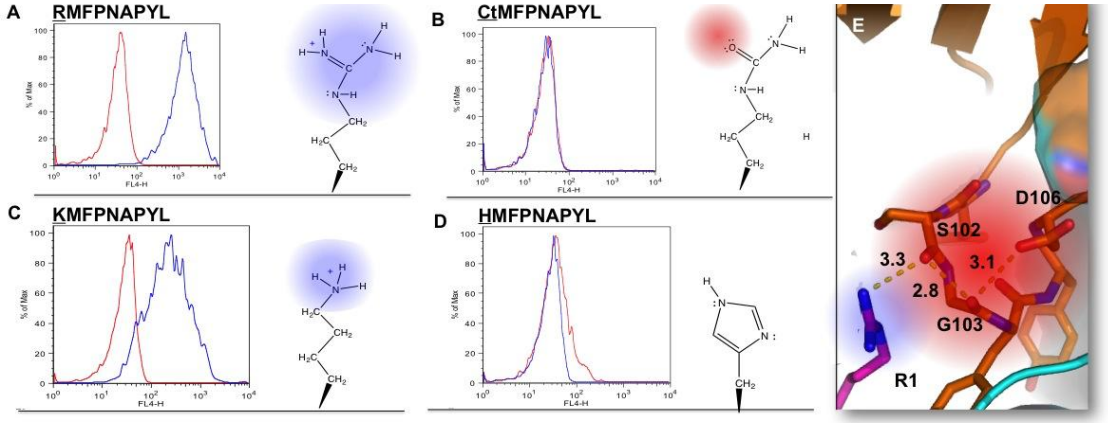

Figure 3.4. Binding results of amino acid substitutions at position 1 of RMF. Flow cytometry binding results of a series of substitutions at position 1 of the RMF peptide are shown with a chemical depiction of the substitution. Regions harboring positive charge are colored blue and those with negative charge, red. Compared to arginine (A), citrulline (B) has similar van der Waals packing and hydrogen bonding but the lack of charge drastically reduces binding. (C) Substitution of lysine, which retains the positive charge of arginine, has forty-fold lower affinity than arginine, but much greater affinity than citrulline. (D) Substitution with histidine, with no similarity to arginine, exhibits no binding. (E) Binding pocket of RMF Arg1.

This pocket acts as an electrostatic lock in which the negatively charged dipoles of the backbone carbonyl oxygens of Ser102, Gly103, and the sidechain of Asp106 converge without countercharge, creating a buried space of focused negative charge. Tyrosine at position 1 does not provide the countercharge needed to fit the electrostatic lock. The crystal structure can help reveal the factors driving specificity and cross reactivity of ESK1 toward other peptide/MHC epitopes. Substitutions along different positions in the peptide demonstrate the sensitivity of various residues.

A loop from the light chain partially shields RMF Pro4 from solvent. Asp94 of the light chain is positioned 3.4 Å away from Pro4. Substitution to glycine, alanine, or serine at RMF position 4 does not significantly affect binding, but substitution to cysteine decreases binding ten-fold (**Figure3.5**). Cysteine modeled into position 4 of RMF sterically clashed with Asp94. Surprisingly, the substitution of tryptophan at position 4 showed no loss in binding affinity. Tryptophan modeled into that position forms potentially favorable cation-π interactions with HLA Lys66. Large residues modeled into the fifth position clash with nearby residues. Other large bulky residues at position five decrease binding over ten-fold (**Figure3.5**).

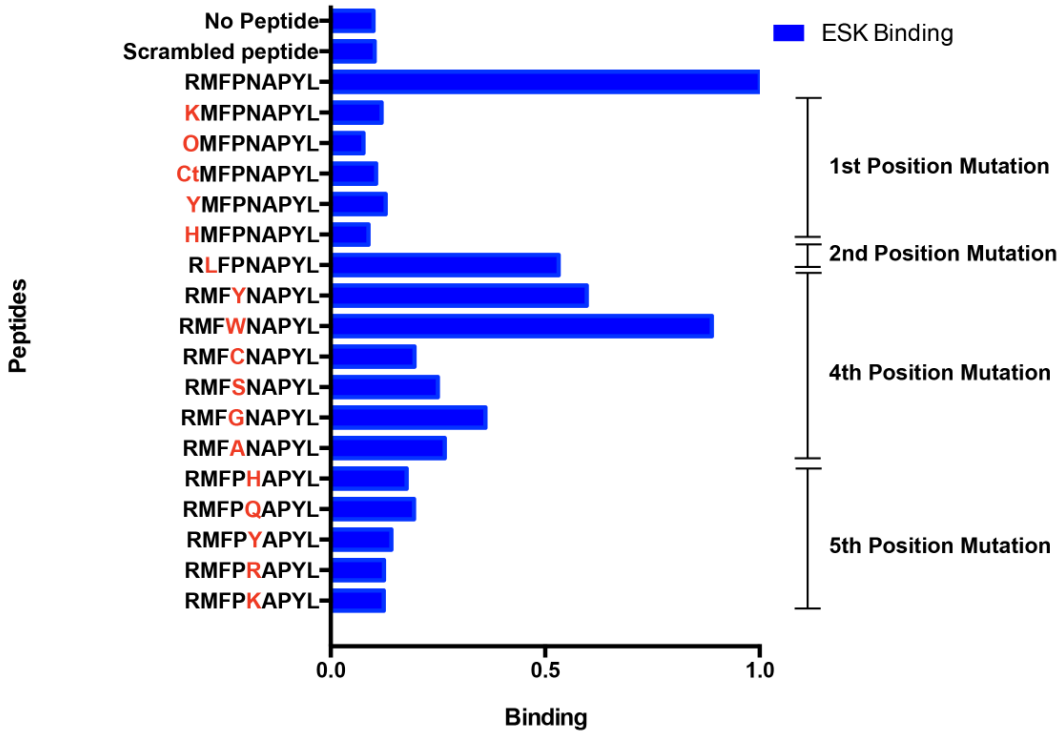

Figure 3.5. Binding avidity of WT1 substituted peptides relative to RMF, as determined by flow cytometry. EW is a peptide (QLQNPSYDK) unrelated to RMF, isolated from Ewing sarcoma, used here as a negative control. Results were normalized to RMF binding. O corresponds to ornithine and Ct corresponds to citrulline; all other amino acid abbreviations are standard.

HLA-A*02 subtype specificity

HLA-A*02 alleles vary widely across different ethnic populations. HLA-A*02:01 is the most commonly found variant, especially in Caucasians in the United States, but other subtypes are more common in other ethnic groups. Six subtypes are found in hundreds of millions of people worldwide that differ from HLA-A*02:01 through 1 to 4 amino acid changes in the side walls of the peptide binding pocket. Models were built of several common HLA-A*02 subtypes, using crystal structure coordinates of the subtype if available

(A*02:03, A*02:06, A*02:07), to predict the effect of binding to RMF and ESK1. All residues that differ between A*02:01 and the other six subtypes do not contact ESK1 (Figure 3.6). Modeling also predicts that RMF binding would be retained across these A*02 subtypes. We predicted and experimentally confirmed that these six subtypes bind RMF and ESK1 (Table 3.2) by surface plasmon resonance using immobilized, biotinylated HLA+RMF. The measured affinity of ESK1 to RMF + A*02:01 is 13.2 nM, lower than measured by the whole cell method. All six HLA variants bind to ESK1 with similar or higher affinity (1.1 nM for A*02:11 to 23.6 nM for A*02:02), supporting patient compatibility.

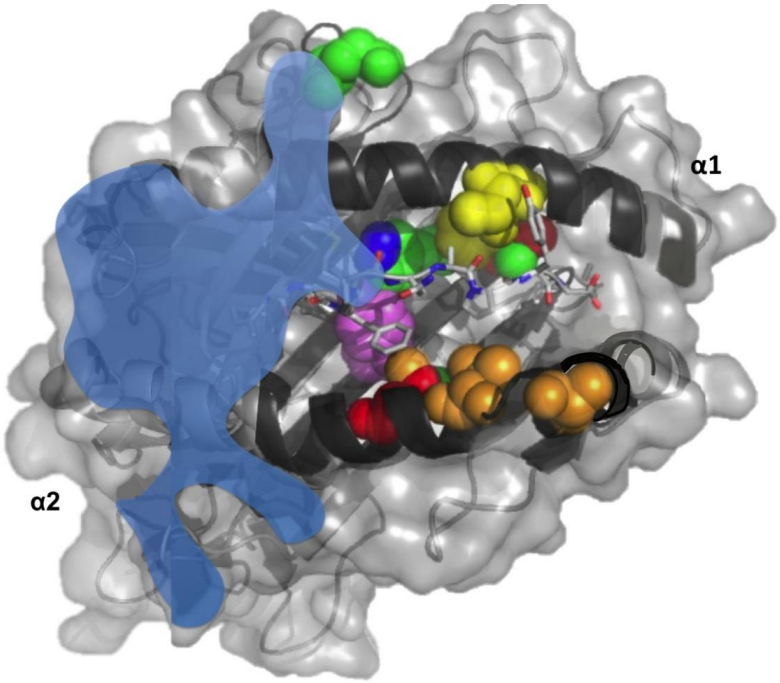

Figure 3.6. Mapped HLA-A*02-subtype differences. Mapped positional differences between the subtypes are colored red: A*02:02, orange: A*02:03, green: A*02:05, blue: A*02:06, magenta: A*02:07, and yellow: A*02:11. The ESK1 footprint is shown in light blue. None of the residues that vary between A*02 subtypes contacts ESK1 (Conducted by N. Ataie).

Table 3.2. Characterization of ESK1 binding to HLA-A*02 variants with RMF. Binding parameters were measured by surface plasmon resonance on a Biacore X100 (Conducted by J. Xiang).

Subtype	k_d [1/s]	Error in k_d [1/s]	k_a [1/Ms]	Error in k_a [1/Ms]	K_D [nM]	Error in K_D [nM]
A0201	1.35E-02	6.70E-04	1.02E+06	4.80E+04	13.2	0.90
A0202	1.40E-02	4.10E-04	5.91E+05	4.30E+04	23.6	1.9
A0203	1.06E-02	2.70E-04	5.24E+05	3.10E+04	20.3	1.3
A0205	5.79E-03	1.10E-04	1.03E+06	1.90E+04	5.6	0.2
A0206	1.91E-03	2.30E-05	9.32E+05	7.50E+03	2.1	0.03
A0207	1.50E-03	3.00E-05	9.53E+05	1.00E+04	1.6	0.04
A0211	9.30E-04	1.80E-05	8.40E+05	5.50E+03	1.1	0.02

Structure-based prediction of potential ESK1 off-target toxicity

A major advantage of antibody over small-molecule therapeutics is that toxicity tends to be more predictable and related to mechanism of action due to their higher specificity (160). Nevertheless, off-target binding is still a serious concern for immunotherapy. Currently, specificity is enforced by counterscreening antibody candidates against nonspecific targets such as cell lysate or MHC receptors bearing untargeted antigen peptides. We demonstrate for the first time that structural knowledge and simple

computational analysis can be used to predict off-targets and further engineer TCRm specificity.

Given the structural and biochemical data supporting the key binding interactions of the ESK1 antibody to RMF positions Arg1, Phe3, and Pro4, we performed a BLAST search for similar expressed human peptide sequences. The peptides were then subjected to binding affinity analysis using NetMHC(138) to predict peptides with a K_d to HLA-A*02:01 < 500 nM. Using artificial neural networks, NetMHC predicts MHC peptide binding with 78% accuracy. The two highest-ranking peptides were identified to be from MED13L (*mediator complex subunit 13-like*), RMFPTPPSL, and PIGQ (*phosphatidylinositol glycan anchor biosynthesis*, *class Q*), RMFPGEVAL, and were tested as potential off-targets to validate our hypothesis. ESK1 bound cell surface MHC with either peptide (Figure 3.7). Structural modeling supports compatibility of these two peptides with HLA-A*02:01 and ESK1 binding. *In silico* mutagenesis of the RMF peptide in the ESK1/HLA/RMF crystal structure showed that the sequences in the MED13L and PIGQ peptides could be accommodated with little change to HLA and ESK1 binding surfaces.

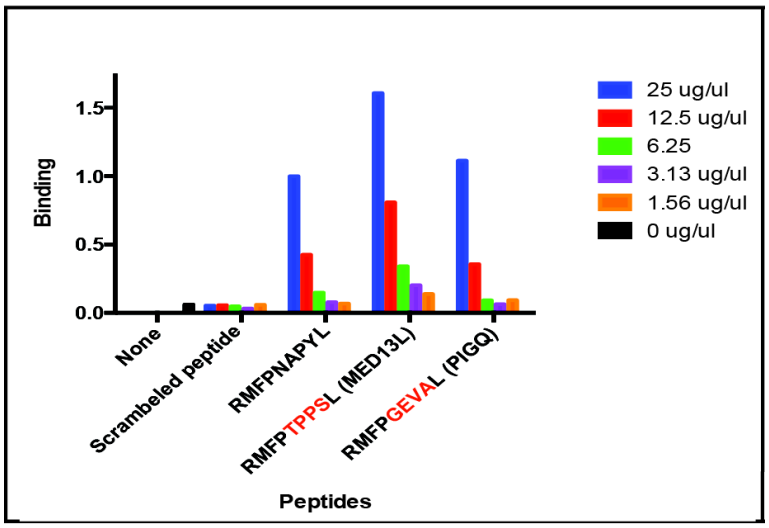

Figure 3.7. Validation of predictions of potential ESK1 off-target epitopes. ESK1 binding was measured by flow cytometry. Relative binding was normalized to 25 µg/mL RMF. Relative binding of a scrambled control peptide or two identified peptides derived from MED13L and PIGQ is shown.

Studies on normal donor peripheral blood monocyte cells showed potential off-target binding of ESK1 to a small subset of healthy donor CD19 + B-cells, which were WT1 negative. In this way, it is possible that ESK1 binding to this subset of cells may be attributable to non-WT1-derived epitopes, which data suggests could be from two or more of the identified off target epitopes MED13L or PIGQ. We observed higher expression of off-target genes MED13L and PIGQ in ESK+ CD19+ cells, when compared wo ESK-/CD19+ cells (Figure 3.8).

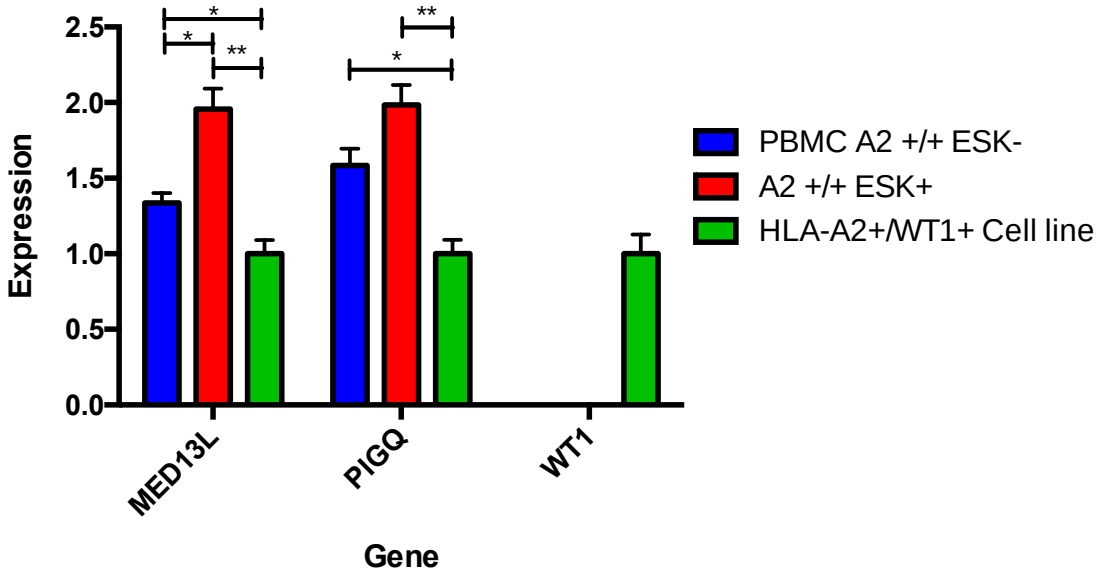

Figure 3.8. Gene expression of MED13L, PIGQ, and WT1 in PBMC with low and high binding of ESK1. PBMC from a normal healthy donor were taken and sorted for CD19+ ESK- and ESK+ populations by FACS. RNA was extracted and qPCR for MED13L, PIGQ, and WT1 genes was performed and normalized to TBP.

DISCUSSION

TCRs with moderate affinity (K_d = 1–100 μM) to antigens are produced in the body and provide the basis for a number of therapeutic agents, including soluble TCR-based constructs, TCR engineered cells, and peptide vaccines. TCR-based drugs have several potentially serious limitations. One is their restriction to a specific HLA subtype, reducing the potential patient population that may benefit from the therapeutic approach to a small fraction of afflicted patients. An additional limitation is cross-reactivity of typically low affinity TCRs to other peptide epitopes presented by MHC molecules that has resulted in severe toxicity in human trials(135). The current state of the art of antibody engineering is more advanced than with TCRs, allowing for greater structural and binding diversity. Here we present the first use of structural and biochemical characterization of the interaction of a TCRm antibody to its cognate pMHC epitope in an effort to investigate and overcome both these limitations.

An essential feature in the development of a TCRm is high specificity to the molecular complex of both the MHC molecule and presented peptide simultaneously, as mAb reactivity with the MHC alone would confer reactivity with every nucleated cell. Phage display can produce much higher-affinity TCRm antibodies such as ESK1 than occurs *in vivo* with TCRs, while simultaneously selecting against antibodies that may cross-react with the MHC complex alone. Second, the high affinity of TCRm antibodies allows pharmacologic dosing and retention of the drug at the cancer cell site *in vivo*.

The TCRm, ESK1, binds with subnanomolar affinity, over 1000-fold more tightly than natural TCRs. Our data demonstrate the molecular basis for both the specificity and the affinity of ESK1.

Surprisingly, the high-affinity binding was mainly driven by interactions between the antibody and HLA receptor that are restricted to regions identical with or similar between at least six common HLA-A*02 subtypes that vary in different ethnic groups worldwide. This result led us to hypothesize that ESK1 could bind to the same WT1 peptide epitope when presented by various other HLA-A*02 subtypes in addition to HLA-A*02:01. Experimental confirmation of ESK1 binding to these HLA-A*02 variants extends the potential scope of ESK1 therapy to millions of additional patients. In addition to its pharmacologic advantages, this unexpected finding shows that the use of a TCRm therapy may be a novel strategy to overcome the limits of HLA-subtype restriction of typical TCR-based therapy and therefore have broader therapeutic applications.

Naturally occurring TCR can bind off-target peptides(161, 162). We were able to use the structural information to predict potential cross-reactive peptides of ESK1 in humans. When bound to the HLA receptor, ESK1 primarily interacts with the N-terminus of RMF. As a consequence, other peptides expressed in humans that are homologous to the N terminus of RMF and that bind to HLA-A*02 with the anchor residue at position 9 but that differ at positions 5–8 in the C terminus might be ESK1 off-targets. We confirmed that such peptides in complex with HLA-A*02:01 can bind to ESK1 on peptide-

pulsed T2 cells*in vitro*. Thus, it may be possible to account for both structure and potential off-targets using a bioinformatics approach as we have shown with ESK1 mAb with WT1/HLA-A*02:01. The determination of whether these alternate targets are processed and expressed on the surface in normal tissues would be challenging, but identification of these targets in advance of clinical trials may allow for appropriate prospective clinical observation. In conclusion, we demonstrate for the first time that detailed, integrated structural, genetic, and biochemical analysis can provide a platform for appropriate selection and stratification of patient in efforts to maximize treatment efficacy and minimize toxicity. As such, this structure-based approach may serve as a key step toward personalized and precision medicine.

Acknowledgments

We thank Aina Cohen (SSRL) for assistance with diffraction data collection. This work was supported by University of Hawaii startup funds (H.L.N.), the Leukemia and Lymphoma Society (D.A.S.), National Institutes of Health (NIH) grants R01CA55349 (D.A.S.) and P01 23766 (D.A.S.), NIH National Institute of General Medical Sciences Medical Scientist Training Program grant GM007739 (E.J.B.), NIH National Institute of General Medical Sciences grants P41GM103393 (D.A.S.) and P30 CA008748 (D.A.S.), and the Major Family Fund (D.A.S.). Use of the Stanford Synchrotron Radiation Lightsource, SLAC National Accelerator Laboratory, is supported by the U.S. Department of Energy, Office of Science, Office of Basic Energy Sciences under Contract No. DE-AC02-76SF00515. The SSRL Structural Molecular Biology Program is supported by the Department of Energy, Office of Biological and Environmental Research.

CHAPTER 4: IDENTIFYING AND BYPASSING MECHANISMS OF RESISTANCE TO ESKM IN ACUTE LEUKEMIA[3,4]

INTRODUCTION

Previous work has demonstrated that ESKM is an effective mAb for the treatment of acute leukemias, including both ALL and AML. Widespread expression of WT1 is seen in multiple cancers, including both ALL and AML. Limited expression in normal tissues has also been observed, making WT1 an attractive target. Much work has been dedicated toward targeting WT1, either through vaccination with peptides derived from WT1, or adoptive T-cell therapy with TCR directed toward WT1+ tumors presenting peptides on MHC-I.

Work in our group has shown that a TCRm mAb directed toward WT1 is an effective therapeutic strategy to treat acute leukemias. ESKM is a TCRm that targets a specific 9 amino acid epitope, RMFPNAPYL, derived from the oncoprotein WT1 that is presented on HLA-A02+ tumors. This has shown to be effective in treatment both in vitro and in vivo against human acute leukemias. While initial response is seen to ESKM, it is not curative even under continuous therapy. Thus, further investigation into strategies that may

[3] Modified from Dubrovsky LD, Pankov D, Brea EJ*et al*. Blood. 2014 and Dubrovsky LD, Brea EJ, *et al.* Submitted 2016

[4] Some experiments were designed and conducted by or in collaboration with Leonid Dubrovksy and Dmitry Pankov as noted in the text.

lead to synergy between ESKM and targeted therapy or immunotherapy is warranted.

Acute lymphoblastic leukemia contain a fusion BCR-Abl protein, from the t(9:22) translocation, also referred to as the Philadelphia translocation (Ph+) in up to 20% of cases in adults, and 5% in children(83). The BCR-Abl fusion protein is necessary for oncogenic transformation and hyperproliferative phenotype of leukemia cells containing this translocation, making it an attractive theapetuic target. Imatinib was approved by the FDA for treatment of Ph+ chronic myelogenous leukemia, but this treatment was also tested in Ph+ ALL as well. Responses were not as drastic or durable in ALL as CML with Ph+ translocation, but more potent BCR-Abl inhibitors such as dasatanib are currently approved as part of therapy in Ph+ ALL(163).

We predicted that use of BCR-Abl inhibitors such as dasatanib, which demonstrated activity in ALL could be useful as a combination therapy with ESKM in BCR-Abl+ WT1+ leukemias. ESKM has shown to be effective in treatment of th BCR-Abl translocated, WT1+ cell line BV173 (50).

Mechanisms of resistance to ESKM

While use of kinase inhibitors in combination with ESKM has shown potential for cure of disseminated leukemia in murine xenograft models of human ALL, no specific FDA approved kinase inhibitors are available for AML. We showed activity of ESKM in vitro and in vivo against human AML cell lines and patient derived xenografts (50, 130). While response to ESKM was seen against the

AML cell lines in vivo, responses were not durable and the leukemia quickly escaped ESKM therapy.

We evaluated mechanisms of ESKM resistant to leukemias by examining whether the leukemia cells downregulated target, alteration of sensitivity to ESKM mediated killing in vitro, and paucity of effector cells available for ADCC mediating killing. Downregulation of target has been seen previously in resistance to antibody therapy in the case of rituximab for non-Hodgkins lymphoma (164). Resistance due to downstream mutations of a receptor have been seen with antibodies such as cetuximab in colorectal cancer(165). Polymorphisms in Fc receptor encoding gene FcϒRIIIahas also been linked to lack of efficacy of antibodies(166). Lack of effectors has also been seen as a mechanism of resistance or failure of antibody therapy.

ESKM has activity solely through antibody dependent cellular cytotoxicity, and lacks complement mediated cytotoxicity or direct killing ability in the absent of human effector cells such as neutrophils, macrophages, and NK cells(50). Activity of ESKM can be increased by a defucosylated Fc enhanced variant in comparison to the ESK-1 with normal fucosylation (130).

We therefore proposed looking at mechanisms of resistance to ESKM. We utilized an immunodeficient mouse strain lacking B cells, T cells, and NK cells, with macrophages and neutrophils as the main effector cells. This allowed us to study resistance to ESKM and discover approaches to enhance sensitivity as combination therapy.

MATERIALS AND METHODS

ADCC

ADCC was evaluated by chromium release assay, incubating target cells in 50 µCi Cr^{51} for 1 hour before 3 washes, with the determined optimal ADCC time of 6 hours. Three effector to target (E:T) ratios were used (either 10:1, 30:1, and 100:1 or 25:1, 50:1, and 100:1). Effector peripheral blood mononuclear cells (PBMCs) were derived from healthy donors by Ficoll density centrifugation, after obtaining informed consent on a Memorial Sloan-Kettering institutional review board–approved protocol. This study was conducted in accordance with the Declaration of Helsinki.

One to three day ADCC assay was performed by incubating healthy donor PBMCs isolated by Ficoll with target leukemia cells at E:T 50:1 and 25:1 in triplicate. Treatment groups had ESKM added to media at 3 µg/ml, while control groups had no antibody added. The SET2 cells used in these assays were GFP tagged, and flow cytometry was utilized to measure the concentration of live (DAPI negative) GFP positive cells in solution compared to total number of cells. Constitutively on GFP was transduced with a lentiviral GFP vector specifically for the purpose of easily identifying these cells in the *in vitro* ADCC assays.

BV173R Synthesis

The BV173R cell line was engineered to harbor the T315I BCR-ABL using a Clonetech pMSCV Puro vector with the T315I BCR-ABL gene, a kind gift from Charles Sawyers (167). BV173-luc-gfp cells were transduced with the retroviral vector, selected, and expanded in media with puromycin. The presence of the resistant T315I mutation was confirmed by polymerase chain reaction (PCR) for the plasmid, as well as ABL sequencing of cDNA and genomic DNA in the resultant BV173R cell line.

Flow cytometry

Fortessa flow cytometer (BD Biosciences) was utilized for all flow cytometry measurements. Evaluation of ESKM binding to target cells and cell surface HLA-A*02:01 expression was done by direct flow cytometry. ESK was labeled with APC using the Innova Biosciences Lightning-Link Allophycocyanin (APC) kit.

For both *in vitro* and *in vivo* studies, APC or PE tagged BB7 antibody (BioLegend) was utilized to measure HLA-A02 expression on cell surface. After mouse BM resection in xenograft models, APC-tagged ESK1 antibody (Innova Biosciences - Lightning-Link® Allophycocyanin), was used to measure RMF expression on cell surface. Xenografted SET2 cells were identified by CD33-BV711, and BV173 by CD19-PE (BioLegend). While the Xenografted SET2 and BV173 leukemia cells were both GFP positive, it was very dim in

the cell lines used for *in vivo* studies, and was therefore not used for flow cytometry.

PCR analysis

Minimal residual disease of cell lines in mouse bone marrow (BM) was evaluated using custom-made primers to the Firefly Luciferase gene with SYBR Green using GAPDH as a control.

Trials of ESKM with TKIs in vivo in mice

Trials of ESKM were done using xenograft models, in nonobese diabetic/severe combined immunodeficient (NOD/SCID) mice with IL2 γ receptor knockout (NSG) mice engrafted with BV173 Ph^+ leukemias. The BV173 and BV173R cell lines used for all in vivo studies stably expressed the firefly luciferase gene, and disseminated engraftment of leukemia was confirmed 6 days after tail vein injection by bioluminescent imaging (BLI) before treatments. Mouse research was approved by the MSKCC institutional review board under protocol 96-11-044.

Preliminary drug dosing studies in NSG mice demonstrated the maximum tolerated dose (MTD) of imatinib to be 50 mg/kg intraperitoneally (IP) daily, with higher dosing resulting in diarrhea and severe toxicity. Dasatinib was also initially tested, with the MTD of 40 mg/kg (0.8 mg/mouse) resulting in no appreciable short-term toxicity. However, longer-term trials of dasatinib resulted in mouse sudden deaths, and the dose was therefore lowered for

subsequent experiments to 20 mg/kg and then to 10 mg/kg to eliminate drug-related mortality. For mice receiving ponatinib, the initial published dose of 5 mg/kg showed inadequate leukemic affect without any evident health side effects, and therefore ponatinib doses were increased to 10 mg/kg. At this dose, toxicity was comparable with 50 mg/kg of imatinib, with intermittent diarrhea and poor growth.

All TKIs, including imatinib, dasatinib, and ponatinib, as well as plerixafor, were purchased from Selleckchem or Fisher Scientific. The plerixafor stock solution was made in phosphate-buffered saline at 200 µg/mL and stored at room temperature. Mice received 1 mg/kg (20 µg/mouse) daily by IP injection, as was used in previous studies(168). No toxicity was noted during therapy. Before its use in vivo, stock solutions of TKIs were prepared in dimethyl sulfoxide (DMSO), with the scheduled dose of TKI in 50 µL DMSO per mouse. All TKIs and ESKM treatments were administered IP at these schedules: ESKM 100 µg twice weekly and TKIs daily. Male NSG mice, aged 6 to 8 weeks, were purchased from Jackson Labs(169). Three million leukemic cells (BV173 or BV173R) were injected per mouse by tail vein on day 0. Luciferin/luciferase BLI was then performed on day 6, with therapy commencing immediately after confirmation of equivalent levels of disseminated leukemia by imaging. IVIS 200 and IVIS Spectrum machines were used for BLI.

ESKM therapy in vivo

Luciferase tagged SET2, BV173, and SET2-S cell lines were used in all xenograft models, and leukemia growth was measured by bioluminescent imaging (BLI) using the IVIS Spectrum, with intraperitoneal luciferin injections 5 minutes prior to imaging. Day 0 of studies were defined as day of leukemia injection by tail vein. Because no differences were noted in therapeutic effect between biweekly ESKM dosing of 100 µg and 50 µg per dose, 50 µg ESKM biweekly IP were used in these studies. GM-CSF was dosed at 1 µg, administered daily IP. For SET2-S cell line experiments, the two experimental groups of five mice each were administered doxycycline via food pellets (625 mg/kg) (Harlan-Teklad) starting on day 6 and continued until the end of the experiment.

Cloning, vector construction, and purification of SET2-S

The 3rd generation lentiviral vector pLV was obtained from VectorBuilder (Santa Clara, CA, USA) and the human CDKN1B (p27kip) cDNA was cloned was under the TRE3G inducible promoter with a C-terminal FLAG tag and IRES for expression of tdTomato. The pLV vector also had constitutive expression of rtTA3 under the CMV promoter. HEK293T cells were used to produce lentiviral particles using the pRSV (Addgene #12253), pMDL (Addgene #12251), and pMD2.G (Addgene #12259) vectors along with the CDKN1B gene (coding for $p27^{Kip1}$ protein). Viral supernatant was harvested from HEK293T cells and used to transduce SET2 GFP-Luciferase expressing

cells using spinfection at $1x10^6$ cells in 8 µg/ml polybrene with viral supernatant at 2000x g, 2 hours, for two rounds on transduction. A clonogenic assay was set up to insure 100% purity of transduced SET2-S cells. Colonies positive for tdTomato after 2 µg/ml doxycycline induction were pooled and expanded for downstream use.

Flag-tag specific antibody used in Western blot assay were purchased from Cell Signaling Technologies (#14793). Doxycycline was obtained from Sigma. SET2 stably transduced with CDKN1B were exposed to increasing doses of doxycycline for 48 hours and 96 hours. Cell-Titer Glo (Promega) was performed at indicated time points to assess viability. Flow cytometry studies for tdTomato expression was performed on the Accuri C6 flow cytometer (BD Biosciences). Flow cytometry for ESKM binding was performed using ESK conjugated with APC fluorophore. Cells were stained with 3 µg/ml ESK-APC for 45 m on ice. DAPI was used for viability assessment. Cells were analyzed using the Fortessa flow cytometer (BD Biosciences)

RESULTS

ESKMtherapyofPh$^+$ ALLinNSGmice

Imatinib is a tyrosine kinase inhibitor that targets Ph+ BCR-Abl. BV173 is a human ALL cell line confirmed to have Ph$^+$ BCR-Abl translocation, and is also HLA-A*02:01$^+$(170).BLI confirmed engraftment of luciferase-tagged BV173 Ph$^+$ ALL in NSG mice 6 days after tail vein injection. Mice were randomly assorted into 4 groups: no therapy, imatinib only, ESKM only, or a combination therapy. ESKM therapy was superior to imatinib therapy after 5 weeks of therapy (78% vs 52% tumor growth reduction, $p< .01$) (Figure 4.1A).The combination of ESKM and imatinib was superior tosingle agent therapy ($P < .001$), decreasing tumor growth by 94% (Figure 4.1B) BV173 cells were isolated from bone marrow and analyzed by flow cytometry for HLA-A expression and ESKM binding immediately after completion of therapy (Figure 4.1C), with detectable BV173 cells in all groups.

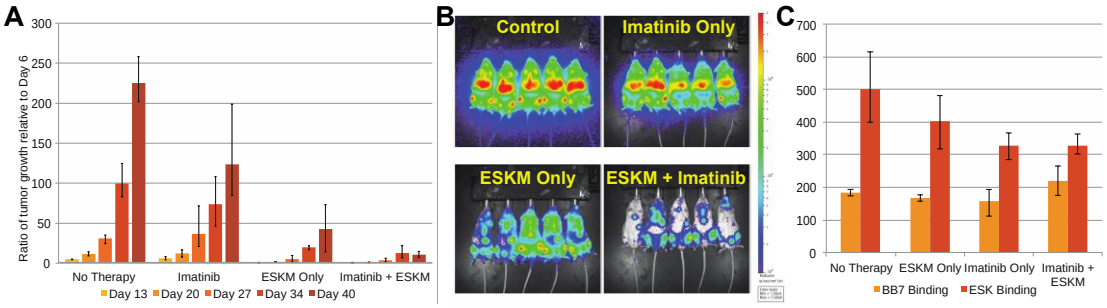

Figure 4.1. BV173 human ALL xenograft NSG mouse model with combination imatinib and ESKM at optimal efficacious doses. Mice received 5 weeks of 100 ug ESKM bw, 50 mg/kg imatinib qd, combination therapy, or no therapy (control). Error bars show 5th and 95th percentiles. **A.** Leukemic growth as measured by bioluminescent imaging for each of the four groups of mice. **B.** BLI at end of therapy (5 weeks of therapy) for each of the four groups of mice. **C.** Flow cytometry for HLA-A02 and ESK binding. Three out of five mice where randomly chosen from each of the four groups. BM was harvested and cells were evaluated by flow cytometry. Cells were gated on human CD19+ population and evaluated for BB7.2 (HLA-A*02:01) and ESK binding (Conducted by L. Dubrovsky).

ESKM therapy in combination with dasatanib

Dasatinib is a more potent FDA approved second-generation TKI of Abl than imatinib with activity (171).Similar to as was evaluated for imatinib, dasatinib was administered at 40 mg/kg qd IP in combination with ESKM. The combination therapy lead to durable response and molecular remission in 75% of mice (**Figure 4.2**), which was confirmed by quantitative PCR of bone marrow 3 weeks after the end of therapy (Table 4.1 MRD < 0.001%). No remissions were seen in mice treated with single agent therapy. The single mouse treated with combination ESKM and dasatanib that relapsed had CNS tumor burden. This is notable because antibodies do not readily enter the CNS (172). At this dasatinib dose, all mice receiving the TKI became ill about 1

week into therapy, with 1 mouse fatality on day 8 of treatment. All dasatinib-treated mice sustained temporary BLI remissions, but those not treated with ESKM relapsed 2 to 3 weeks after cessation of therapy.

Table 4.1. MRD from NSG mouse bone marrow. Quantitative PCR for the luciferase gene from mouse bone marrows of three mice treated with combination therapy ESKM and dasatanib whose images were negative on BLI 3 weeks after end of therapy with high dose dasatinib for 11 days and concurrent ESKM for 4 weeks. The positive control mouse was treated with dasatinib only and had positive BLI signal (relapsed). BV173 cells mixed with healthy donor cells (negative for luciferase gene) at known ratios and qPCR done on mixture as control.

Sample	**Calculated Gene Expression**
BV173 cells 100% positive Control	**100.00%**
BV173 1% cells positiveControl	**0.37%**
BV173 0.01% cells positiveControl	**0.02%**
Cell Line Negative Control	**<0.001%**
ESKM + Dasatinib treated Mouse #2	**<0.001%**
ESKM + Dasatinib treated Mouse #3	**<0.001%**
ESKM + Dasatinib treated Mouse #5	**<0.001%**
Dasatinib alone treated mouse positive Control	**2.22%**

Figure
4.2 CombinationtherapywithESKManddasatanibshowssuperioritytoimatinibintreatmentofxenograftmodelofALL. Errorbarsshow 5thand 95thpercentiles. (A) BV173 growthmeasuredbyBLIinmicetreatedwithhighdosedasatinibtherapy (40 mg/kgqdfor 8 daysthenreducedto 20 mg/kgx3 daysforatotal 11 daysoftreatmentandthendiscontinuedsecondarytohightoxicity), ESKMonlyfor 4 weeks, combinationtherapyandcontrol (notherapy). (B) BLIonDay 55, 3 weeksafterendoftherapy. Mouse #1 incombinationdasatinibwithESKMdiedsecondarytodasatinibtoxicityonDay 13, andmouse #4 appearstohaverelapsedinCNS. (C) HighdosedasatinibplusESKMgroupBLIimages, showingprogressionofrelapseinmouse #4. (D) LeukemicgrowthmeasuredbyBLIinmicetreatedwithdasatinibtherapyat 20 mg/kgqdfor 18 days, thendiscontinuedduetohightoxicity. ESKMwasgiventosixmice (day 18 today 42). Allmicerelapsed, thoughESKMmicerelapsedwasdelaryedsignificantlyandprolongedlifespanby 1 week. Lastdatapointpertainstowhenmiceweresacrificedduetoillness. (E) BLIattheendofESKMtherapy (day 42). MicereceivedESKMfollowingdiscontinuationofdasatinib (Dasatinib→ESKM 1 and 2) andcomparedtoonecage (5 mice) thatreceivednoadditionaltherapy. ESKMsalvagedmicehavesubstantiallylesstumorburdenthendasatinibonlymice. Allmicerelapsed (Conducted by L. Dubrovsky).

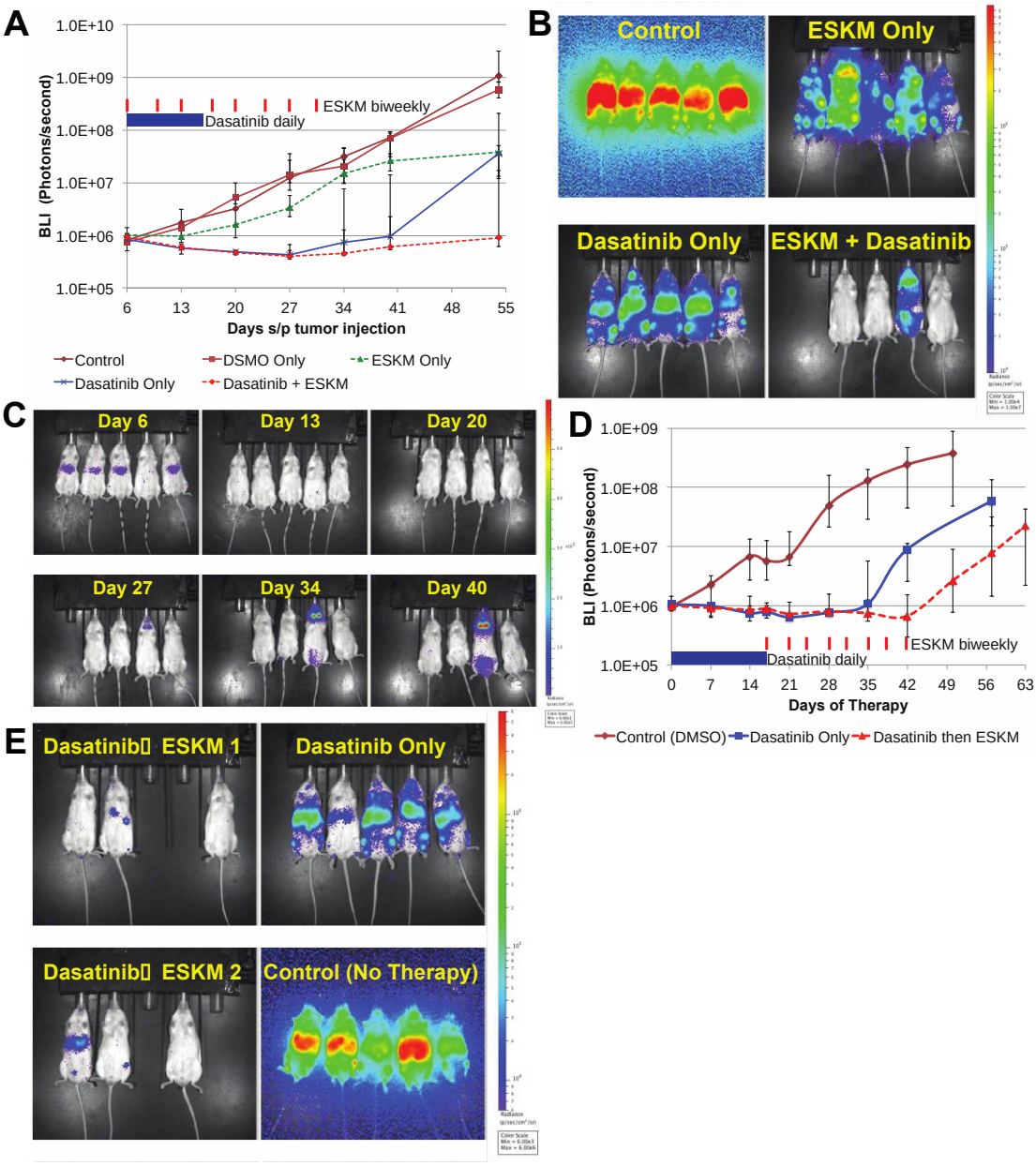
A
1.0E+10
1.0E+09
1.0E+08
1.0E+07
1.0E+06
1.0E+05
BLI (Photons/second)
ESKM biweekly
Dasatinib daily
6
13
20
27
34
41
48
55
Days s/p tumor injection
Control
DSMO Only
ESKM Only
Dasatinib Only
Dasatinib + ESKM
B
Control
ESKM Only
Dasatinib Only
ESKM + Dasatinib
C
Day 6
Day 13
Day 20
Day 27
Day 34
Day 40
D
1.0E+09
1.0E+08
1.0E+07
1.0E+06
1.0E+05
BLI (Photons/second)
ESKM biweekly
Dasatinib daily
0
7
14
21
28
35
42
49
56
63
Days of Therapy
Control (DMSO)
Dasatinib Only
Dasatinib then ESKM
E
Dasatinib ESKM 1
Dasatinib Only
Dasatinib ESKM 2
Control (No Therapy)

Therapy of T315I Resistant Ph+ Leukemia Therapy

BV173R (TKI resistant T315I mutant) leukemia xenografted NSG mice were initially treated with ESKM, imatinib, dasatinib and concurrent combinations of imatinib plus ESKM and dasatinib plus ESKM. Only 3 weeks of therapy were given, as the leukemia proved resistant to the first andsecond generation TKIs. In contrast, ESKM retained full and equivalent efficacy against the resistant BV173R leukemia compared to TKI sensitive leukemia BV173 (Figure 4.3A) as quantified by luciferase imaging during treatment. These findings are consistent with *in vitro* studies indicating that in ADCC assays, ESKM is as active against BV173R as it is against BV173 (Figure 4.3B). Dasatinib provided only modest slowing of leukemic growth with leukemic burden rising five-fold over the same time period. The combination of ESKM and dasatinib showed substantial reduction in leukemia burden, though no mice were cured. As in the prior experiments with BV173 treated with the combination ESKM plus dasatinib, relapse was *lymphoidtumors* rather than diffuse leukemia (Figure 4.3C).

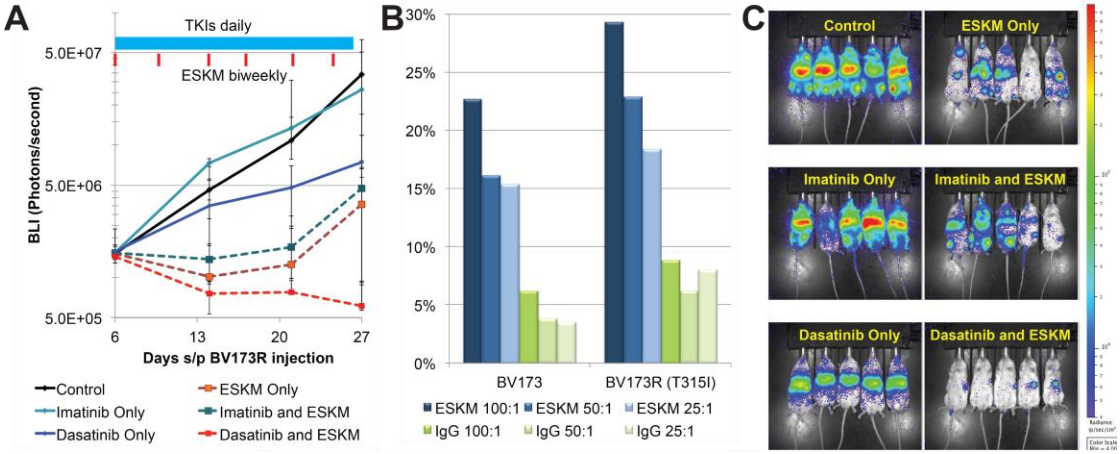

Figure 4.3. BV173R (with T315I mutation) treated with dasatinib 10 mg/kg and imatinib 50 mg/kg qd IP for 21 days with and without biweekly ESKM therapy (6 doses of ESKM). Error bars show 5th and 95th percentiles. **A.** Exponential growth curves, from start of therapy (day 6). The blue bar shows duration of TKI therapy and the red lines are doses of ESKM. **B.** The susceptibility of cell line BV173, resistant cell line BV173R (with BCR-ABL T315I mutation) to ESKM directed ADCC with human PBMCs and different effector to target ratios.**C**. BLI imaging at the end of ESKM/TKI therapy (day 27). ESKM is superior to imatinib and dasatinib for treatment of resistant Ph+ ALL (Conducted by L. Dubrovsky).

NSG mice engrafted with this T315I Ph+ resistant leukemia were then treated with the third generation drug, ponatinib. Leukemic regression was seen in all ponatinib treated mice, with negative BLI showing no disease at the end of therapy on day 34 (Figure 4.4A). Mice treated with ponatinib monotherapy subsequently developed systemic leukemic relapse within two weeks after end of treatment, while those treated with the combination of ESKM and ponatinib developed either *focal lymphoid* relapse (3/5), or had no evidence of disease (2/5) 4 weeks after completion of therapy (Figure 4.4B).

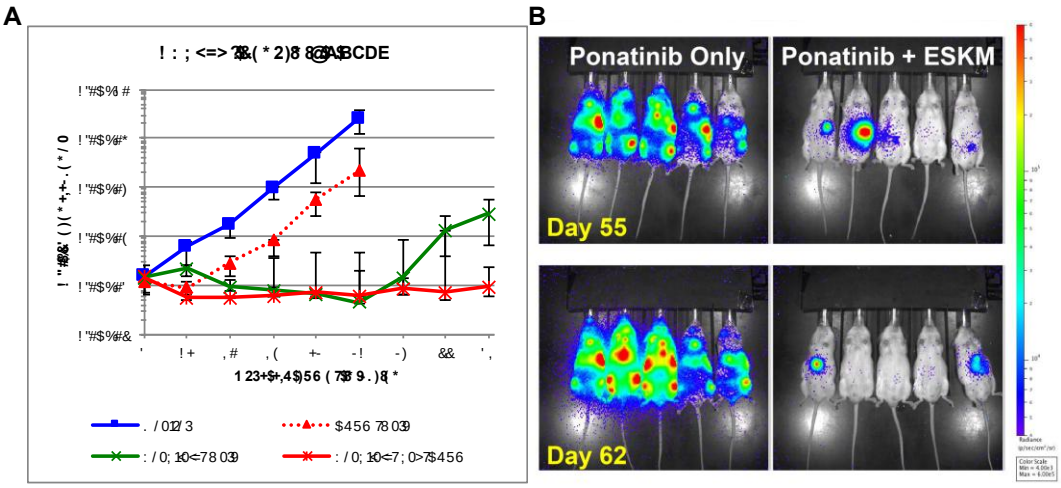

Figure 4.4. BLI of NSG mice engrafted with resistant T315I cell line BV173R. Therapy with ponatinib and ESKM began on day 6 after injection, and ponatinib dose was escalated from 5 mg/kg to 10 mg/kg on day 13 secondary to initial lack of side effects. All treatments ended on day 34. **A**. Median BLI values for all four treatment groups, with error bars indicating 5 – 95% confidence intervals. **B**. BLI imaging for ponatinib and ponatinib + ESKM treated mice 3 and 4 weeks after conclusion of therapy. All ponatinib-alone mice have diffusely relapsed leukemia, while combination therapy mice have focal tumor relapse or no evidence of disease by BLI. Mouse #2 showed no signal on day 62, which was an error in injection of luciferin(Conducted by L. Dubrovsky).

In Vivo Leukemia Growth Characterization and Resistance to ESKM

While ESKM was notably efficacious in Ph+ ALL, which allows for combination with TKI such as imatanib and dasatanib which can lead to durable response in xenograft models, AML has proven more difficult to treat in xenograft mouse models with ESKM.

The AML cell line SET2 grows as discrete tumor cells in the BM (Figure 4.5AB). Initial treatments of SET2 with ESKM resulted in modest, short-lived therapeutic effects (Figure 4.5C). Increasing E:T ratio by decreasing the number of injected SET2 cells from 3 x 10^6 to 0.5 x 10^6 per mouse improved

initial cytotoxicity, but ultimately did not prevent rapid leukemic overgrowth. Increasing E:T further with GM-CSF did not increase ADCC/ADCP potency in this model (Figure 4.5D).

Pre-treatment of mice with ESKM prior to injection of leukemia, which should provide a situation of maximum effector to target ratio, did not change outcome when compared to therapy on already engrafted SET2 cells in the mouse BM (Figure 4.5E). Furthermore, after the first week of ESKM therapy, additional mAb doses had minimal efficacy of slowing leukemic growth (Figure 4.5F), implying the outgrowth of a resistant clone or the failure of therapy after leukemic overgrowth past a certain tumor burden.

Figure 4.5. SET2 cell line engrafted xenograft NSG mouse model growth patterns. Error bars: 5^{th} to 95^{th} percentile. All BLI imaging and growth curves use exponential scale. **A.** IHC for CD33, outlining discreet SET2 cells in mouse BM with no therapy, 3 weeks after injection. **B.** CD33 IHC of SET2 cells in mouse BM 3 weeks after injection on 2 weeks of ESKM therapy (started on day 6). **C.** *In vivo* SET2 growth quantification by BLI over time, with 3×10^6 cells injected on day 0, with and without ESKM therapy. **D.** *In vivo* SET2 growth quantification by BLI over time with and without ESKM therapy. Effector to target ratios are increased from (c) with only 5×10^5 cells injected on day 0 and the addition of GM-CSF. **E.** SET2 growth by BLI quantification, comparing starting ESKM after leukemic BM engraftment (on day 6) to leukemic growth in ESKM pre-treated mice (ESKM injected 2 hours prior to injection of SET2). **F.** SET2 growth by BLI quantification comparing 4 weeks of continuous (bi-weekly) ESKM therapy to only 1 week of treatment(Conducted by L. Dubrovsky).

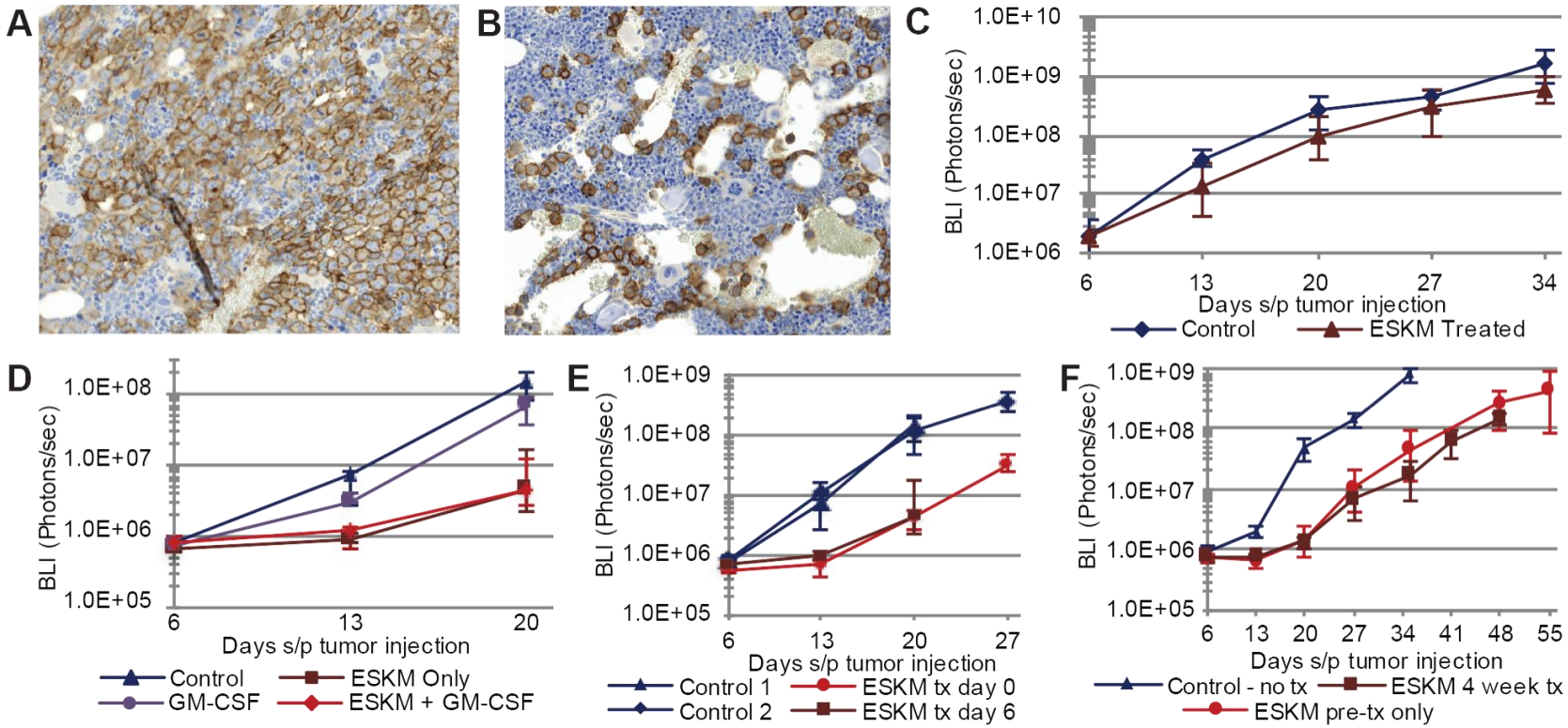
A
B
C
1.0E+10
1.0E+09
1.0E+08
1.0E+07
1.0E+06
BLI (Photons/sec)
6
13
20
27
34
Days s/p tumor injection
Control
ESKM Treated
D
1.0E+08
1.0E+07
1.0E+06
1.0E+05
BLI (Photons/sec)
6
13
20
Days s/p tumor injection
Control
ESKM Only
GM-CSF
ESKM + GM-CSF
E
1.0E+09
1.0E+08
1.0E+07
1.0E+06
1.0E+05
BLI (Photons/sec)
6
13
20
27
Days s/p tumor injection
Control 1
ESKM tx day 0
Control 2
ESKM tx day 6
F
1.0E+09
1.0E+08
1.0E+07
1.0E+06
1.0E+05
BLI (Photons/sec)
6
13
20
27
34
41
48
55
Days s/p tumor injection
Control - no tx
ESKM 4 week tx
ESKM pre-tx only

Selection of germline or epigenetic durable resistance *in vivo* and *in vitro*

SET2 cells harvested from mouse BM likewise did not down regulate the target antigen as measured by flow cytometry or HLA-A02 (Figure 4.6AB). However, these data do not rule out other forms of intrinsic resistance such as the outgrowth of an ADCC/ADCP resistant clone. Therefore, SET2 cells were extracted from the BM of ESKM treated and untreated mice, and then passaged in naive NSG mice. The resistant tumor cells extracted from the ESKM treated mice showed no durable resistance to renewed ESKM therapy compared to their untreated counterparts (Figure 4.6C).

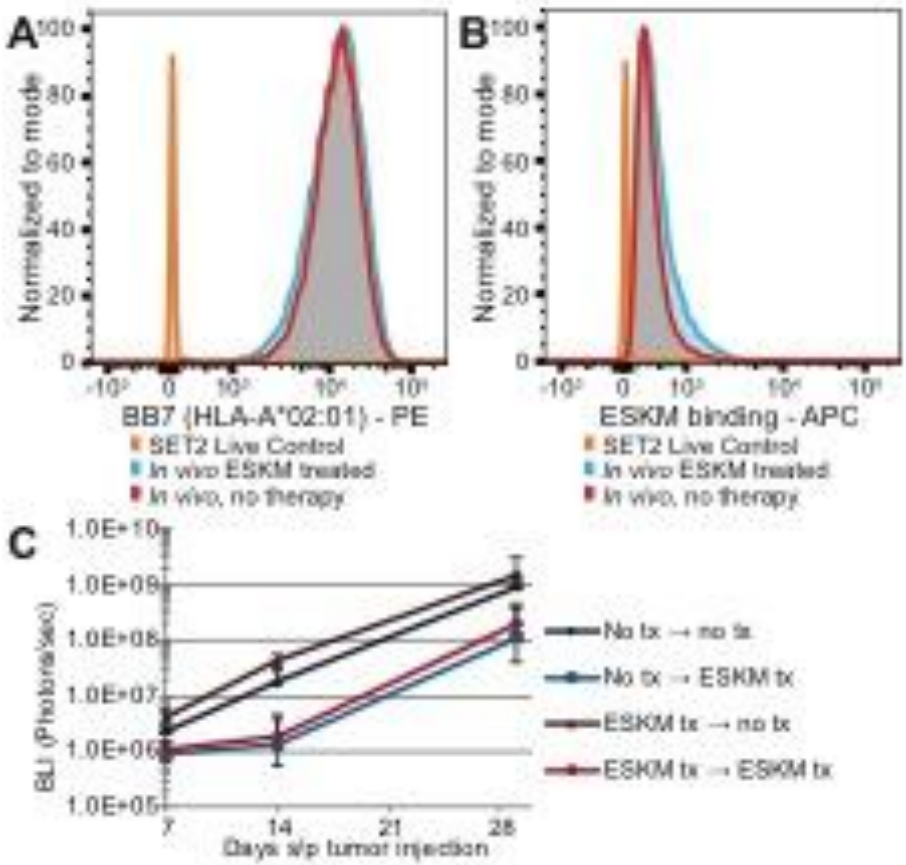

Figure 4.6. SET2 cell evaluation status-post harvest from murine BM. **A.** Flow cytometry for surface HLA-A*02:01 expression, showing no difference between SET2 cells harvested from control mice and those treated with ESKM. **B.** Same cells as in (a), evaluating for ESKM binding, showing no difference between cells extracted from ESKM treated and untreated mice. **C.** SET2 cells from ESKM treated and untreated mice were harvested and passaged into a secondary group of mice. Ten initial mice (5 control, 5 treated) had BM harvested, and the SET2 cells extracted by Ficoll from each mouse were injected into two mice, (a control mouse and an ESKM pre-treated mouse). Error bars: 5th to 95th percentile. BLI growth curve utilizing exponential scale.

We also explored whether resistance to ADCC could be selected for in vitro, using healthy volunteer PBMCs as effectors and SET2 target cells. A three day ADCC assay with E:T 25:1 was set up, with flow cytometry used to evaluate cytotoxicity and HLA expression. No plateau in killing of SET2 was

observed, and HLA-A*02 expression actually increased, likely due to cytokine release by the effector cells (Figure 4.7A-B).

Increasing E:T to 50:1 greatly improved cytotoxicity overnight to 93.1% (± 0.9%, 5%-95% confidence). To definitively assess whether a resistant SET2 clone existed in this model, SET2 cells were exposed to 2 days of ADCC with E:T 50:1. The reaction was then quenched by killing the effector cells with puromycin (to which the SET2 target cells were made resistant). The remaining cells then underwent a second 18 hour ADCC with E:T 50:1, and results were compared to SET2 with PBMCs without ESKM. The pre-treated SET2 cells remained susceptible to ADCC with 97.8% cytotoxicity, and no evidence of target loss (Figure 4.7C). These results make treatment escape via selection and outgrowth of an intrinsically resistant SET2 clone very unlikely. Rather, a kinetic escape mechanism is strongly suggested.

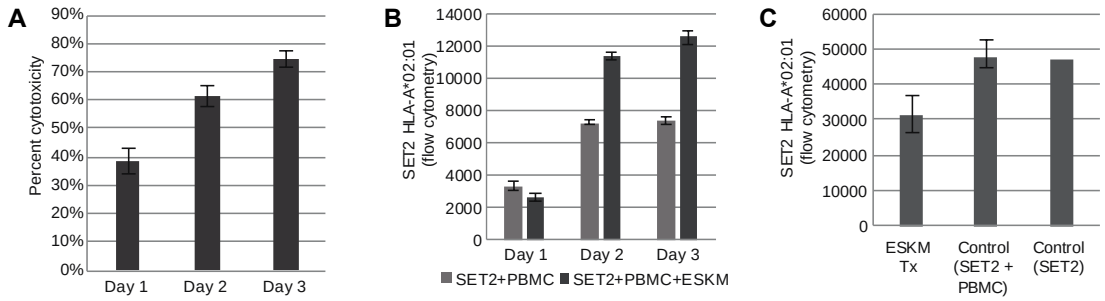

Figure 4.7. Lack of outgrowth of resistant SET2 cells *in vitro*. Error bars: 5th to 95th percentile. **A.** 3 day ADCC: daily cytotoxicity as measured by flow cytometry. Effector to target ratio set at 25:1, with normal donor PBMCs used as effectors. Cytotoxicity measured as ratio of live SET2 cells with:without ESKM in media. **B.** Median HLA-A*02:01 cell surface expression of cells in (a) on days 1-3 of ADCC by flow cytometry. HLA-A*02:01 increases in cells exposed to PBMC with ESKM compared to SET2 cells with PBMC without ESKM likely due to inflammatory cytokines. **C.** Median surface HLA-A*02:01 expression by flow cytometry of passaged SET2 cells, status-post 2nd round of ADCC.

Slowing leukemia growth kinetics improved therapeutic efficacy

The evaluation of the kinetic escape hypothesis required the controlled slowing of leukemic growth without direct toxicity to the cell. This has been previously done in another model by inducing the overexpression of the cyclin-dependent kinase inhibitor p27^{Kip1} inducing cell cycle arrest without apoptosis[30]. We transduced SET2 with a doxycycline inducible vector coding for CDKN1B gene (coding for p27^{Kip1} protein). The SET2 p27^{Kip1} expressing cell line (SET2-S) responded to doxycycline mediated induction of p27^{Kip1} with dose dependent growth inhibition (Figure 4.8A-C). In the NSG mouse model, ESKM mediated ADCC was dramatically improved by slowing SET2-S growth

by $p27^{Kip1}$ overexpression (Figure 4.8D-E). $p27^{Kip1}$ overexpression alone slowed growth but was not therapeutically effective. A comparison of the doxycycline treated SET2-S growth *in vivo* with and without ESKM therapy demonstrates that even a modest slowing of leukemic growth results in dramatic increase in therapeutic effect (Figure 4.8E). Evaluation of this $p27^{Kip1}$ cell line by flow cytometry revealed no down regulation of ESKM binding with the overexpression of $p27^{Kip1}$ (Figure 4.8F). *In vitro* ADCC performed by chromium assay showed minimal differences in ESKM mediated toxicity of SET2-S between normal and high $p27^{Kip1}$ expressing cells (Figure 4.8G). The highly improved potency of ADCC/ADCP in these experiments in vivo appears to result from slower tumor growth, and therefore supports the hypothesis of kinetic escape mechanism of ADCC resistance.

Figure 4.8. SET2-S cell evaluation *in vitro* and *in vivo*. Error bars: 5th to 95th percentile. BLI imaging and growth curves use exponential scale. **A.** Western blot evaluating the protein expression of p27^{Kip1} measured using a FLAG specific antibody. **B.** Dose dependent growth inhibition of SET2-S cells *in vitro* with increasing doxycycline concentrations. **C.** Competition assay demonstrating decrease in population of SET2-S cells when compared to SET2 cells. SET2 and SET2-S cells were mixed 50:50 at t=0 hrs and 2 µg/ml doxycycline was added to the media. Expression of tdTomato, marking SET-S cells, was measured over time. **D.** BLI at the end of 3 weeks of therapy in NSG mouse model of SET2-S leukemia (day 28 status-post leukemic injection). Controls had injections of SET2-S cells and no therapy. ESKM treated mice received the antibody only on day 6 onwards. The other two groups got doxycycline alone or doxycycline with ESKM. **E.** A plot on log scale of the mice treated in panel D over one month. SET2-S *in vivo* growth, by BLI, evaluating ESKM ADCC with and without p27^{Kip1} overexpression, demonstrating clear superiority of ADCC treatment on slower growing SET2-S cells compared to wild type controls. **F.** Flow cytometry of SET2-S cells with and without doxycycline exposure, evaluating ESKM binding. **G.** ADCC of SET2-S with and without upregulation of p27^{Kip1}, activated by doxycycline exposure. The overexpression of p27^{Kip1} appears to stabilize SET2-S, decreasing the chromium release of both control and ESKM treated cells.

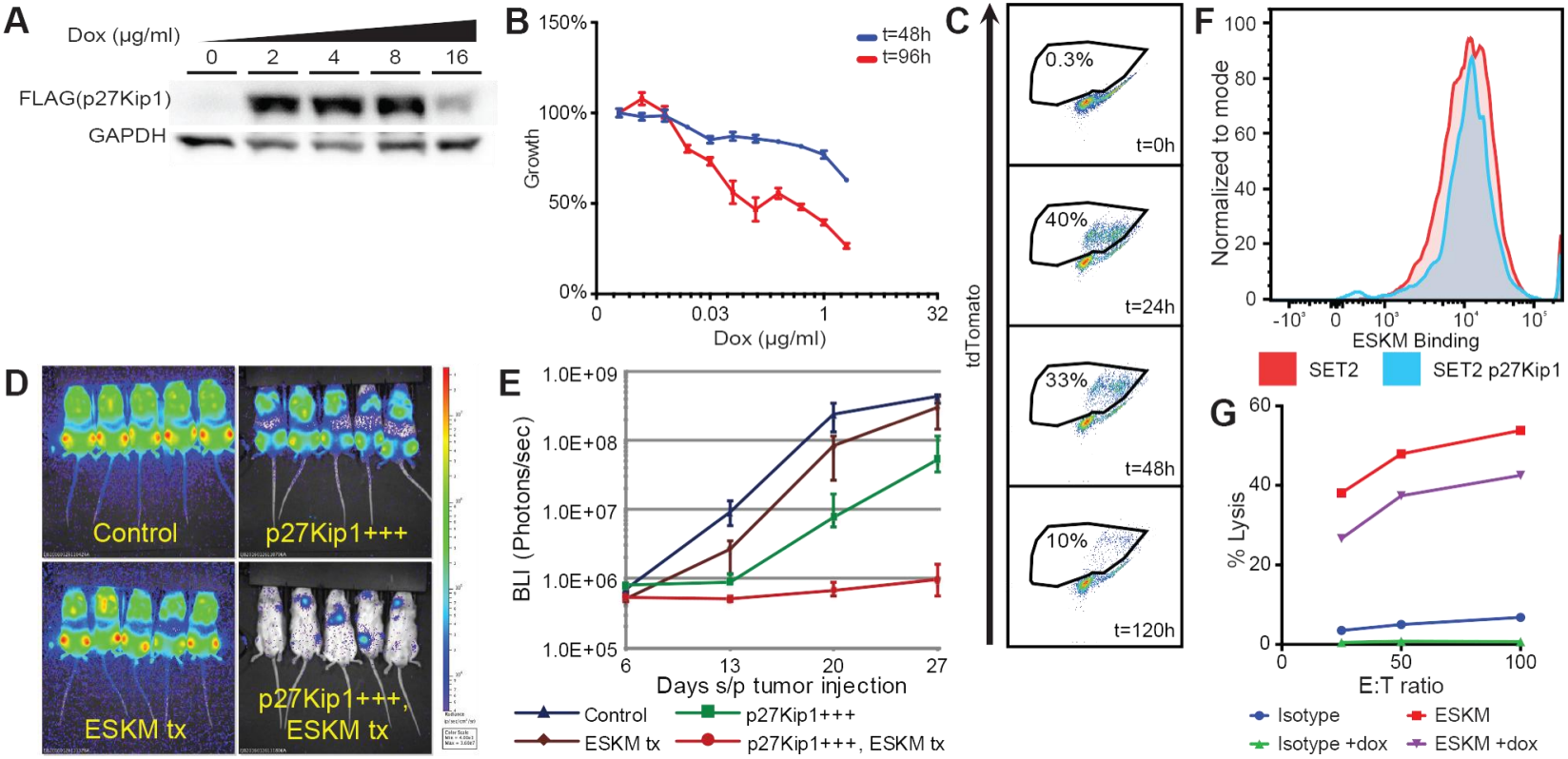
A
Dox (μg/ml)
0
2
4
8
16
FLAG(p27Kip1)
GAPDH
B
150%
100%
50%
0%
Growth
t=48h
t=96h
0
0.03
1
32
Dox (μg/ml)
C
0.3%
t=0h
40%
t=24h
33%
t=48h
10%
t=120h
tdTomato
F
100
80
60
40
20
0
Normalized to mode
-10³
0
10³
10⁴
10⁵
ESKM Binding
SET2
SET2 p27Kip1
D
Control
p27Kip1+++
ESKM tx
p27Kip1+++, ESKM tx
E
1.0E+09
1.0E+08
1.0E+07
1.0E+06
1.0E+05
BLI (Photons/sec)
6
13
20
27
Days s/p tumor injection
Control
p27Kip1+++
ESKM tx
p27Kip1+++, ESKM tx
G
60
40
20
0
% Lysis
0
50
100
E:T ratio
Isotype
ESKM
Isotype +dox
ESKM +dox

DISCUSSION

Antibody therapies are effective at targeting tumor specific antigens, modulating the immune system to increase immune cell mediated killing of tumor cells, or by blockade of oncogenic signaling pathways. One limitation of targeting tumor antigens is lack of therapeutic efficacy as a single agent modality. Other than mAbs that mediate the up-regulation of T-cell activity via checkpoint blockade, a mechanism of action completely independent of ADCC, most native mAb alone do not result in complete remissions or long-term survivals. Even more complex constructs, such as brentuximab vedontin, are used in combination or sequenced with chemotherapy(173). Other effective mAb, such as rituximab and trastuzumab, rely on additional mechanisms of action such as signaling blockade to inhibit cellular proliferation(174). The lack of mAb ADCC/ADCP potency is a significant limitation for this class of drugs, given the ability to specifically target a large number of new antigens. While combining antibody therapy with chemotherapy has improved outcomes, these two treatments may not synergize well in many instances, since chemotherapeutic agents can be naturally toxic to the effector cells required for ADCC.

ESKM as a therapy for BCR-Abl resistant ALL

ESKM is a potent mAb therapy that is not susceptible to tumor escape by gatekeeper mutations in the Abl domain, a known clinical mechanism of resistance to TKI targeting the BCR-Abl fusion (171). ESKM is also a therapeutically effective antibody in mouse models of other human leukemias

and solid tumors(128, 130). However, as monotherapy, the antibody was unable to achieve cures in these models. In combination, TKIs and ESKM did not exhibit enhanced toxicity, had at least an additive therapeutic effect and resulted in molecular cures of Ph+ ALL in mice. BM relapse of leukemia post treatment may reflect inadequate effector cells rather than loss of antigen, or local stromal cell protection, since RMF/HLA-A*02:01 was still expressed on leukemia cells at the end of therapy and reducing leukemic cell adherence to stromal cells with plerixafor did not significantly increase antileukemic activity.

The data support a more generally accepted hypothesis that mAb therapies would likely benefit from combination therapy to decrease cancer burden and keep cancer growth rates low, thereby fostering more effective ADCC *in vivo* at increased E:T ratios. Thus, patients with CML in remission on TKIs may be ideal candidates for ESKM treatment, since they have minimal residual leukemic burden and slow cancer growth. The main mechanism of escape of ALL for ESKM monotherapy seemed to be inadequate effector function, as target down-regulation and intrinsic resistance to ESKM mediated ADCC was not observed.

An important advantage to TCRm antibody therapy was its efficacy against pan-resistant Ph+ leukemias. First and second generation TKI's are not effective against leukemias that carry the BCR-ABL T315I resistance mutation. Such mutations occur in 12-15% of screened patients with CML and are a source of relapse and failure of treatment(175). While a third generation TKI, ponatinib, is effective in the presence of this mutation, its use is currently

restricted because of severe vascular toxicity(176). Therefore, there is an urgent need for alternative therapies in patients with these mutations. ESKM works through an entirely different mechanism than the TKI's, and our experiments demonstrated equal efficacy of the TCRm mediated ADCC against both TKI sensitive BV173 and its resistant mutant BV173R *in vitro* and *in vivo*. Combining ESKM with another TKI could result in faster remissions and possible cure, which may allow a shorter course of these expensive, potentially toxic and non-curative drugs.

While these data strongly support the effectiveness of combining TKIs with ESKM, there are limitations. The patients must be HLA-A*02+, and have leukemias expressing WT1. Leukemias with reduced HLA-A*02 expression may be resistant to ESKM. Additionally, low WT1 expression, or inadequate concentrations of effector cells such as in a leukemia packed bone marrow, may also limit cytotoxic activity of this TCRm antibody. Importantly, despite its potent activity against Ph+ ALL, ESKM had no discernable effect on normal human BM progenitor cells within these model systems. Because of its specificity for the leukemia cells, ESKM should cause minimal toxicity. In addition, this antibody could be evaluated in human clinical trials during the peri-stem cell transplant time frame.

Resistance to ESKM mediated ADCC in AML

ESKM relies solely on ADCC for its cytotoxic effect in vitro and in vivo. While we have demonstrated efficacy in both ALL and AML models with

ESKM, as a single agent durable remission is difficult to achieve. The data here are derived from experiments that utilize the antibody ESKMto elucidate the *in vitro* and *in vivo* factors which result in leukemic escape. The data do not support down-regulation of target epitope, inadequate pharmacokinetics of the mAb, the inhibition of effector cells, suboptimal effector to target ratio in the BM, or the microenvironment as important mechanisms of mAb therapy failure. Instead, we observed that growth kinetics of the leukemia, and the quality and number of effectors, was critical to leukemic relapse. This was demonstrated by the superior efficacy of ESKM in mice on slower growing clones of AML cells, which differed from the parental line only by the introduction of an inducible cyclin-dependent kinase inhibitor $p27^{Kip1}$ to slow the AML cell cycling time. These results indicate that leukemia may be able to evade ADCC and ADCP by outgrowing effectors. These findings are especially relevant for the use of mAb in the setting of rapidly growing population of leukemia cells, with a limited number of effectors whose activity may be suppressed by chemotherapy or the disease itself. For mAb that act via other mechanisms not requiring effectors, such as the direct killing demonstrated by rituximab or traztuzumab, these issues may be less important and may warrant use of cytostatic drugs, by targeting growth pathways such as MAPK, in combination with ESKM and other TCRm to yield synergy(177, 178).

The concept of outgrowing antibody mediated destruction in humans has been documented in another disease. In idiopathic thrombocytopenia

purpura (ITP), the antibody mediated destruction of platelets can be treated by thrombopoietic agents, which are very effective at increasing platelet numbers simply by increasing platelet production(179). The converse therefore is feasible, and documented by our data: slowing down target cell growth increases susceptibility to the effector mechanisms. Interestingly, the escape mechanism does not appear to be simply a matter of inadequate E:T ratios as the initiation of therapy at time zero or addition of more effectors, either by infusion or cytokine induction, did not prevent relapse.

These findings may be highly relevant currently, given the rapid development and approval of many cellular growth pathway inhibitors, each targeting specific overactive signaling pathways in cancer cells, many of which are cytostatic. With the ever-increasing ability to detect cell growth drivers and an expanding library of small molecules, such as tyrosine kinase inhibitors, including BRAF inhibitors, MEK inhibitors, and JAK inhibitors, it will soon be possible to slow the growth of many tumor cells safely *in vivo*. Indeed, we showed that in mouse models of Ph+ ALL, ESKM plus imatinib was more than additive, and ESKM plus dasatinib was in some cases curative. Combining cytostatic therapy with targeted immune therapy, such as mAbs, may therefore result in synergistic and possibly curative outcomes without resorting to cytotoxic chemotherapy. Furthermore, chemotherapy may contribute to the effector cell dysfunction. Of course, chemotherapy may still be required to lower tumor burden for more optimal E:T ratios.

THESIS SUMMARY

USE OF POOLED shRNA SCREENS TO DISCOVER REGULATORS OF MHC-I

We demonstrated the use of a pooled shRNA screen to study regulation of the surface molecule MHC-I on tumor cells. This is the first comprehensive study of kinases which regulate surface levels of MHC-I on tumor cells. Using a hypothesis driven screen is a useful starting point for discovering regulation of a pathway. We hypothesized that kinases, which are involved in dysregulating oncogenic signaling, would influence surface levels of MHC-I. Interferon gamma, a known pharmacologic regulation of MHC-I, works through signaling of the JAK-STAT kinase pathway, so it is not surprising that other kinases are involved in the regulation.

MEK and EGFR were validated as regulators of MHC-I in tumor cells. MEK has been demonstrated to regulate MHC-I in gastric cancer, and melanoma. We validated these data in our mesothelioma cell lines and also broad tumor types, ranging from melanoma, NSCLC, thyroid cancer, colorectal cancer, and pancreatic cancer. Given that immunotherapies are being evaluated for many, if not all of these neoplasms regulating antigen presentation may be a beneficial strategy to increasing therapeutic efficacy.

Future directions

The use of a pooled shRNA screen, coupled with FACS and next generation sequencing to deconvolute shRNA construct identity and abundance is a novel concept that could be applied broadly to other surface

antigen targets, and potentially any protein with a specific antibody compatibly with flow cytometric based assays. One could envision looking at regulation of checkpoint inhibitors such as PD-L1 using a screen similar to this one, or for looking at genes affected phosphorylation of ERK.

Utilizing a similar screening platform, this could be done with CRISPR based knockout of genes, which may lead to more potent phenotypes than what was seen with shRNA based loss of function screens. In some cases, complete knockout is required for a phenotype to be observed, and this screening strategy would be amenable to CRISPR based lentiviral pooled screens (180). Gain of function screens using ORF based libraries could also be used if FACS based screens(181).

THE MAPK PATHWAY REGULATIONS MHC-I

The MAPK pathway is responsible for growth, proliferation, gene expression, and differentiation of many tissues. This pathway is often activated in cancers, and is part of the oncogenic process. We discovered two hits in our screen which are part of the MAPK pathway, EGFR and MEK, as negative regulators of MHC-I. Inhibition of these kinases, either by shRNA or by specific small molecule inhibition led to increased surface MHC-I.

EGFR is a receptor tyrosine kinase which is often constitutively activated in various cancers, such as NSCLC via mutations in the tyrosine kinase domain or via overexpression in colorectal cancer and others (182, 183). EGFR signals downstream into PI3K, MAPK, and STAT, leading to

broad effects on angiogenesis, motility, survival, proliferation, and differentiation (184).

We demonstrated that EGFR is a potent regulator of surface MHC-I in tumors with activated signaling due to activating EGFR mutations. Knockdown of EGFR with shRNA led to an increase in surface MHC-I. We further phenocopied this effect using specific small molecule inhibitors, either erlotinib or afatanib. We were able to increase tumor antigen presentation by measuring WT1 tumor antigen presentation with ESKM upon treatment of a mesothelioma cell line. EGFRi in NSCLC cell lines with activating EGFR mutations led to increased levels of HLAA, TAP1, TAP2, and B2M, which are key components of MHC-I and antigen presentation machinery. We also observed dose dependent increases in HLAA and B2M with increasing EGFRi.

MAP2K1 or MEK was also validated as a regulator of MHC-I. Work previously has demonstrated the role of MEK in regulating gastric cancer MHC-I. MEK was identified in our unbiased kinome screen as well to regulated MHC-I expression in mesothelioma, and we were able to further validate these effects in broad tumor types such as melanoma, colorectal cancer, pancreatic cancer, and thyroid cancer cell lines. Given that many cancers have activation of the MAPK pathway, and immunotherapy is being evaluated in many of these same cancers it may be relevant to consider regulating antigen presentation and MHC-I expression in addition to treatment with an immunomodulatory drug(79, 185).

Future directions

The work described here sets up a framework for evaluation of kinase targets that are commonly activated via mutations, amplifications, deletions, or autocrine signaling to be utilized as targets in up-regulation of MHC-I and tumor antigen presentation. In particular, many kinases are known to feed into the MAPK pathway, identified as a key regulator in tumor cells of MHC-I expression. While we focused on EGFR and MEK, other kinases have been shown to feed into the MAPK pathway. We have some preliminary data on RET regulating MHC-I. Other RTK such as ALK, overexpressed in certain NSCLC tumors, and MET, amplified also in NSCLC and hepatocellular carcinoma, are therapeutic targets that could also be evaluated for their role on regulating MHC-I.

Discovering the downstream effectors that regulate MHC-I, along with components of the antigen presentation machinery would also be of interest. We have data suggesting a role for STAT1, and this could be followed up mechanistically with CHiP experiments to definitively show the role of STAT1 in regulating MHC-I upon MAPK inhibition. The regulation of MHC-I may also depend on where the activated signaling originates from, as RTK may signal to a different set of pathways than a downstream BRAF mutation. This may also be relevant in predicting the response to MAPKi in regulating MHC-I.

USE OF KINASE INHIBITION IN COMBINATION WITH IMMUNOTHERAPY FOR SUPERIOR THERAPUETIC EFFICACY

Kinase inhibitors have been utilized for over two decades now as FDA approved therapies for cancer, starting with the approval of imatinib for CML with BCR-Abl translocations. Since then, many cancers have been appreciated to have presence of genetic, epigenetic, or autocrine/paracrine dysregulation leading to chronic signaling of oncogenic pathways. Blocking cancer cells from their addiction to oncogenic signaling has demonstrated to have therapeutic efficacy in many cancers(186).

While the mechanisms of various immunotherapies are being fully worked out, it is understood that antigen presentation on MHC-I plays an important and vital role in the response to immunotherapy. Mutational burden, leading to robust neo-antigen presentation on MHC-I has been shown to be predictive of response to immunotherapy (107, 108). We propose that limited presentation of these antigens may lead to ineffective response to various immunotherapies dependent on antigen presentation.

By utilizing inhibition of two well characterized targets, EGFR and MEK, to up-regulate MHC-I this provides for a rational combination therapy which targets tumor growth and also antigen presentation to the immune system. We demonstrated that use of MEKi can increase two forms of immunotherapy, using TCRm antibodies in combination with trametinib, or with p-mel specific T-cells against a murine melanoma treated with MEKi. Others have shown that

it is possible to combine MEKi with CTLA-4 and PD-1 checkpoint blockade in syngeneic mouse tumor models (110, 111, 113).

Further models to demonstrate the use of EGFRi in combination with immunotherapy are warranted. We did not have a model in place to ideally evaluate this, but use of genetically engineered mouse models with transgenic expression of EGFR mutations serve as an ideal platform to evaluate combination with PD-1 therapy. Others have published on increased PD-L1 and PD-1 expression in the tumor of transgenic EGFR mutant lung adenocarcinoma mouse models, and we also examined the data and showed decreased levels of MHC-I and antigen presentation components (101). This could set up a model by which tumors, through EGFR signaling, would activate PD-L1 expression on tumors and down-regulate MHC-I and antigen presentation machinery such as TAP1 and TAP2 to allow for immune escape and sustained proliferation of the tumor. Our data support this model, and we expect that combined blockade of PD-1 along with EGFRi to be complementary therapies.

These data support a model by which inhibiting constitutively activated kinases that feed into the MAPK pathway, such as EGFR and MEK, or other kinases whereby constitutive activation has been demonstrated to play a role in the MAPK pathway could be treated with specific small molecule inhibitors to increase immunogenicity of the tumor. This would also be compatible with use of an immunotherapy dependent on antigen presentation, such as checkpoint blockade, vaccination, adoptive T-cell therapy, or TCRm mAb. This

may argue for upfront use of combined kinase inhibition with immunotherapy versus using agents sequentially after a patient has failed therapy with one treatment.

Future directions

The work described here sets up an ideal set of in vivo combination therapies to evaluate. We have tried work with ESKM in combination with MEKi but have not seen synergy that was observed in vitro. Off target effects on activation and proliferation of leukocytes has been seen with MEKi, which act as the main effector for ESKM (110, 114, 187). Optimal dosing schedules will be required in order to properly sequence this with immunotherapy.

EGFRi may be a more attractive target for immunotherapy combinations, since this has not been seen to affect immune effector cells. Utilizing a transgenic EGFRm mouse model, we could evaluate combinations of EGFRi with anti PD-1/PD-L1 therapies. One issue is that the transgenic models respond exquisitely well to monotherapy EGFRi, leaving a very small window for effective combination (90). Another approach is use of humanized mouse models, which have been shown to be useful for preclinical immunotherapy studies such as anti-CTLA4 and anti-PD1/PD-L1 with human tumors in murine models. We plan to evaluate use of EGFRm human NSCLC in humanized mice for combination therapy with EGFRi and anti PD-1 therapy with pembrolizumab.

STRUCTURE OF A TCR MIMIC ANTIBODY WITH TARGET PREDICTS PHARMACOGENETICS AND POTENTIAL OFF TARGETS

Use of a TCR mimic against the oncoprotein WT1 has demonstrated potent in vitro and in vivo efficacy. We have examined the sequence specificity of ESK previously, but have never completely understood the determinants for specificity and binding. Utilizing an x-ray crystal structure of ESK in complex with HLA*A02 and the WT1 derived peptide target RMFPNAPYL we have gained insight into the basis of ESKM on target binding and affinity. We also learned of the broaded of potential haplotypes of HLA*A02 which ESK is compatible with, a unique property of this TCRm.

ESK was found to bind in a manner differently than how TCR bind to the HLA molecule. ESK contacts both the HLA molecule and the RMF peptide, similar to a TCR. The difference is the location of the contacts between the ESK fab, which are located over regions rich in Arg residues on the HLA*A02 molecule and RMF peptide. ESK primarily contacts the first 3-4 amino acids of the RMF peptide. This is an unusually interesting property, which given the counter negative charges on the ESK Fab region may explain the observed sub-nanomolar affinity seen with the TCRm, when compared to TCR which bind with micromolar affinity, despite both binding with comparable surface areas to the HLA*A02 and peptide portions.

The structure also allowed for explanation of another interesting property of ESK, which is the broad binding to various HLA*A02 subtypes, such as HLA*A0203, HLA*A0207 and others. This is a unique property of

ESK, whereas this is not seen with TCR. This provides a huge advantage to use of ESK as a targeting modality for WT1+ HLA*A02 tumors, as there are TCR based therapies currently in clinical trials against WT1+ tumors but are limited to the specific subtype HLA*A0201(26). Our structural data revealed that ESK binds to regions that are conserved amongst the different HLA*A02 polymorphisms, allowing for subtype universal TCRm. This may argue for TCRm based therapies to be utilized in adoptive T-cell and CAR-T cell based therapies, allowing for an expanded patient population to benefit from these therapies.

Lastly, we wanted to examine the potential off targets of ESK by utilizing a bioinformatics based approach informed by our structural studies. By using BLAST and NETMHC algorithms, we were able to identify some potential off target peptides of ESK, derived from two genes, MED13L and PIGQ. These were confirmed to bind to the HLA*A02 molecule and were conducive to ESK binding at similar levels to what is seen with RMF binding. While it has been demonstrated that ESK did bind a small subset of normal human B-cells, it is uncertain what non WT1 target was contributing to the binding. This data suggests these proteins, amongst other potential off targets, may contribute to the off target binding of ESK. This has the potential to influence how off targets of TCR and TCRm based therapies are evaluated.

Future directions

The structure of ESK1 in complex with the target WT1 peptide and HLA*A02 can be utilized for future development of more specific TCRm mAb to avoid biasing in binding that leave open opportunities for off target peptides to be bound and potentially elicit killing by effector cells. We already have utilized the structural information to develop second generation versions of ESK, which bind closer to the orientation which TCR bind to pMHC complexes and have in preliminary experiments demonstrated higher specificity for WT1+ cells. Utilizing better screening strategies, we can develop more specific, potent therapeutic TCRm for immunotherapy.

IDENTIFYING AND BYPASSING RESISTANCE TO ESKM IN ACUTE LEUKEMIA

ESKM is an ideal therapy to target WT1+ acute leukemias, which currently only have one FDA approved biologic therapy, blinotinumab for CD19+ ALL. We propose that targeting WT1+ leukemias is a viable therapeutic strategy. Previous work demonstrated efficacy of ESK1 in acute leukemia in vitro and in vivo(50). We went on further to show that in BCR-Abl positive ALL, ESKM could be used in combination with TKI targeting BCR-Abl in WT1+ leukemias. Interestingly, ESKM was more potent that first generation imatanib in BCR-Abl+ ALL. We also showed that combination with the more potent dasatinib, in combination with ESKM, could result in curative strategies in ALL.

We also demonstrated that in nearly pan resistant BCR-Abl with T315I gatekeeper mutation in ALL, ESKM was still an effective therapy. Superior therapy was also seen by combining ESKM with ponatinib, the only FDA approved TKI therapy for T315I mutated BCR-Abl. Given the life threatening toxicity seen with ponatinib, leading to its temporary withdrawal as an FDA approved drug, we believe that ESKM may be a complementary therapy for use in T315I ALL and CML, which may have minimal side effects as seen in preclinical toxicity studies(130, 176).

While we had seen some efficacy with ESKM in AML, the therapy was inferior to what was seen in ALL despite tumors having similar levels of binding and killing of ESKM. Another issue for AML is the lack of targeted therapies approved for AML, with the exception being ATRA in PML-RARA translocated AML.

Using xenograft mouse models of AML cell line SET2 in NSG mice, we evaluated potential mechanisms of resistance to ESKM in vivo. Target down-regulation was not observed. Nor was intrinsic resistance to ADCC, the predominant mechanism by which ESKM works in vivo. We evaluated insufficient effector cells by engrafting fewer leukemia cells, thereby increasing the effector to target ratio. The leukemia was still able to growout of continuous ESKM therapy. Drug penetrance into tumor was not observed as a limitation.

We hypothesized a kinetic mechanism by which ESKM is unable to kill at a fast enough rate. This was demonstrated by slowing down the kinetics of

SET2 by overexpression of a cell cycle blocking protein, p27kip, which led to slower cell cycling but not apoptosis. Overexpression of p27kip did not lead to alterations in binding of ESKM or more sensitivity to ADCC. In vivo, overexpression of p27kip in combination with ESKM led to a greater than additive effect in leukemia growth inhibition when compared to either overexpression alone, or ESKM treatment alone.

The kinetics of leukemia growth leading to sensitivity to an antibody therapy depedent on ADCC may have broad implication for trial design. This may indicate that ESKM for AML should be paired with leukemias that are being treated with cytostatic therapies. While overexpression of p27kip is not physiologic, it has been shown that hypomethylating agents such as decitabine and azacytadine can lead to increased levels of p27kip(188). We expect that more targeted therapies such as FLT3 inhibitors will become available for use in leukemia and may by ideal candidates for combination therapy with TCRm mAb such as ESKM.

Future directions

The data shown for ESKM has demonstrated that kinetics plays a role in outgrowth and resistance by leukemia. We are interested to see if this applies to other TCRm, and other antibodies. While other antibodies have multiple mechanisms of action, such as direct killing by signal blockade or induction of apoptosis, ADCC remains an important mainstay of therapeutic activity of

mAb. This may also be relevant to antibody therapies that target much lower epitope densities

Other mechanisms besides slowing down tumor growth could include boosting the ability for effector cells to kill target cells. We have preliminary data on use of CD47 antagonists that increase efficacy of multiple TCRm in vitro and in vivo by promoting antibody dependent cellular phagocytosis, a major form of killing utilized by macrophages.

References

1. Newberg MH, et al. (1996) Importance of MHC class 1 alpha2 and alpha3 domains in the recognition of self and non-self MHC molecules. *J Immunol* 156(7):2473–2480.
2. Salter RD, Cresswell P (1986) Impaired assembly and transport of HLA-A and -B antigens in a mutant TxB cell hybrid. *EMBO J* 5(5):943–949.
3. Schubert U, et al. (2000) Rapid degradation of a large fraction of newly synthesized proteins by proteasomes. *Nature* 404(6779):770–4.
4. Princiotta MF, et al. (2003) Quantitating Protein Synthesis, Degradation, and Endogenous Antigen Processing. *Immunity* 18(3):343–354.
5. Rock KL, et al. (1994) Inhibitors of the proteasome block the degradation of most cell proteins and the generation of peptides presented on MHC class I molecules. *Cell* 78(5):761–771.
6. Reits EA, Vos JC, Grommé M, Neefjes J (2000) The major substrates for TAP in vivo are derived from newly synthesized proteins. *Nature* 404(6779):774–8.
7. Hewitt EW (2003) The MHC class I antigen presentation pathway: strategies for viral immune evasion. *Immunology* 110(2):163–9.
8. Neefjes J, Jongsma MLM, Paul P, Bakke O (2011) Towards a systems understanding of MHC class I and MHC class II antigen presentation. *Nat Rev Immunol* 11(12):823–836.
9. Hunt DF, et al. (1992) Characterization of Peptides Bound to the Class I MHC Molecule HLA-A2.1 by Mass Spectrometry. *Science (80-)* 255(5049):1261–1263.
10. Suri A, et al. (2012) Cancer testis antigens: A new paradigm for cancer therapy. *Oncoimmunology* 1(7):1194–1196.
11. Simpson AJG, Caballero OL, Jungbluth A, Chen Y-T, Old LJ (2005) Cancer/testis antigens, gametogenesis and cancer. *Nat Rev Cancer* 5(8):615–25.
12. Atanackovic D, et al. (2008) Booster vaccination of cancer patients with MAGE-A3 protein reveals long-term immunological memory or tolerance depending on priming. *Proc Natl Acad Sci U S A* 105(5):1650–5.
13. Matsushita H, et al. (2012) Cancer Exome Analysis Reveals a T Cell Dependent Mechanism of Cancer Immunoediting. *Nature* 482(7385). doi:10.1038/nature10755.
14. Schumacher TN, Schreiber RD (2015) Neoantigens in cancer immunotherapy. *Science (80-)* 348(6230):69–74.
15. Dunn GP, Bruce AT, Ikeda H, Old LJ, Schreiber RD (2002) Cancer immunoediting: from immunosurveillance to tumor escape. *Nat Immunol* 3(11):991–998.
16. Gilboa E (1999) The Makings of a Tumor Rejection Antigen. *Immunity* 11(3):263–270.
17. Sahin U, et al. (1995) Human neoplasms elicit multiple specific immune responses in the autologous host. *Proc Natl Acad Sci U S A* 92(25):11810–3.

18. van der Bruggen P, et al. (1991) A gene encoding an antigen recognized by cytolytic T lymphocytes on a human melanoma. *Science (80-)* 254(5038):1643–1647.
19. Chen Y-TT, et al. (1997) A testicular antigen aberrantly expressed in human cancers detected by autologous antibody screening. *Proc Natl Acad Sci* 94(5):1914–1918.
20. Overwijk WW, et al. (2003) Tumor regression and autoimmunity after reversal of a functionally tolerant state of self-reactive CD8+ T cells. *J Exp Med* 198(4):569–80.
21. Krug LM, et al. (2010) WT1 peptide vaccinations induce CD4 and CD8 T cell immune responses in patients with mesothelioma and non-small cell lung cancer. *Cancer Immunol Immunother* 59(10):1467–79.
22. Filipazzi P, et al. (2012) Limited Induction of Tumor Cross-Reactive T Cells without a Measurable Clinical Benefit in Early Melanoma Patients Vaccinated with Human Leukocyte Antigen Class I–Modified Peptides. *Clin Cancer Res* 18(23):6485–6496.
23. Jäger E, Jäger D, Knuth A (2002) Clinical cancer vaccine trials. *Curr Opin Immunol* 14(2):178–182.
24. Rosenberg SA, Restifo NP, Yang JC, Morgan RA, Dudley ME (2008) Adoptive cell transfer: a clinical path to effective cancer immunotherapy. *Nat Rev Cancer* 8(4):299–308.
25. Dudley ME, Rosenberg SA (2003) Adoptive-cell-transfer therapy for the treatment of patients with cancer. *Nat Rev Cancer* 3(9):666–675.
26. Chapuis AG, et al. (2013) Transferred WT1-reactive CD8+ T cells can mediate antileukemic activity and persist in post-transplant patients. *Sci Transl Med* 5(174):174ra27.
27. Morgan RA, et al. (2003) High Efficiency TCR Gene Transfer into Primary Human Lymphocytes Affords Avid Recognition of Melanoma Tumor Antigen Glycoprotein 100 and Does Not Alter the Recognition of Autologous Melanoma Antigens. *J Immunol* 171(6):3287–3295.
28. Morgan RA, et al. (2006) Cancer regression in patients after transfer of genetically engineered lymphocytes. *Science* 314(5796):126–9.
29. Liddy N, et al. (2012) Monoclonal TCR-redirected tumor cell killing. *Nat Med* 18(6):980–7.
30. Hathcock K, et al. (1993) Identification of an alternative CTLA-4 ligand costimulatory for T cell activation. *Science (80-)* 262(5135):905–907.
31. Parry R V, et al. (2005) CTLA-4 and PD-1 receptors inhibit T-cell activation by distinct mechanisms. *Mol Cell Biol* 25(21):9543–53.
32. Tivol EA, et al. (1995) Loss of CTLA-4 leads to massive lymphoproliferation and fatal multiorgan tissue destruction, revealing a critical negative regulatory role of CTLA-4. *Immunity* 3(5):541–7.
33. Leach DR, Krummel MF, Allison JP (1996) Enhancement of Antitumor Immunity by CTLA-4 Blockade. *Science (80-)* 271(5256):1734–1736.
34. Hodi FS, et al. (2010) Improved Survival with Ipilimumab in Patients with Metastatic Melanoma. *N Engl J Med* 363(8):711–723.

35. Nishimura H, Nose M, Hiai H, Minato N, Honjo T (1999) Development of Lupus-like Autoimmune Diseases by Disruption of the PD-1 Gene Encoding an ITIM Motif-Carrying Immunoreceptor. *Immunity* 11(2):141–151.
36. Dong H, et al. (2002) Tumor-associated B7-H1 promotes T-cell apoptosis: A potential mechanism of immune evasion. *Nat Med* (4):793–800.
37. Freeman GJ, et al. (2000) Engagement of the PD-1 immunoinhibitory receptor by a novel B7 family member leads to negative regulation of lymphocyte activation. *J Exp Med* 192(7):1027–34.
38. Iwai Y, et al. (2002) Involvement of PD-L1 on tumor cells in the escape from host immune system and tumor immunotherapy by PD-L1 blockade. *Proc Natl Acad Sci* 99(19):12293–12297.
39. Topalian SL, et al. (2012) Safety, activity, and immune correlates of anti-PD-1 antibody in cancer. *N Engl J Med* 366(26):2443–54.
40. Yang L, et al. (2007) A tumor suppressor and oncogene: the WT1 story. *Leukemia* 21(5):868–876.
41. Oji Y, et al. (1999) Expression of the Wilms' tumor gene WT1 in solid tumors and its involvement in tumor cell growth. *Japanese J cancer Res* 90(February):194–204.
42. Cheever MA, et al. (2009) The Prioritization of Cancer Antigens: A National Cancer Institute Pilot Project for the Acceleration of Translational Research. *Clin Cancer Res* 15(17):5323–5337.
43. Oka Y, et al. (2000) Human cytotoxic T-lymphocyte responses specific for peptides of the wild-type Wilms' tumor gene (WT1) product. *Immunogenetics* 51(2):99–107.
44. Oka Y, et al. (2000) Cancer Immunotherapy Targeting Wilms' Tumor Gene WT1 Product. *J Immunol* 164(4):1873–1880.
45. May RJ, et al. (2007) Peptide Epitopes from the Wilms' Tumor 1 Oncoprotein Stimulate CD4+ and CD8+ T Cells That Recognize and Kill Human Malignant Mesothelioma Tumor Cells. *Clin Cancer Res* 13(15):4547–4555.
46. Pinilla-Ibarz J, et al. (2006) Improved human T-cell responses against synthetic HLA-0201 analog peptides derived from the WT1 oncoprotein. *Leukemia* 20(11):2025–33.
47. Denkberg G, et al. (2002) Direct visualization of distinct T cell epitopes derived from a melanoma tumor-associated antigen by using human recombinant antibodies with MHC- restricted T cell receptor-like specificity. *Proc Natl Acad Sci* 99(14):9421–9426.
48. Weidanz JA, Hawkins O, Verma B, Hildebrand WH (2011) TCR-like biomolecules target peptide/MHC Class I complexes on the surface of infected and cancerous cells. *Int Rev Immunol* 30(5-6):328–340.
49. Sergeeva A, et al. (2011) An anti–PR1/HLA-A2 T-cell receptor–like antibody mediates complement-dependent cytotoxicity against acute myeloid leukemia progenitor cells. *Blood* 117(16):4262–4272.

50. Dao T, et al. (2013) Targeting the Intracellular WT1 Oncogene Product with a Therapeutic Human Antibody. *Sci Transl Med* 5(176):176ra33–176ra33.
51. Ferrone S, Marincola FM (1995) Loss of HLA class I antigens by melanoma cells: molecular mechanisms, functional significance and clinical relevance. *Immunol Today* 16(10):487–494.
52. Leone P, et al. (2013) MHC Class I Antigen Processing and Presenting Machinery: Organization, Function, and Defects in Tumor Cells. *JNCI J Natl Cancer Inst* 105(16):1172–1187.
53. Hicklin DJ, Marincola FM, Ferrone S (1999) HLA class I antigen downregulation in human cancers: T-cell immunotherapy revives an old story. *Mol Med Today* 5(4):178–186.
54. Reichel J, et al. (2015) Flow sorting and exome sequencing reveal the oncogenome of primary Hodgkin and Reed-Sternberg cells. *Blood* 125(7):1061–72.
55. Shukla SA, et al. (2015) Comprehensive analysis of cancer-associated somatic mutations in class I HLA genes. *Nat Biotechnol* 33(11):1152–1158.
56. Storkus WJ, Alexander J, Payne J a, Dawson JR, Cresswell P (1989) Reversal of natural killing susceptibility in target cells expressing transfected class I HLA genes. *Proc Natl Acad Sci U S A* 86(7):2361–4.
57. Ljunggren HG, Kärre K (1985) Host resistance directed selectively against H-2-deficient lymphoma variants. Analysis of the mechanism. *J Exp Med* 162(6):1745–59.
58. Wallach D, Fellous M, Revel M (1982) Preferential effect of γ interferon on the synthesis of HLA antigens and their mRNAs in human cells. *Nature* 299(5886):833–836.
59. Ma W, Lehner PJ, Cresswell P, Pober JS, Johnson DR (1997) Interferon- Rapidly Increases Peptide Transporter (TAP) Subunit Expression and Peptide Transport Capacity in Endothelial Cells. *J Biol Chem* 272(26):16585–16590.
60. Y Shirayoshi PABEAKO (1988) Interferon-induced transcription of a major histocompatibility class I gene accompanies binding of inducible nuclear factors to the interferon consensus sequence. *Proc Natl Acad Sci U S A* 85(16):5884.
61. Decker T, Kovarik P (2000) Serine phosphorylation of STATs. *Oncogene* 19(21):2628–37.
62. Baldeon ME, Neece DJ, Nandi D, Monaco JJ, Gaskins HR (1997) Interferon- Independently Activates the MHC Class I Antigen Processing Pathway and Diminishes Glucose Responsiveness in Pancreatic -Cell Lines. *Diabetes* 46(5):770–778.
63. Saura M, Zaragoza C, Bao C, McMillan A, Lowenstein CJ (1999) Interaction of interferon regulatory factor-1 and nuclear factor kappaB during activation of inducible nitric oxide synthase transcription. *J Mol Biol* 289(3):459–71.

64. LEE AH, HONG J-H, SEO Y-S (2000) Tumour necrosis factor-α and interferon-γ synergistically activate the RANTES promoter through nuclear factor κB and interferon regulatory factor 1 (IRF-1) transcription factors. *Biochem J* 350(1):131–138.
65. Basler M, Kirk CJ, Groettrup M (2013) The immunoproteasome in antigen processing and other immunological functions. *Curr Opin Immunol* 25(1):74–80.
66. Dunn GP, Koebel CM, Schreiber RD (2006) Interferons, immunity and cancer immunoediting. *Nat Rev Immunol* 6(11):836–48.
67. Latchman Y, et al. (2001) PD-L2 is a second ligand for PD-1 and inhibits T cell activation. *Nat Immunol* 2(3):261–8.
68. Tempero MA, et al. (1990) Phase II trial of interferon gamma and monoclonal antibody 17-1A in pancreatic cancer: Biologic and clinical effects. *J Clin Oncol* 8(12):2019–2026.
69. Paul P, et al. (2011) A Genome-wide Multidimensional RNAi Screen Reveals Pathways Controlling MHC Class II Antigen Presentation. *Cell* 145(2):268–283.
70. Bernstein E, Caudy AA, Hammond SM, Hannon GJ (2001) Role for a bidentate ribonuclease in the initiation step of RNA interference. *Nature* 409(6818):363–6.
71. Sims D, et al. (2011) High-throughput RNA interference screening using pooled shRNA libraries and next generation sequencing. *Genome Biol* 12(10):R104.
72. Workman P (2005) Drugging the cancer kinome: progress and challenges in developing personalized molecular cancer therapeutics. *Cold Spring Harb Symp Quant Biol* 70:499–515.
73. Manning G, Whyte DB, Martinez R, Hunter T, Sudarsanam S (2002) The protein kinase complement of the human genome. *Science* 298(5600):1912–34.
74. Zuber J, et al. (2011) RNAi screen identifies Brd4 as a therapeutic target in acute myeloid leukaemia. *Nature* 478(7370):524–528.
75. Zuber J, et al. (2011) Toolkit for evaluating genes required for proliferation and survival using tetracycline-regulated RNAi. *Nat Biotechnol* 29(1):79–83.
76. Fellmann C, et al. (2013) An Optimized microRNA Backbone for Effective Single-Copy RNAi. *Cell Rep* 5(6):1704–1713.
77. Hanahan D, Weinberg RA (2011) Hallmarks of cancer: the next generation. *Cell* 144(5):646–74.
78. Roberts PJ, Der CJ (2007) Targeting the Raf-MEK-ERK mitogen-activated protein kinase cascade for the treatment of cancer. *Oncogene* 26(22):3291–310.
79. Dhillon AS, Hagan S, Rath O, Kolch W (2007) MAP kinase signalling pathways in cancer. *Oncogene* 26(22):3279–90.
80. Egan SE, et al. (1993) Association of Sos Ras exchange protein with Grb2 is implicated in tyrosine kinase signal transduction and

transformation. *Nature* 363(6424):45–51.
81. Macdonald SG, et al. (1993) Reconstitution of the Raf-1-MEK-ERK signal transduction pathway in vitro. *Mol Cell Biol* 13(11):6615–6620.
82. Warrell Jr. RP, et al. (1991) Differentiation therapy of acute promyelocytic leukemia with tretinoin (all-trans-retinoic acid). *N Engl J Med* 324(20):1385–1393.
83. Specchia G, et al. (1995) Ph positive acute lymphoblastic leukemia in adults: molecular and clinical studies. *Leuk Lymphoma* 18 Suppl 1:37–42.
84. Kantarjian H, et al. (2002) Hematologic and cytogenetic responses to imatinib mesylate in chronic myelogenous leukemia. *N Engl J Med* 346(9):645–52.
85. Smit VTHBM, et al. (1988) KRAS codon 12 mutations occur very frequently in pancreatic adenocarcinomas. *Nucleic Acids Res* 16(16):7773–7782.
86. Brose MS, et al. (2002) BRAF and RAS Mutations in Human Lung Cancer and Melanoma. *Cancer Res* 62(23):6997–7000.
87. Brose MS, et al. (2002) BRAF and RAS Mutations in Human Lung Cancer and Melanoma. *Cancer Res* 62(23):6997–7000.
88. Flaherty KT, et al. (2012) Improved Survival with MEK Inhibition in BRAF-Mutated Melanoma. *N Engl J Med* 367(2):107–114.
89. Solit DB, et al. (2006) BRAF mutation predicts sensitivity to MEK inhibition. *Nature* 439(7074):358–362.
90. Politi K, et al. (2006) Lung adenocarcinomas induced in mice by mutant EGF receptors found in human lung cancers respond to a tyrosine kinase inhibitor or to down-regulation of the receptors. *Genes Dev* 20(11):1496–510.
91. Maverakis E, et al. (2015) MEK inhibitors and their potential in the treatment of advanced melanoma: the advantages of combination therapy. *Drug Des Devel Ther* Volume 10:43.
92. Killock D (2015) Lung cancer: A new generation of EGFR inhibition. *Nat Rev Clin Oncol* 12(7):373–373.
93. Kobayashi S, et al. (2005) EGFR mutation and resistance of non-small-cell lung cancer to gefitinib. *N Engl J Med* 352(8):786–92.
94. Liao B-C, Lin C-C, Yang JC-H (2015) Second and third-generation epidermal growth factor receptor tyrosine kinase inhibitors in advanced nonsmall cell lung cancer. *Curr Opin Oncol* 27(2):94–101.
95. Eberlein CA, et al. (2015) Acquired Resistance to the Mutant-Selective EGFR Inhibitor AZD9291 Is Associated with Increased Dependence on RAS Signaling in Preclinical Models. *Cancer Res* 75(12):2489–500.
96. Gobin SJP, Biesta P, Elsen PJ Van den (2003) Regulation of human β2-microglobulin transactivation in hematopoietic cells. *Blood* 101(8):3058–3064.
97. Gobin SJP, et al. (1998) The RFX complex is crucial for the constitutive and CIITA-mediated transactivation of MHC class I and ??2-

microglobulin genes. *Immunity* 9(4):531–541.
98. Johnson DR (2003) Locus-specific constitutive and cytokine-induced HLA class I gene expression. *J Immunol* 170(4):1894–1902.
99. Wolchok JD, Vilček J (1992) Induction of HLA class I mRNA by cytokines in human fibroblasts: comparison of TNF, IL-1 and IFN-β. *Cytokine* 4(6):520–527.
100. Regales L, et al. (2009) Dual targeting of EGFR can overcome a major drug resistance mutation in mouse models of EGFR mutant lung cancer. *J Clin Invest* 119(10):3000–10.
101. Akbay EA, et al. (2013) Activation of the PD-1 Pathway Contributes to Immune Escape in EGFR-Driven Lung Tumors. *Cancer Discov* 3(12):1355–1363.
102. Sugiyama H (2001) Wilms' Tumor Gene WT1: Its Oncogenic Function and Clinical Application. *Int J Hematol* 73(2):177–187.
103. Tsuboi A, et al. (2012) Long-term WT1 peptide vaccination for patients with acute myeloid leukemia with minimal residual disease. *Leukemia* 26(6):1410–1413.
104. Quintarelli C, et al. (2008) Cytotoxic T lymphocytes directed to the preferentially expressed antigen of melanoma (PRAME) target chronic myeloid leukemia. *Blood* 112(5):1876–85.
105. Chang, Aaron, Dao, Tao, Scott, Andrew, Dubrovsky, Leonid, Liu, Cheng, Scheinberg D (2015) A Therapeutic TCR Mimic Monoclonal Antibody for Intracellular PRAME Protein in Leukemias. *American Society of Hematology* Available at: https://ash.confex.com/ash/2015/webprogram/Paper82235.html [Accessed February 11, 2016].
106. Budhu S, et al. (2010) CD8+ T cell concentration determines their efficiency in killing cognate antigen-expressing syngeneic mammalian cells in vitro and in mouse tissues. *J Exp Med* 207(1):223–35.
107. Rizvi NA, et al. (2015) Mutational landscape determines sensitivity to PD-1 blockade in non-small cell lung cancer. *Science (80-)* 348(6230):124–128.
108. Snyder A, et al. (2014) Genetic Basis for Clinical Response to CTLA-4 Blockade in Melanoma. *N Engl J Med* 371(23):2189–2199.
109. Van Allen EM, et al. (2015) Genomic correlates of response to CTLA4 blockade in metastatic melanoma. *Science (80-)* 350(6257):207–211.
110. Liu L, et al. (2015) The BRAF and MEK Inhibitors Dabrafenib and Trametinib: Effects on Immune Function and in Combination with Immunomodulatory Antibodies Targeting PD1, PD-L1 and CTLA-4. *Clin Cancer Res An Off J Am Assoc Cancer Res*. doi:10.1158/1078-0432.CCR-14-2339.
111. Hu-Lieskovan S, et al. (2015) Improved antitumor activity of immunotherapy with BRAF and MEK inhibitors in BRAF(V600E) melanoma. *Sci Transl Med* 7(279):279ra41.
112. Kortum RL, Rouquette-Jazdanian AK, Samelson LE (2013) Ras and

extracellular signal-regulated kinase signaling in thymocytes and T cells. *Trends Immunol* 34(6):259–268.
113. Ebert PJR, et al. (2016) Article MAP Kinase Inhibition Promotes T Cell and Anti- tumor Activity in Combination with PD-L1 MAP Kinase Inhibition Promotes T Cell and Anti-tumor Activity in Combination with PD-L1 Checkpoint Blockade. *Immunity*:1–13.
114. Vella LJ, et al. (2014) MEK inhibition, alone or in combination with BRAF inhibition, affects multiple functions of isolated normal human lymphocytes and dendritic cells. *Cancer Immunol Res*:canimm.0181.2013.
115. Wolchok D, Goodman A (1994) induction cells of NF-xB may be necessary but is not sufficient for of H-2 antigens by TNF in J558L murine myeloma. *Cytokines* 55(January):7–12.
116. Girdlestone J, Isamat M, Gewert D, Milstein C (1993) Transcriptional regulation of HLA-A and -B: differential binding of members of the Rel and IRF families of transcription factors. *Proc Natl Acad Sci U S A* 90(24):11568–11572.
117. Zaidi MR, Merlino G (2011) The Two Faces of Interferon-γ in Cancer. *Clin Cancer Res* 17(19):6118–6124.
118. Pollack BP, Sapkota B, Cartee T V. (2011) Epidermal Growth Factor Receptor Inhibition Augments the Expression of MHC Class I and II Genes. *Clin Cancer Res* 17(13):4400–4413.
119. Mimura K, et al. (2013) The MAPK pathway is a predominant regulator of HLA-A expression in esophageal and gastric cancer. *J Immunol* 191(12):6261–72.
120. Fogdell-Hahn A, Ligers A, Gronning M, Hillert J, Olerup O (2000) Multiple sclerosis: a modifying influence of HLA class I genes in an HLA class II associated autoimmune disease. *Tissue Antigens* 55(2):140–148.
121. Brown MA, Kenna T, Wordsworth BP (2016) Genetics of ankylosing spondylitis-insights into pathogenesis. *Nat Rev Rheumatol* 12(2):81–91.
122. Caroline Robert, M.D and Thomas S. Kupper M. (1999) Inflammatory Skin Diseases, T Cells, and Immune Surveillance — NEJM. *N Engl J Med* 341(10):1817–1828.
123. Scott AM, Wolchok JD, Old LJ (2012) Antibody therapy of cancer. *Nat Rev Cancer* 12(4):278–87.
124. Yan C, Higgins PJ (2013) Drugging the undruggable: transcription therapy for cancer. *Biochim Biophys Acta* 1835(1):76–85.
125. Dahan R, Reiter Y (2012) T-cell-receptor-like antibodies - generation, function and applications. *Expert Rev Mol Med* 14:e6.
126. Keilholz U, et al. (2005) Wilms' tumour gene 1 (WT1) in human neoplasia. *Leukemia* 19(8):1318–23.
127. Ohminami H, Yasukawa M, Fujita S (2000) HLA class I-restricted lysis of leukemia cells by a CD8(+) cytotoxic T-lymphocyte clone specific for WT1 peptide. *Blood* 95(1):286–293.

128. Dao T, et al. (2013) Targeting the intracellular WT1 oncogene product with a therapeutic human antibody. *Sci Transl Med* 5(176):176ra33.
129. Dubrovsky L, et al. (2014) A TCR-mimic antibody to WT1 bypasses tyrosine kinase inhibitor resistance in human BCR-ABL+ leukemias. *Blood* 123(21):3296–3304.
130. Veomett N, et al. (2014) Therapeutic Efficacy of an Fc-Enhanced TCR-like Antibody to the Intracellular WT1 Oncoprotein. *Clin Cancer Res* 20(15):4036–4046.
131. Ding Y-H, et al. (1998) Two Human T Cell Receptors Bind in a Similar Diagonal Mode to the HLA-A2/Tax Peptide Complex Using Different TCR Amino Acids. *Immunity* 8(4):403–411.
132. Ding Y-H, Baker BM, Garboczi DN, Biddison WE, Wiley DC (1999) Four A6-TCR/Peptide/HLA-A2 Structures that Generate Very Different T Cell Signals Are Nearly Identical. *Immunity* 11(1):45–56.
133. Stewart-jones G, et al. (2009) Correction for Stewart-Jones et al., Rational development of high-affinity T-cell receptor-like antibodies. *Proc Natl Acad Sci* 106(26):10872–10872.
134. Mareeva T, Martinez-Hackert E, Sykulev Y (2008) How a T cell receptor-like antibody recognizes major histocompatibility complex-bound peptide. *J Biol Chem* 283(43):29053–9.
135. Linette GP, et al. (2013) Cardiovascular toxicity and titin cross-reactivity of affinity-enhanced T cells in myeloma and melanoma. *Blood* 122(6):863–71.
136. Ellis JM, et al. (2000) Frequencies of HLA-A2 alleles in five U.S. population groups. Predominance Of A*02011 and identification of HLA-A*0231. *Hum Immunol* 61(3):334–340.
137. Gonzalez-Galarza FF, Christmas S, Middleton D, Jones AR (2011) Allele frequency net: a database and online repository for immune gene frequencies in worldwide populations. *Nucleic Acids Res* 39(Database issue):D913–919.
138. Lundegaard C, et al. (2008) NetMHC-3.0: accurate web accessible predictions of human, mouse and monkey MHC class I affinities for peptides of length 8-11. *Nucleic Acids Res* 36(Web Server issue):W509–12.
139. Marsh SGE, Parham P, Barber LD (1999) *The HLA Facts Book* (Academic Press).
140. Altman JD, Davis MM (2001) MHC-Peptide Tetramers to Visualize Antigen-Specific T Cells. *Current Protocols in Immunology* (John Wiley & Sons, Inc.).
141. Soltis SM, et al. (2008) New paradigm for macromolecular crystallography experiments at SSRL: automated crystal screening and remote data collection. *Acta Crystallogr D Biol Crystallogr* 64(Pt 12):1210–1221.
142. Otwinowski Z, Minor, Wladek (1997) Processing of X-ray diffraction data collected in oscillation mode. *Methods Enzymol* 276:307–326.

143. Kabsch W (2010) XDS. *Acta Crystallogr Sect D Biol Crystallogr* 66(2):125–132.
144. Vagin A, Teplyakov A (2010) Molecular replacement with MOLREP. *Acta Crystallogr D Biol Crystallogr* 66(Pt 1):22–25.
145. McCoy AJ, et al. (2007) *Phaser* crystallographic software. *J Appl Crystallogr* 40(4):658–674.
146. Murshudov GN, Vagin AA, Dodson EJ (1997) Refinement of Macromolecular Structures by the Maximum-Likelihood Method. *Acta Crystallogr Sect D Biol Crystallogr* 53(3):240–255.
147. Emsley P, Cowtan K (2004) Coot: model-building tools for molecular graphics. *Acta Crystallogr D Biol Crystallogr* 60(Pt 12 Pt 1):2126–2132.
148. Krissinel E, Henrick K (2007) Inference of macromolecular assemblies from crystalline state. *J Mol Biol* 372(3):774–797.
149. Borbulevych OY, Do P, Baker BM (2010) Structures of native and affinity-enhanced WT1 epitopes bound to HLA-A*0201: implications for WT1-based cancer therapeutics. *Mol Immunol* 47(15):2519–2524.
150. Ding YH, et al. (1998) Two human T cell receptors bind in a similar diagonal mode to the HLA-A2/Tax peptide complex using different TCR amino acids. *Immunity* 8(4):403–411.
151. Ding YH, Baker BM, Garboczi DN, Biddison WE, Wiley DC (1999) Four A6-TCR/peptide/HLA-A2 structures that generate very different T cell signals are nearly identical. *Immunity* 11(1):45–56.
152. Garboczi DN, et al. (2010) Structure of the complex between human T-cell receptor, viral peptide and HLA-A2. Nature. 1996. 384: 134-141. *J Immunol (Baltimore, Md 1950)* 185(11):6394–6401.
153. Stewart-Jones G, et al. (2009) Rational development of high-affinity T-cell receptor-like antibodies. *Proc Natl Acad Sci U S A* 106(14):5784–5788.
154. Sami M, et al. (2007) Crystal structures of high affinity human T-cell receptors bound to peptide major histocompatibility complex reveal native diagonal binding geometry. *Protein Eng Des Sel PEDS* 20(8):397–403.
155. Borbulevych OY, Piepenbrink KH, Baker BM (2011) Conformational melding permits a conserved binding geometry in TCR recognition of foreign and self molecular mimics. *J Immunol (Baltimore, Md 1950)* 186(5):2950–2958.
156. Borbulevych OY, et al. (2009) T cell receptor cross-reactivity directed by antigen-dependent tuning of peptide-MHC molecular flexibility. *Immunity* 31(6):885–896.
157. Armstrong KM, Insaidoo FK, Baker BM (2008) Thermodynamics of T-cell receptor-peptide/MHC interactions: progress and opportunities. *J Mol Recognit JMR* 21(4):275–287.
158. Willcox BE, et al. (1999) TCR binding to peptide-MHC stabilizes a flexible recognition interface. *Immunity* 10(3):357–365.
159. Davis-Harrison RL, Armstrong KM, Baker BM (2005) Two different T cell

receptors use different thermodynamic strategies to recognize the same peptide/MHC ligand. *J Mol Biol* 346(2):533–550.
160. Brennan FR, et al. (2014) Safety and immunotoxicity assessment of immunomodulatory monoclonal antibodies. *MAbs* 2(3):233–255.
161. Reiser J-B, et al. (2003) CDR3 loop flexibility contributes to the degeneracy of TCR recognition. *Nat Immunol* 4(3):241–7.
162. Birnbaum ME, et al. (2014) Deconstructing the Peptide-MHC Specificity of T Cell Recognition. *Cell* 157(5):1073–1087.
163. Steinberg M (2007) Dasatinib: A tyrosine kinase inhibitor for the treatment of chronic myelogenous leukemia and philadelphia chromosome-positive acute lymphoblastic leukemia. *Clin Ther* 29(11):2289–2308.
164. Davis TA, Czerwinski DK, Levy R (1999) Therapy of B-Cell Lymphoma with Anti-CD20 Antibodies Can Result in the Loss of CD20 Antigen Expression. *Clin Cancer Res* 5(3):611–615.
165. Karapetis CS, et al. (2008) K-ras mutations and benefit from cetuximab in advanced colorectal cancer. *N Engl J Med* 359(17):1757–65.
166. Cartron G (2002) Therapeutic activity of humanized anti-CD20 monoclonal antibody and polymorphism in IgG Fc receptor Fcgamma RIIIa gene. *Blood* 99(3):754–758.
167. Burgess MR, Skaggs BJ, Shah NP, Lee FY, Sawyers CL (2005) Comparative analysis of two clinically active BCR-ABL kinase inhibitors reveals the role of conformation-specific binding in resistance. *Proc Natl Acad Sci U S A* 102(9):3395–400.
168. Hu Y, et al. (2012) Enhancement of the anti-tumor activity of therapeutic monoclonal antibodies by CXCR4 antagonists. *Leuk Lymphoma* 53(1):130–8.
169. Shultz LD, Ishikawa F, Greiner DL (2007) Humanized mice in translational biomedical research. *Nat Rev Immunol* 7(2):118–130.
170. Pegoraro L, et al. (1983) Establishment of a Ph1-positive human cell line (BV173). *J Natl Cancer Inst* 70(3):447–53.
171. Talpaz M, et al. (2006) Dasatinib in imatinib-resistant Philadelphia chromosome-positive leukemias. *N Engl J Med* 354(24):2531–41.
172. Seitz RJ, Heininger K, Schwendemann G, Toyka K V., Wechsler W (1985) The mouse blood-brain barrier and blood-nerve barrier for IgG: A tracer study by use of the avidin-biotin system. *Acta Neuropathol* 68(1):15–21.
173. Younes A, Yasothan U, Kirkpatrick P (2012) Brentuximab vedotin. *Nat Rev Drug Discov* 11(1):19–20.
174. Adams GP, Weiner LM (2005) Monoclonal antibody therapy of cancer. *Nat Biotechnol* 23(9):1147–1157.
175. Branford S (2002) High frequency of point mutations clustered within the adenosine triphosphate-binding region of BCR/ABL in patients with chronic myeloid leukemia or Ph-positive acute lymphoblastic leukemia who develop imatinib (STI571) resistance. *Blood* 99(9):3472–3475.

176. Moslehi JJ, Deininger M (2015) Tyrosine Kinase Inhibitor-Associated Cardiovascular Toxicity in Chronic Myeloid Leukemia. *J Clin Oncol* 33(35):4210–8.
177. Vu T, Claret FX (2012) Trastuzumab: updated mechanisms of action and resistance in breast cancer. *Front Oncol* 2:62.
178. Maloney DG, Smith B, Rose A (2002) Rituximab: Mechanism of action and resistance. *Semin Oncol* 29(1):2–9.
179. Frampton JE, Lyseng-Williamson KA (2009) Romiplostim. *Drugs* 69(3):307–17.
180. Shalem O, et al. (2014) Genome-scale CRISPR-Cas9 knockout screening in human cells. *Science* 343(6166):84–7.
181. Johannessen CM, et al. (2013) A melanocyte lineage program confers resistance to MAP kinase pathway inhibition. *Nature* 504(7478):138–42.
182. Santarius T, Shipley J, Brewer D, Stratton MR, Cooper CS (2010) A census of amplified and overexpressed human cancer genes. *Nat Rev Cancer* 10(1):59–64.
183. Pao W, Chmielecki J (2010) Rational, biologically based treatment of EGFR-mutant non-small-cell lung cancer. *Nat Rev Cancer* 10(11):760–74.
184. da Cunha Santos G, Shepherd FA, Tsao MS (2011) EGFR mutations and lung cancer. *Annu Rev Pathol* 6:49–69.
185. Chen L, Han X (2015) Anti-PD-1/PD-L1 therapy of human cancer: past, present, and future. *J Clin Invest* 125(9):3384–91.
186. Adjei AA, Hidalgo M (2005) Intracellular signal transduction pathway proteins as targets for cancer therapy. *J Clin Oncol* 23(23):5386–403.
187. Vella LJ, et al. The kinase inhibitors dabrafenib and trametinib affect isolated immune cell populations. *Oncoimmunology* 3(7):e946367.
188. Sánchez-Abarca LI, et al. (2010) Immunomodulatory effect of 5-azacytidine (5-azaC): potential role in the transplantation setting. *Blood* 115(1):107–21.